Cortical plasticity following injury in primate visual system

Dissertation

zur Erlangung des Grades eines

Doktors der Naturwissenschaften

der Mathematisch-Naturwissenschaftlichen Fakultät

und

der Medizinischen Fakultät

der Eberhard-Karls-Universität Tübingen

vorgelegt

von

Yibin Shao

aus Heilongjiang, China

October - 2014

Tag der mündlichen Prüfung: _____2015. 3. 23_____

Dekan der Math.-Nat. Fakultät: Prof. Dr. W. Rosenstiel
Dekan der Medizinischen Fakultät: Prof. Dr. I. B. Autenrieth

1. Berichterstatter: Prof. Dr. / PD Dr. / Dr. __Stelios Smirnakis_____

2. Berichterstatter: Prof. Dr. / PD Dr. / Dr. __Cornelius Schwarz_____

Prüfungskommission: Prof. Dr. / PD Dr. / Dr. __Nikos Logothetis_____

                            Prof. Dr. / PD Dr. / Dr. __Georgios Keliris_____

Erklärung / Declaration:

Ich erkläre, dass ich die zur Promotion eingereichte Arbeit mit dem Titel:

"   Cortical plasticity following injury in primate visual system

                                                                                                            "
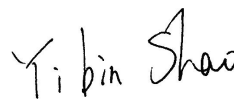
selbständig verfasst, nur die angegebenen Quellen und Hilfsmittel benutzt und wörtlich oder inhaltlich übernommene Stellen als solche gekennzeichnet habe. Ich versichere an Eides statt, dass diese Angaben wahr sind und dass ich nichts verschwiegen habe. Mir ist bekannt, dass die falsche Abgabe einer Versicherung an Eides statt mit Freiheitsstrafe bis zu drei Jahren oder mit Geldstrafe bestraft wird.

I hereby declare that I have produced the work entitled "……", submitted for the award of a doctorate, on my own (without external help), have used only the sources and aids indicated and have marked passages included from other works, whether verbatim or in content, as such. I swear upon oath that these statements are true and that I have not concealed anything. I am aware that making a false declaration under oath is punishable by a term of imprisonment of up to three years or by a fine.

Tübingen,

den _____   2015. 10. 14   _____   _____
                 Datum / Date   Unterschrift /Signature

Synopsis

Contents

Chapter 1 Introduction

Several brain areas are capable of reorganization after injury though the extent and limits of reorganization differ from area to area. Studying the visual system has several advantages: 1) its precise topography increases the sensitivity and specificity of reorganization measurements, 2) the background information that exists about the connectivity pattern and function of visual areas permits the formulation of precise hypotheses about the mechanism of recovery. Understanding the potential for plasticity inherent in different processing levels of the adult visual has potential implications for the rehabilitation of visual system disorders.

The aim of this dissertation is to study whether and how much the visual cortex changes following injury at different levels of the visual system. Damage at any level of the visual system induces changes in anatomy, connectivity and function throughout the rest of the system. Using fMRI we have the advantage of observing changes over the entire brain that enables comparisons of how different areas reorganize following lesions. Chapter 2 provides a brief overview of our work, which is described in detail in the original papers and manuscripts contained in the second part of this thesis.

Chapter 3 focuses on plasticity after damage of the first relay of the visual system, the retina. First a major cause of blindness in human, macular degeneration is introduced, followed by our study on a rhesus macaque with naturally occurring bilateral macular dystrophy. Then results are presented mapping visual cortical organization under two conditions: 1) naturally occurring chronic macular degeneration and 2) laser induced retinal lesions (data from the literature) [1]. Chapter 4 concentrates on studying visual cortical organization after damage of the major entry point of cortical visual processing, the primary visual cortex (V1). Despite the importance of V1 as a relay of information to extrastriate cortex, visual performance does not always degrade completely following V1 damage. This intriguing phenomenon, called "blindsight," is described here. Later in this chapter, studies of visual cortex organization following V1 lesions are critically

reviewed. In Chapter 5, I discuss select studies of plasticity after extrastriate cortex injury, as well as plasticity that occurs with training in subjects with healthy visual system. At the end, I summarize our findings and put them in context in the literature.

Chapter 2 Brief overview of papers

2.1 Detailed functional and structural characterization of a macular lesion in a rhesus macaque

In this study we present detailed structural and functional findings of a rhesus macaque suffering from a naturally occurring bilateral macular dystrophy, partial optic atrophy and corresponding reduction of central V1 signals in visual fMRI experiments [2]. Detailed structural and functional examinations in the affected animal and a healthy macaque of similar age were performed. Structural assessment showed a symmetric macular dystrophy combined with reduced vascularization and partial optic nerve atrophy in the otherwise healthy animal. Functional deficits reflected the loss of central retinal function. Altered macular morphology corresponded to a preferential reduction of central signals in the multifocal electroretinography and to a specific attenuation of cone-derived responses in the Ganzfeld electroretinography, while rod function remained normal.
In conclusion, we provided detailed characterization of a primate macular disorder. This study served to stimulate awareness and further investigation in primates with naturally occurring macular disorders. Identifying a primate animal model of juvenile macular degeneration would be useful in facilitating the preclinical development of therapeutic strategies.

2.2 Visual Cortex Organization in a Macaque Monkey with Macular Degeneration

The visual field is retinotopically represented in early visual areas. It has been suggested that when adult primary visual cortex (V1) is deprived of normal retinal input, it is capable of large-scale reorganization, with neurons inside the lesion projection zone

(LPZ) being visually driven by inputs from intact retinal regions. Early functional magnetic resonance imaging (fMRI) studies in humans with macular degeneration (MD) report more than 1cm spread of activity inside the LPZ border, whereas recent results report no shift of the LPZ border [1]. Here, we used fMRI population receptive field measurements to study, for the first time, the visual cortex organization of one macaque monkey with MD and to compare it with normal controls [3]. Our results showed that the border of the V1 LPZ remained stable suggesting that the deafferented area V1 zone of the MD animal has limited capacity for reorganization. Interestingly we found that V5/MT has a higher potential for reorganization after macular degeneration than earlier visual cortex.

2.3 Macaque area V2/V3 organization following homonymous retinal lesions

A major problem in neuroscience is to understand the capacity of the adult visual system for plasticity. In particular, plasticity of the primary visual cortex (V1) after retinal lesions has been extensively investigated by numerous studies. In contrast, reorganization of extrastriate areas following retinal lesions is less well studied. Here, we used fMRI to study reorganization of visual areas V2/V3 following permanent binocular retinal lesions in 4 adult macaque monkeys [4]. Our results indicate that V2/V3 of adult macaque monkeys has a marked capacity for reorganization following retinal lesions.

2.4 Population receptive field analysis of the primary visual cortex complements perimetry in patients with homonymous visual field defects

Injury to the primary visual cortex (V1) typically leads to loss of conscious vision in the corresponding, homonymous region of the contralateral visual hemi-field (scotoma). Several studies suggest that V1 is highly plastic after injury to the visual pathways, whereas others have called this conclusion into question. We used functional magnetic resonance imaging (fMRI) to measure area V1 population receptive field (pRF) properties in five patients with partial or complete quadrantic visual field loss as a result of partial V1 or optic radiation lesions [5]. Comparisons were made with healthy controls deprived of visual stimulation in one quadrant "artificial scotoma". We observed no large-scale changes in spared V1 topography. However limited reorganization was manifested in some patients by a small shift in the pRF centers toward the border of the scotoma, and a slight increase in V1 pRF sizes near the border of the scotoma as well as in the V1 of the contralesional hemisphere.

Chapter 3 Plasticity after retinal damage

3.1 Macular degeneration

Macular degeneration is a major cause of blindness and has enormous socioeconomic impact [6]. It is a medical condition that usually affects older adults (age-related macular degeneration, or AMD) and results in a loss of vision in the center of visual field because of damage to the retina. Apart from AMD, there are several macular dystrophies that can manifest earlier in life, i.e. the juvenile forms of macular degeneration (JMD) [3]. In subjects with bilateral macular degeneration, the foveal confluence and adjacent cortex is typically deprived of its normal input as a result of damage to the central retina. In humans, any form of macular degeneration results in significant morbidity for the patient, particularly since there are limited therapeutic options available. These macular dystrophies often result in profound visual disability as the central visual input is crucial for reading, face recognition and other key tasks of everyday life[6]. Patients who suffer from macular damage typically spontaneously develop one or more alternative retinal locus that lies in the intact peripheral part of the retina for fixation, called preferred retinal locus (PRL) [7]. Human subjects suffering from macular degeneration exhibit perceptual filling-in of their blind visual field as well as an associated distortion of the visual space [8,9,10,11].

Non-human primates, like the rhesus macaque, proved over the years to be ideal models for studying the pathophysiological processes of aging and retinal disease. Prominent examples are the studies on MD. Common features of MD such as altered pigment distribution, window defects due to retinal pigment epithelial atrophy, soft drusen and changes of Bruch's membrane structure can all be found reliably in elderly monkeys (*Macaca mulatta*) where progression, ultrastructure and functional losses are comparable to those found in humans [12,13].

We studied a rhesus macaque (*Macaca mulatta*) suffering from a chronic MD condition approximating human juvenile macular degeneration (JMD) [2], which is thought to have more capacity of plasticity than the case of AMD [14,15,16,17]. Before studying visual cortical plasticity on this monkey, and in order to clarify the underlying pathophysiology, we carried out a detailed *in vivo* characterization of the structural and functional aspects of this condition using state of the art clinical diagnostic protocols including OCT imaging, fluorescence and indocyanine green angiography and multifocal ERG [2]. Structural assessment showed a symmetric macular dystrophy combined with reduced vascularization and partial optic nerve atrophy in the otherwise healthy animal. Functional deficits reflect the loss of central retinal function.

3.2 Visual cortex (re)-organization after macular degeneration

Early visual areas have a topographically precise, retinotopic, representation of the visual field [18,19,20,21,22]. These maps remain stable over time in healthy adults but are thought to be plastic following injury of the visual pathways [14,15,16,17,23,24,25,26,27,28,29]. Understanding the capacity of the visual system for reorganization following injury is an important step in the long-term effort to design treatments aimed at enhancing the ability of the visual system to recover after injury.

Several groups have used fMRI to study visual cortex reorganization in a human patients suffered from macular degeneration. The first fMRI study was from a 60 year old female subject with age-related macular degeneration. They found a large unresponsive zone in the V1 lesion project zone (LPZ) and large-scale reorganization in V1 to be absent [30]. Several subsequent fMRI case studies on subjects with binocular macular lesions suggested that human primary visual cortex deprived of its normal retinal input by MD undergoes large-scale reorganization spanning centimeters of cortical space [14,15,16,17]. The largest human fMRI study surveying MD patients to date [31], however, recently reported the lack of large-scale reorganization in V1 [1]. To

understand the difference between the results, Masuda et al. used a passive viewing condition and a stimulus-related judgment task. They found that V1 responses into the LPZ happened only under the stimulus related judgment task condition, suggesting that it may be mediated by cortical feedback. They proposed that the reported reorganization is caused by cortical signals initiated by the task demands, and not by reorganization of the feed-forward pathways carrying the retinal stimulation [32].

In [3] we used fMRI population receptive field measurements [33] to study cortical reorganization in a macaque monkey suffering from a chronic MD condition approximating human juvenile macular degeneration (JMD) [2]. We compared our results with both the human fMRI and the macaque fMRI & electrophysiology literature. In this macaque subject with juvenile macular degeneration we found that area area V1 showed at best limited reorganization, in agreement with what [31] found in human MD. Area V2 also showed limited reorganization. In contrast, extrastriate area V5/MT showed considerably more capacity for reorganization: visually modulated MT voxles with ectopic pRFs cover a much larger cortical area than expected in the MD animal compared to "artificial scotoma" controls (by occluding the central part of the visual field). Area V5/MT could therefore potentially serve as the source of relatively strong feedback inside the area V1 lesion projection zone. There was also a suggestions that area V3 could be upregulated in the MD animal, but we did not have enough data to make a definitive statement.

3.3 Extrastriate cortex (re)-organization following induced retinal lesions

Human studies of cortical plasticity following retinal lesions have some disadvantages. For example, because retinal histology cannot be obtained in living subjects, we cannot exclude the possibility that retinal pathology is incomplete or patchy, or that the retinal lesion borders may not be abrupt but tapering. Laser induced retinal lesions in animals can be better standardized. Moreover, by inducing the lesion in adulthood we can

bypass the developmental period of plasticity, which cannot be done for juvenile macular degeneration.

Several groups have studied the capacity of the visual cortex for reorganization following induced retinal lesions in adult animals. The majority of electrophysiology studies after homonymous retinal lesions in adult cats and macaques reported that area V1 exhibits a considerable degree of plasticity into adulthood [23,24,25,28,34]. However, recent studies using cytochrome oxidase [35], electrophysiology [36] and fMRI [1] have put this result to question, and suggest that post lesion responses inside the V1 lesion projection zone (LPZ) are weak or absent. In a recent review, Wandell and Smirnakis [37] suggested that electrophysiological recording selection bias explains the disparity of the results.

Less is known about the capacity of extrastriate cortex to reorganize following retinal lesions. Reports from the literature of filling-in suggest that under the right conditions visual responsiveness in higher areas can be seen in cortical locations that are far away from the visual stimulus. De Weerd et. al. showed that the responses of extrastriate V2/V3 neurons whose receptive fields are contained inside an area devoid of stimulation (artificial scotoma) increase within seconds to reach a level comparable to that elicited by direct stimulation [38]. Enhancements of these pathways provide a possible substrate that might be able to support reorganization.

Here, we extend these results by using fMRI to study the extent to which areas V2/V3 reorganize following permanent bilateral and homonymous retinal lesions induced by photocoagulation in adult macaques [4]. We found that a few hours after the lesion, about half of the area V2/V3 lesion projection zone (LPZ) could already be modulated by visual stimuli. Furthermore, the voxels that did not show visual modulation on the day of the lesion could be visually modulated 2 weeks later, and the mean modulation strength remained approximately stable thereafter for the duration of our observations (4-5 months). The distribution of eccentricities of visually modulated voxels inside the V2/V3 LPZ spanned a wider range than expected post-lesion, suggesting that neurons

inside the LPZ reorganize by receiving input either from the foveal or the peripheral border of the LPZ, depending on proximity. Overall, area V2/V3 of adult rhesus macaques displays a significant capacity for reorganization following retinal lesions that exceeds the capacity of area V1 for reorganization, as well as the range of filling-in exhibited in V2/V3 by the presentation of transient stimuli.

Chapter 4 Plasticity after V1 injury

4.1 Blindsight: residual vision after V1 damage

Blindsight is defined as residual visual capacity following lesions to V1 [39,40]. Despite area V1 being the chief relay of visual input to all exstrastiate visual areas, a series of studies performed over the last 25 years has provided strong evidence that subjects still possess considerable residual visual capacity, including residual visual motion, form and wavelength sensitivity, in the blind part of their visual field following dense area V1 lesions [40,41,42,43,44,45,46,47,48]. These findings have also been replicated in monkeys with V1 injury [49,50]. This phenomenon has been termed "blindsight" to reflect the fact that the residual visual perceptual capacity remaining following V1 lesions is often associated with the absence of visual awareness.

"Blindsight" is generally assumed to be mediated by extra-geniculo-striate retinofugal pathways and modulated by feedback from higher areas [49,51,52,53,54,55], but the precise mechanism has not been deciphered. Therefore it is important to identify candidate areas that might be involved in the residual vision observed in the phenomenon of ''blindsight''.

4.2 Spared V1 (re)-organization after partial V1 lesions

Visual responsiveness of higher cortical visual areas is dependent on V1 input, and it has been shown that transient inactivation of area V1 eliminates more than 95% of visually driven activity seen in retinotopically corresponding locations of extrastriate areas [56,57,58].

However, several extrastriate visual cortices have shown activity with the absence of V1. MT neurons, following the lesion of V1, were found to maintain active, both in monkeys and humans [51,59]. In area V2 and V3, visually driven activity were reported to persists in a patient suffering from hemianopia [60], and macaques with chronic V1 lesion [61].

A more debated issue is whether the adult V1 is able to reorganize adjacent to regions of V1 injury or following lesions of the optic radiation. Enlarged receptive fields have been found in areas surrounding chronic V1 lesions in cats [62,63,64], and visual point spread functions were seen to enlarge over time in the areas surrounding focal V1 lesions in kittens [65]. Smaller, short term changes (2 d after the lesion) have been reported as well [66]. As expected, reorganization is more extensive in young animals [65,67] compared with adults [68].

A recent study in an adult human subject suggested that large-scale reorganization occurs in area V1 after partial de-afferentiation by an optic radiation lesion [69]. However, the cortical measures of reorganization used were not quantitative, and the study lacked the important control of comparison with normal subjects subjected to transient visual deprivation. We measured how spared V1 cortex covers the visual field in five human subjects with chronic V1 injury [5]. We derived detailed retinotopic maps and visual field coverage maps for the spared V1 area of each patient. Comparisons were made with healthy controls deprived of visual stimulation in one quadrant. We observed no large-scale changes in spared-V1 topography as the V1/V2 border remained stable, and pRF eccentricity versus cortical-distance plots were similar to those of controls. However, the distribution of pRF centers in spared-V1 was shifted slightly toward the scotoma border in 2 of 5 patients compared with AS controls; pRF size in spared-V1 was slightly increased in patients near the scotoma border; and pRF size in the contra-lesional hemisphere was slightly increased compared with AS controls. These observations suggest the existence of limited reorganization.

Chapter 5 Summary

5.1 Plasticity after extrastriate cortex damage

Damage to higher-level, extrastriate visual cortex causes more subtle, area-specific abnormalities of visual perception without frank blindness. In humans, temporal cortex lesions predominantly cause abnormalities of face perception (prosopagnosia) and perception of complex objects and shapes [70,71]. Color vision abnormalities usually result from damage to the fusiform and lingual gyri [72,73,74]. Damage to human V5 or the MT + complex, causes deficits of motion perception, often termed motion blindness [75,76,77]. Improvement has been reported following lesions of area V4 [78,79] and area MT/MST in primates [80,81,82,83,84]. In most of the studies involving V4 or MT lesions, improvements were specific to the class of visual stimuli or retinotopic locations trained.

5.2 Plasticity in healthy visual system

Healthy visual systems typically remain plastic in response to changes in environmental inputs throughout the lifespan. A large number of studies showed changes for fundamental stimulus features such as orientation [85,86,87], spatial frequency [86], direction of motion [88], etc can occur with perceptual training. This notion is supported by electrophysiological recordings in monkeys [89,90] as well as fMRI [91,92] and EEG [93] studies in humans. In primate area V4, electrophysiological recordings demonstrated significant changes in both neuronal responsiveness and orientation tuning with perceptual learning [94]. Neurons in area V5/MT change direction selectivity by visual motion discrimination training [95]. In primate inferotemporal (IT) cortex, training with particular stimulus categories alters the neuronal representation of diagnostic features for the trained categories [96].

5.3 Comparison of visual plasticity

Damage at different levels of the visual system can induce anatomical and functional changes throughout the rest of the system.

In area V1 of monkeys with induced or naturally occurring retinal injury [1,3], we found limited reorganization. The border of the V1 LPZ remained stable in both studies. In the case of the fMRI study in human subjects with area V1 lesions, we found that the topography of spared regions of area V1 as well as the V1/V2 border remained stable, suggesting that spared area V1 exhibits at best limited reorganization [5].

In contrast, in both monkey fMRI studies of ours [3,4] we found considerable reorganization in extrastriate areas following acute retinal injury or macular degeneration. However, there are also differences between these two studies: V2/V3 areas seemed to be filled in after acute retinal lesions; yet in the macular degeneration case area V2 showed limited reorganization, area V3 had the tendency to be upregulated, but we cannot make a definitive statement. The size of the lesion may be the difference between the two cases. The lesion in the MD case is larger, especially the fovea is damaged. Perhaps this makes earlier visual areas like V2 more difficult to reorganize. Conversely area V5/MT appears to reorganize after retinal lesions in the MD case. But we have not looked in other cases. It may be that reorganization is amplified if there are more than one processing steps between the area of the lesion and the area where reorganization is measured.

Prior studies in humans and monkeys with V1 lesions also suggest that visually driven BOLD responses persist inside the lesion projection zone in extrastriate areas of V2/V3 and V5/MT [51,59,60,61].

Taken together, these studies show the same trend, which is that extrastriate areas have more capacity for plasticity than V1. In general, the higher one area is in the visual hierarchy, the more sources of input it has. One possible explanation is that when one source of input is eliminated, the others may compensate. It is also possible however that the intrinsic capacity of extrastriate areas for local reorganization is greater.

It is interesting to notice the differences between the plasticity seen in area V2/V3 following a retinal lesion [4] versus following an area V1 lesion [61]. In the case of a retinal lesion of limited extent [4], activity inside V2/V3 LPZ returns to nearly normal levels. By contrast after similar size V1 lesions, V2/V3 activity only returns to ~20-30% of prior activity [61]. This may appear to be counterintuitive, as the retinal lesion cuts off all access to the visual input that corresponds to the lesioned area, whereas V1 lesions leave potential bypassing pathways through LGN, the superior colliculus and the pulvinar intact. This suggests that the existence of intact area V1 and its upstream connections are important for the reorganization of areas V2, V3.

More importantly, the mechanisms likely underlying these two types of plasticities are fundamentally different. In the case of retinal lesions, as information is lost from its origin, we propose the signal arises from surrounding regions [3,4]. Whereas in V1 lesions, it seems that the signal could also arise from subcortical areas such as LGN [50]. Therefore, perhaps one type of plasticity is more akin to "filling-in" in subjects suffering from macular degeneration, the other to "blindsight" in patients with V1 damage.

Abbreviations

fMRI	functional magnetic resonance imaging
BOLD	blood oxygen level dependent
pRF	population receptive field
V1	primary visual cortex
V2/V3	secondary, third visual cortex
V5/MT	middle temporal, visual area implicated in the processing of motion
AS	artificial scotoma
LPZ	lesion projection zone
AMD/JMD	age related, juvenile macular degeneration
PRL	preferred retinal locus
OCT	optical coherence tomography
ERG	electroretinography

Bibliography

1. Smirnakis SM, Brewer AA, Schmid MC, Tolias AS, Schüz A, et al. (2005) Lack of long-term cortical reorganization after macaque retinal lesions. Nature 435: 300-307.
2. Dominik Fischer M, Zobor D, Keliris GA, Shao Y, Seeliger MW, et al. (2012) Detailed functional and structural characterization of a macular lesion in a rhesus macaque. Documenta ophthalmologica Advances in ophthalmology.
3. Shao Y, Keliris GA, Papanikolaou A, Fischer MD, Zobor D, et al. (2013) Visual cortex organisation in a macaque monkey with macular degeneration. The European journal of neuroscience 38: 3456-3464.
4. Shao Y, Keliris GA, Augath M, Logothetis NK, Smirnakis SM (2014) Macaque area V2/V3 organization following homonymous retinal lesions.
5. Papanikolaou A, Keliris GA, Papageorgiou TD, Shao Y, Krapp E, et al. (2014) Population receptive field analysis of the primary visual cortex complements perimetry in patients with homonymous visual field defects. Proceedings of the National Academy of Sciences of the United States of America 111: E1656-1665.
6. Williams RA, Brody BL, Thomas RG, Kaplan RM, Brown SI (1998) The psychosocial impact of macular degeneration. Archives of ophthalmology 116: 514-520.
7. Timberlake GT, Mainster MA, Peli E, Augliere RA, Essock EA, et al. (1986) Reading with a macular scotoma. I. Retinal location of scotoma and fixation area. Investigative Ophthalmology & Visual Science 27: 1137-1147.
8. Gerrits HJ, Timmerman GJ (1969) The filling-in process in patients with retinal scotomata. Vision Research 9: 439-442.
9. Kapadia MK, Gilbert CD, Westheimer G (1994) A quantitative measure for short-term cortical plasticity in human vision. The Journal of neuroscience : the official journal of the Society for Neuroscience 14: 451-457.
10. Burke W (1999) Psychophysical observations concerned with a foveal lesion (macular hole). Vision Research 39: 2421-2427.
11. Zur D, Ullman S (2003) Filling-in of retinal scotomas. Vision Research 43: 971-982.
12. El-Mofty A, Gouras P, Eisner G, Balazs EA (1978) Macular degeneration in rhesus monkey (Macaca mulatta). Experimental eye research 27: 499-502.
13. Dawson WW, Dawson JC, Lake KP, Gonzalez-Martinez J (2008) Maculas, monkeys, models, AMD and aging. Vision Research 48: 360-365.
14. Baker CI (2005) Reorganization of Visual Processing in Macular Degeneration. Journal of Neuroscience 25: 614-618.
15. Baker CI, Dilks DD, Peli E, Kanwisher N (2008) Reorganization of visual processing in macular degeneration: Replication and clues about the role of foveal loss. Vision Research 48: 1910-1919.
16. Schumacher EH, Jacko JA, Primo SA, Main KL, Moloney KP, et al. (2008) Reorganization of visual processing is related to eccentric viewing in patients with macular degeneration. Restorative Neurology and Neuroscience 26: 391-402.
17. Dilks DD, Baker CI, Peli E, Kanwisher N (2009) Reorganization of Visual Processing in Macular Degeneration Is Not Specific to the "Preferred Retinal Locus". Journal of Neuroscience 29: 2768-2773.
18. Van Essen DC, Maunsell JHR (1983) Hierarchical Organization and Functional Streams in the Visual-Cortex. Trends in Neurosciences 6: 370-375.

19. Tootell RB, Switkes E, Silverman MS, Hamilton SL (1988) Functional anatomy of macaque striate cortex. II. Retinotopic organization. Journal of Neuroscience 8: 1531-1568.
20. Brewer AA, Press WA, Logothetis NK, Wandell BA (2002) Visual areas in macaque cortex measured using functional magnetic resonance imaging. Journal of Neuroscience 22: 10416-10426.
21. Gattass R, Nascimento-Silva S, Soares JGM, Lima B, Jansen AK, et al. (2005) Cortical visual areas in monkeys: location, topography, connections, columns, plasticity and cortical dynamics. Philosophical Transactions of the Royal Society B: Biological Sciences 360: 709-731.
22. Wandell BA, Dumoulin SO, Brewer AA (2007) Visual field maps in human cortex. Neuron 56: 366-383.
23. Kaas JH, Krubitzer LA, Chino YM, Langston AL, Polley EH, et al. (1990) Reorganization of retinotopic cortical maps in adult mammals after lesions of the retina. Science 248: 229-231.
24. Heinen SJ, Skavenski AA (1991) Recovery of Visual Responses in Foveal V1 Neurons Following Bilateral Foveal Lesions in Adult Monkey. Experimental Brain Research 83: 670-674.
25. Gilbert CD, Wiesel TN (1992) Receptive-Field Dynamics in Adult Primary Visual-Cortex. Nature 356: 150-152.
26. Chino YM, Smith EL, Kaas JH, Sasaki Y, Cheng H (1995) Receptive-Field Properties of Deafferentated Visual Cortical-Neurons after Topographic Map Reorganization in Adult Cats. Journal of Neuroscience 15: 2417-2433.
27. Morland AB, Baseler HA, Hoffmann MB, Sharpe LT, Wandell BA (2001) Abnormal retinotopic representations in human visual cortex revealed by fMRI. Acta psychologica 107: 229-247.
28. Giannikopoulos DV (2006) Dynamics and specificity of cortical map reorganization after retinal lesions. Proceedings of the National Academy of Sciences 103: 10805-10810.
29. Levin N, Dumoulin SO, Winawer J, Dougherty RF, Wandell BA (2010) Cortical Maps and White Matter Tracts following Long Period of Visual Deprivation and Retinal Image Restoration. Neuron 65: 21-31.
30. Sunness JS, Liu T, Yantis S (2004) Retinotopic mapping of the visual cortex using functional magnetic resonance imaging in a patient with central scotomas from atrophic macular degeneration. Ophthalmology 111: 1595-1598.
31. Baseler HA, Gouws A, Haak KV, Racey C, Crossland MD, et al. (2011) Large-scale remapping of visual cortex is absent in adult humans with macular degeneration. Nature Neuroscience 14: 649-655.
32. Masuda Y, Dumoulin SO, Nakadomari S, Wandell BA (2008) V1 Projection Zone Signals in Human Macular Degeneration Depend on Task, not Stimulus. Cerebral Cortex 18: 2483-2493.
33. Dumoulin SO, Wandell BA (2008) Population receptive field estimates in human visual cortex. Neuroimage 39: 647-660.
34. Gilbert CD, Li W (2012) Adult visual cortical plasticity. Neuron 75: 250-264.
35. Horton JC, Hocking DR (1998) Monocular core zones and binocular border strips in primate striate cortex revealed by the contrasting effects of enucleation, eyelid suture, and retinal laser lesions on cytochrome oxidase activity. Journal of Neuroscience 18: 5433-5455.
36. Murakami I, Komatsu H, Kinoshita M (1997) Perceptual filling-in at the scotoma following a monocular retinal lesion in the monkey. Visual Neuroscience 14: 89-101.
37. Wandell BA, Smirnakis SM (2009) Plasticity and stability of visual field maps in adult primary visual cortex. Nature Reviews Neuroscience 10: 873-884.
38. De Weerd P, Gattass R, Desimone R, Ungerleider LG (1995) Responses of cells in monkey visual cortex during perceptual filling-in of an artificial scotoma. Nature 377: 731-734.
39. Weiskrantz L, Warrington EK, Sanders MD, Marshall J (1974) Visual capacity in the hemianopic field following a restricted occipital ablation. Brain : a journal of neurology 97: 709-728.

40. Weiskrantz L, Warrington EK (1986) The Problem of Form Discrimination in Blindsight. Behavioural Brain Research 20: 157-158.
41. Riddoch G (1917) Dissociation of visual perceptions due to occipital injuries, with especial reference to appreciation of movement. Brain 40: 15-57.
42. Poppel E, Held R, Frost D (1973) Leter: Residual visual function after brain wounds involving the central visual pathways in man. Nature 243: 295-296.
43. Barbur JL, Harlow AJ, Weiskrantz L (1994) Spatial and temporal response properties of residual vision in a case of hemianopia. Philosophical transactions of the Royal Society of London Series B, Biological sciences 343: 157-166.
44. Morland AB, Jones SR, Finlay AL, Deyzac E, Le S, et al. (1999) Visual perception of motion, luminance and colour in a human hemianope. Brain : a journal of neurology 122 (Pt 6): 1183-1198.
45. Weiskrantz L (1996) Blindsight revisited. Current Opinion in Neurobiology 6: 215-220.
46. Blythe IM, Kennard C, Ruddock KH (1987) Residual Vision in Patients with Retrogeniculate Lesions of the Visual Pathways. Brain 110: 887-905.
47. Weiskrantz L, Harlow A, Barbur JL (1991) Factors Affecting Visual Sensitivity in a Hemianopic Subject. Brain 114: 2269-2282.
48. Zeki S, Ffytche DH (1998) The Riddoch syndrome: insights into the neurobiology of conscious vision. Brain : a journal of neurology 121 (Pt 1): 25-45.
49. Cowey A, Stoerig P (1995) Blindsight in Monkeys. Nature 373: 247-249.
50. Schmid MC, Mrowka SW, Turchi J, Saunders RC, Wilke M, et al. (2010) Blindsight depends on the lateral geniculate nucleus. Nature 466: 373-377.
51. Rodman HR, Gross CG, Albright TD (1989) Afferent Basis of Visual Response Properties in Area Mt of the Macaque .I. Effects of Striate Cortex Removal. Journal of Neuroscience 9: 2033-2050.
52. Cowey A, Stoerig P (1991) The neurobiology of blindsight. Trends in Neurosciences 14: 140-145.
53. Moore T, Rodman HR, Gross CG (2001) Direction of motion discrimination after early lesions of striate cortex (V1) of the macaque monkey. Proceedings of the National Academy of Sciences of the United States of America 98: 325-330.
54. Stoerig P, Cowey A (2007) Blindsight. Current Biology 17: R822-R824.
55. Weiskrantz L (2004) Roots of blindsight. Progress in brain research 144: 229-241.
56. Schiller PH, Malpeli JG (1977) Effect of Striate Cortex Cooling on Area 18 Cells in Monkey. Brain Research 126: 366-369.
57. Girard P, Bullier J (1989) Visual activity in area V2 during reversible inactivation of area 17 in the macaque monkey. Journal of Neurophysiology 62: 1287-1302.
58. Girard P, Salin PA, Bullier J (1991) Visual activity in areas V3a and V3 during reversible inactivation of area V1 in the macaque monkey. Journal of Neurophysiology 66: 1493-1503.
59. Goebel R, Muckli L, Zanella FE, Singer W, Stoerig P (2001) Sustained extrastriate cortical activation without visual awareness revealed by fMRI studies of hemianopic patients. Vision Research 41: 1459-1474.
60. Baseler HA, Morland AB, Wandell BA (1999) Topographic organization of human visual areas in the absence of input from primary cortex. Journal of Neuroscience 19: 2619-2627.
61. Schmid MC, Panagiotaropoulos T, Augath MA, Logothetis NK, Smirnakis SM (2009) Visually driven activation in macaque areas V2 and V3 without input from the primary visual cortex. PLoS One 4: e5527.
62. Eysel UT, Schmidtkastner R (1991) Neuronal Dysfunction at the Border of Focal Lesions in Cat Visual-Cortex. Neuroscience Letters 131: 45-48.
63. Eysel UT, Schweigart G (1999) Increased receptive field size in the surround of chronic lesions in the adult cat visual cortex. Cerebral Cortex 9: 101-109.

64. Eysel UT, Schweigart G, Mittmann T, Eyding D, Qu Y, et al. (1999) Reorganization in the visual cortex after retinal and cortical damage. Restorative Neurology and Neuroscience 15: 153-164.

65. Zepeda A, Vaca L, Arias C, Sengpiel F (2003) Reorganization of visual cortical maps after focal ischemic lesions. Journal of cerebral blood flow and metabolism : official journal of the International Society of Cerebral Blood Flow and Metabolism 23: 811-820.

66. Schweigart G, Eysel UT (2002) Activity-dependent receptive field changes in the surround of adult cat visual cortex lesions. The European journal of neuroscience 15: 1585-1596.

67. Payne BR, Lomber SG (2002) Plasticity of the visual cortex after injury: what's different about the young brain? The Neuroscientist : a review journal bringing neurobiology, neurology and psychiatry 8: 174-185.

68. Yinon U, Shemesh R, Arda H, Dobin G, Jaros PP (1993) Physiological studies in deafferented visual cortex cells of cats following transplantation of fetal xenografts from the rat's cortex. Experimental neurology 122: 335-341.

69. Dilks DD, Serences JT, Rosenau BJ, Yantis S, McCloskey M (2007) Human adult cortical reorganization and consequent visual distortion. The Journal of neuroscience : the official journal of the Society for Neuroscience 27: 9585-9594.

70. Damasio AR, Damasio H, Van Hoesen GW (1982) Prosopagnosia: anatomic basis and behavioral mechanisms. Neurology 32: 331-341.

71. Huxlin KR, Merigan WH (1998) Deficits in complex visual perception following unilateral temporal lobectomy. Journal of Cognitive Neuroscience 10: 395-407.

72. Damasio A, Yamada T, Damasio H, Corbett J, McKee J (1980) Central achromatopsia: behavioral, anatomic, and physiologic aspects. Neurology 30: 1064-1071.

73. Zeki S (1990) A century of cerebral achromatopsia. Brain : a journal of neurology 113 (Pt 6): 1721-1777.

74. Zeki S, Marini L (1998) Three cortical stages of colour processing in the human brain. Brain : a journal of neurology 121 (Pt 9): 1669-1685.

75. Zeki S (1991) Cerebral akinetopsia (visual motion blindness). A review. Brain : a journal of neurology 114 (Pt 2): 811-824.

76. Zihl J, von Cramon D, Mai N, Schmid C (1991) Disturbance of movement vision after bilateral posterior brain damage. Further evidence and follow up observations. Brain : a journal of neurology 114 (Pt 5): 2235-2252.

77. Vaina LM, Cowey A, Eskew RT, Jr., LeMay M, Kemper T (2001) Regional cerebral correlates of global motion perception: evidence from unilateral cerebral brain damage. Brain : a journal of neurology 124: 310-321.

78. Schiller PH (1993) The effects of V4 and middle temporal (MT) area lesions on visual performance in the rhesus monkey. Visual Neuroscience 10: 717-746.

79. Merigan WH, Pham HA (1998) V4 lesions in macaques affect both single- and multiple-viewpoint shape discriminations. Visual Neuroscience 15: 359-367.

80. Newsome WT, Wurtz RH, Dursteler MR, Mikami A (1985) Deficits in visual motion processing following ibotenic acid lesions of the middle temporal visual area of the macaque monkey. The Journal of neuroscience : the official journal of the Society for Neuroscience 5: 825-840.

81. Newsome WT, Pare EB (1988) A selective impairment of motion perception following lesions of the middle temporal visual area (MT). The Journal of neuroscience : the official journal of the Society for Neuroscience 8: 2201-2211.

82. Bisley JW, Pasternak T (2000) The multiple roles of visual cortical areas MT/MST in remembering the direction of visual motion. Cerebral Cortex 10: 1053-1065.

83. Yamasaki DS, Wurtz RH (1991) Recovery of function after lesions in the superior temporal sulcus in the monkey. Journal of Neurophysiology 66: 651-673.

84. Rudolph K, Pasternak T (1999) Transient and permanent deficits in motion perception after lesions of cortical areas MT and MST in the macaque monkey. Cerebral Cortex 9: 90-100.

85. Ramachandran VS, Braddick O (1973) Orientation-specific learning in stereopsis. Perception 2: 371-376.

86. Fiorentini A, Berardi N (1980) Perceptual learning specific for orientation and spatial frequency. Nature 287: 43-44.

87. Crist RE, Kapadia MK, Westheimer G, Gilbert CD (1997) Perceptual learning of spatial localization: specificity for orientation, position, and context. Journal of Neurophysiology 78: 2889-2894.

88. Ball K, Sekuler R (1987) Direction-specific improvement in motion discrimination. Vision Research 27: 953-965.

89. Crist RE, Li W, Gilbert CD (2001) Learning to see: experience and attention in primary visual cortex. Nature Neuroscience 4: 519-525.

90. Schoups A, Vogels R, Qian N, Orban G (2001) Practising orientation identification improves orientation coding in V1 neurons. Nature 412: 549-553.

91. Schwartz S, Maquet P, Frith C (2002) Neural correlates of perceptual learning: a functional MRI study of visual texture discrimination. Proceedings of the National Academy of Sciences of the United States of America 99: 17137-17142.

92. Furmanski CS, Schluppeck D, Engel SA (2004) Learning strengthens the response of primary visual cortex to simple patterns. Current biology : CB 14: 573-578.

93. Pourtois G, Rauss KS, Vuilleumier P, Schwartz S (2008) Effects of perceptual learning on primary visual cortex activity in humans. Vision Research 48: 55-62.

94. Yang T, Maunsell JH (2004) The effect of perceptual learning on neuronal responses in monkey visual area V4. The Journal of neuroscience : the official journal of the Society for Neuroscience 24: 1617-1626.

95. Lu H, Qian N, Liu Z (2004) Learning motion discrimination with suppressed MT. Vision Research 44: 1817-1825.

96. Sigala N, Logothetis NK (2002) Visual categorization shapes feature selectivity in the primate temporal cortex. Nature 415: 318-320.

Personal contributions to papers and manuscripts

Detailed functional and structural characterization of a macular lesion in a rhesus macaque

Fischer MD, Zobor D, Keliris GA, <u>Shao Y</u>, Seeliger MW, Haverkamp S, Jägle H, Logothetis NK and Smirnakis SM (August-2012) *Documenta Ophthalmologica* **125(3)** 179-194.

I performed some of the experiments, conducted corresponding analysis and wrote part of the paper.

Visual cortex organization in a macaque monkey with macular degeneration

<u>Shao Y</u>, Keliris GA, Papanikolaou A, Fischer MD, Zobor D, Jägle H, Logothetis NK and Smirnakis SM (November-2013) *European Journal of Neuroscience* **38(10)** 3456–3464.

I performed the experiments, analysis and wrote the manuscript.

Macaque area V2/V3 reorganization following homonymous retinal lesions

<u>Shao Y</u>, Keliris GA, Augath M, Logothetis NK and Smirnakis SM
Manuscript ready to submit

I conducted the analysis and wrote the manuscript.

Population receptive field analysis of the primary visual cortex complements perimetry in patients with homonymous visual field defects

Papanikolaou A, Keliris GA, Papageorgiou TD, <u>Shao Y</u>, Krapp E, Papageorgiou E, Stingl K, Bruckmann A, Schiefer U, Logothetis NK and Smirnakis SM (April-2014) *Proceedings of the National Academy of Sciences of the United States of America* **111(16)** E1656–E1665.

I gave feedback on the analysis and the manuscript.

Published papers and manuscripts

Detailed functional and structural characterization of a macular lesion in a rhesus macaque

Visual cortex organization in a macaque monkey with macular degeneration

Macaque area V2/V3 reorganization following homonymous retinal lesions

Population receptive field analysis of the primary visual cortex complements perimetry in patients with homonymous visual field defects

Acknowledgements

Detailed functional and structural characterization of a macular lesion in a rhesus macaque

**M. Dominik Fischer · Ditta Zobor · Georgios A. Keliris ·
Yibin Shao · Mathias W. Seeliger · Silke Haverkamp ·
Herbert Jägle · Nikos K. Logothetis · Stelios M. Smirnakis**

Abstract

Purpose Animal models are powerful tools to broaden our understanding of disease mechanisms and to develop future treatment strategies. Here we present detailed structural and functional findings of a rhesus macaque suffering from a naturally occurring bilateral macular dystrophy (BMD), partial optic atrophy and corresponding reduction of central V1 signals in visual fMRI experiments when compared to data in a healthy macaque (CTRL) of similar age.

Methods Retinal imaging included infrared and auto-fluorescence recordings, fluorescein and indocyanine green angiography and spectral domain optical coherence tomography (OCT) on the Spectralis HRA + OCT platform. Electroretinography included multifocal and Ganzfeld-ERG recordings. Animals were killed and eyes analyzed by immunohistochemistry.

Results Angiography showed reduced macular vascularization with significantly larger foveal avascular zones (FAZ) in the affected animal ($FAZ_{BMD} = 8.85$ mm^2 vs. $FAZ_{CTRL} = 0.32$ mm^2). OCT showed bilateral thinning

M. Dominik Fischer and Ditta Zobor have contributed equally to the manuscript.

M. Dominik Fischer
Centre for Ophthalmology, University Eye Hospital, Schleichstr. 12-14, 72076 Tübingen, Germany

M. Dominik Fischer · D. Zobor · M. W. Seeliger
Institute for Ophthalmic Research, Centre for Ophthalmology, Schleichstr. 12-14, 72076 Tübingen, Germany

Present Address:
M. Dominik Fischer (✉)
Nuffield Laboratory of Ophthalmology, University of Oxford, Levels 5 and 6 West Wing, The John Radcliffe Hospital, Oxford OX3 9DU, UK
e-mail: Dominik.Fischer@ndcn.ox.ac.uk

G. A. Keliris · Y. Shao · N. K. Logothetis ·
S. M. Smirnakis
Max-Planck Institute for Biological Cybernetics, Spemannstr. 38-44, 72076 Tübingen, Germany

S. Haverkamp
Neuroanatomy, Max Planck Institute for Brain Research, Deutschordenstr. 46, 60528 Frankfurt a.M., Germany

H. Jägle
University Eye Clinic, University of Regensburg, Franz-Josef-Strauß-Allee 11, 93053 Regensburg, Germany

S. M. Smirnakis
Department of Neuroscience and Neurology, Baylor College of Medicine, One Baylor Plaza, Houston, TX 77030, USA

of the macula within the FAZ (total retinal thickness, $TRT_{BMD} = 174 \pm 9$ μm) and partial optic nerve atrophy when compared to control ($TRT_{CTRL} = 303 \pm 45$ μm). Segmentation analysis revealed that inner retinal layers were primarily affected (inner retinal thickness, $IRT_{BMD} = 33 \pm 9$ μm vs. $IRT_{CTRL} = 143 \pm 45$ μm), while the outer retina essentially maintained its thickness ($ORT_{BMD} = 141 \pm 7$ μm vs. $ORT_{CTRL} = 160 \pm 11$ μm). Altered macular morphology corresponded to a preferential reduction of central signals in the multifocal electroretinography and to a specific attenuation of cone-derived responses in the Ganzfeld electroretinography, while rod function remained normal. *Conclusion* We provided detailed characterization of a primate macular disorder. This study aims to stimulate awareness and further investigation in primates with macular disorders eventually leading to the identification of a primate animal model and facilitating the preclinical development of therapeutic strategies.

Keywords Macular disorder · Neurodegeneration · Functional MRI · Optical coherence tomography · Electroretinography

Introduction

Nonhuman primates, like the rhesus macaque, proved over the years to be ideal models for studying the pathophysiological processes of aging and retinal disease. Prominent examples are the studies on age-related macular degeneration (AMD), a blinding disorder with large socioeconomic impact. Common features of AMD such as altered pigment distribution, window defects due to retinal pigment epithelial atrophy, soft drusen and changes of Bruch's membrane structure can all be found reliably in elderly monkeys (*Macaca mulatta*) where progression, ultrastructure and functional losses are comparable to those found in humans [1, 2].

In humans, any form of macular degeneration results in significant morbidity for the patient, particularly since there are still no therapeutic options available—with the exception of anti-VEGF treatment in exudative (wet) AMD. Apart from AMD, there is a group of inherited retinal degenerations that are frequently seen in human patients. Various forms of macular dystrophy with different inheritance patterns,

clinical phenotype and rate of progression can manifest already early in life [3]. These macular dystrophies often result in profound visual disability as the central visual input is crucial for reading, face recognition and other key tasks of everyday life [4].

Unfortunately, progress in studying the pathogenesis, and consequently the development of treatment options in inherited degenerations has been hampered by the lack of appropriate animal models. While a large number of genetically modified rodent and lapine animal models exist for the study of the visual system, their applicability is questionable since these animals do not have a significant central retinal region comparable to the human and/or primate macula [5]. The retinal structure in rhesus macaques on the other hand corresponds well to human retinal architecture, making them an ideal candidate for studying retinal disorders and for testing the development of new therapeutic strategies [6].

Here we study in detail the case of a naturally occurring bilateral macular dystrophy (BMD) in a rhesus macaque (*Macaca mulatta*). The visual field loss in this animal was first detected during functional magnetic resonance (fMRI) experiments designed to map its visual cortex. Results from these experiments demonstrated a central loss of visually driven area V1 activity, which corresponded in extent to the expected retinotopic projection of the retinal lesion. In order to explain the lack of foveal responses and to clarify the underlying pathophysiology, we carried out a detailed in vivo characterization of the structural and functional aspects of this condition using state-of-the-art clinical diagnostic protocols including fMRI, Spectralis® HRA + OCT imaging, fluorescence and indocyanine green angiography and Ganzfeld and multifocal ERG. To the best of our knowledge, this is the first presentation of such an unusual macular lesion and its extensive in vivo characterization in a primate.

Methods

Ethics statement

Animals were treated in accordance with the recommendations of the Weatherall report (http://www.mrc.ac.uk/Utilities/Documentrecord/index.htm?d=MRC0

03440), and all experiments were conducted with great care to ensure the well-being of the animals. Specifically, group housing was maintained to increase quality of life by social interaction and stimulation for play. Animals were kept in large cages that allow swinging and jumping, and equipment or toys were changed frequently. To ameliorate suffering, high-quality anesthesia procedures were used during experimentation (described in detail below). All procedures involving animals were performed with the approval of the Regierungspraesidium Tuebingen (Trial No. KY 2/06) and in full compliance with the guidelines of the local authorities and the European Community (EUVD 86/609/EEC) for the care and use of laboratory animals.

Animals

A detailed ophthalmological examination of a rhesus macaque (*Macaca mulatta*, male, aged 6 years) with bilateral macular dystrophy (BMD) was performed, including a 1-year follow-up. At baseline, three healthy macaques (two males, aged 9 years; and a female, aged 6 years) served as control (CTRL). FMRI experiments were performed on one male, one female and the BML animal, and retinal imaging (OCT) and electrophysiological recordings were performed on one male and the BML animal. All animals were treated in accordance with the recommendations of the Weatherall report.

Preparation

First, blood samples were taken from both animals for toxicological and genetic analysis. Then, experiments were performed under general anesthesia described in detail elsewhere [7]. Briefly, the animals were premedicated with glycopyrolate (0.01 mg/kg, intramuscular) and ketamine (15 mg/kg, intramuscular), and then deep anesthesia was induced by fentanyl (3 µg/kg), thiopental (5 mg/kg) and succinyl chloride (3 mg/kg). Anesthesia was maintained with remifentanil (0.5–2 µg/kg/min) and mivacurium chloride (3–6 mg/kg/h) to ensure the suppression of eye movements. Heart rate and blood oxygen saturation were monitored continuously with a pulse-oxymeter. Prone position was maintained, and the head was fixed via stereotax. Wire specula were used for lid retraction. Pupillary mydriasis was produced by

tropicamide eye drops (Mydriaticum Stulln©, Pharma Stulln, Germany). During examinations the cornea was kept well hydrated to provide clear optical media.

Intraocular pressure (IOP) was measured four times on each eye using a Tono-Pen (Tono-Pen® XL Applanation Tonometer, Reichert Technologies, Depew, NY, USA) and averaged.

Functional MRI

FMRI experiments were performed on a 4.7T vertical scanner (Bruker Biospec, Bruker Biospin GmbH, Ettlingen, Germany) equipped with 48 mT/m gradients. Typically, 17 axial slices were acquired with an eight-segment gradient-echo EPI with field of view (FOV) 128×128 mm^2, matrix 128×128, slice thickness 2 mm, flip angle (FA) 40°, echo time (TE) 20 ms and repetition time (TR) 750 ms. For anatomical measurements we used FLASH with the same FOV 128×128 mm^2, matrix 256×256, slice thickness 2 mm, FA 70° and TE 10 ms. A high-resolution 3D-MDEFT anatomical image with an isotropic resolution of 0.5 mm was acquired during a separate session and was used for co-registration with the FLASH and EPI images. For more details on the fMRI methods see [7, 8]. Visual stimulation was delivered monocularly to the left eye by using a custom in-house–made system that projected the images to MRI-compatible goggles through a fiberoptic guide with resolution 640×480 pixels. The horizontal field of view was 30° and the vertical 23. The stimuli consisted of bar apertures (2° thickness) moving by 1° per volume acquisition (6 s) over a flickering polar checkerboard in four different directions (down, right, up and left). Each fMRI scan included 2 repetitions of the stimuli, and we acquired 5–7 scans for each session. Data were analyzed by using the voxel-based population receptive field (pRF) analysis method described by Dumoulin et al. [9]. The activity of each voxel was fit by using a two-dimensional Gaussian function with three parameters (the visual field spatial coordinates x, y reflecting the center of the pRF and a standard deviation reflecting the pRF size). The gray–white matter boundary was segmented using the high-resolution 3D-MDEFT anatomical images, and 3D cortical surface and flat mesh models were created [10]. Functional activation maps of the explained variance were thresholded at 0.15 and were overlaid on the 3D and flat meshes. Activation maps were also

calculated using other threshold values (not shown) without significant changes to the map and the border of the lesion projection zone (LPZ), demonstrating that activity is changing sharply across the border. The expected cortical representation of the retinal lesion was calculated from Tootell et al.'s [11] retinotopic organization maps of V1 obtained via the ^{14}c-2-deoxy-D-glucose staining technique, and from electrophysiological cortical magnification measurements M_1 $(r) = 13r^{-1.22}$ [12], or M_2 $(r) = 15.7$ $(r + 1.62)^{-1}$ [13], where r is the eccentricity from the center of the visual field, and M is the magnification factor in millimeter per degree. Then, the radius D from the fovea of the representation of the central part of the visual field in area V1 from eccentricity $1°$ to eccentricity E can be calculated by integrating the magnification factor equation. Cortical distance from $0°$ to $1°$ eccentricity was estimated using D_f $(r) = 7 \ln(r + 0.33)$ [14].

Retinal imaging

High-resolution spectral domain OCT (SD-OCT) imaging was done in the same session as ERG recordings as previously described [15–17] using the commercially available Spectralis® HRA + OCT device from Heidelberg Engineering. For acquisition of scans, a mean of 16 images was calculated with automated alignment of iterative recordings using the Automated Real Time mode, thereby increasing the signal-to-noise ratio by a factor of four [18]. For quantification of retinal dimensions, we used the proprietary software package version 3.1 from Heidelberg Engineering according to the instructions by the manufacturer. Briefly, the "measure distance tool" was used to quantify the horizontal extent of the lesion between the foveola and the "hard border" (i.e., where the retinal thickness stopped to be minimal) as well as the "soft border" (i.e., where the retinal thickness reaches normal thickness). For quantification of retinal thickness, we used the automatic layer segmentation of the software that identifies the inner- and outermost border of the retina (inner limiting membrane to retinal pigment epithelium) and analyzed the retinal thickness in horizontal cross sections centered on the foveola at 16 equidistant loci (every 500 μm) along the length of the scan. Because the built-in software from Heidelberg Engineering did not reliably detect the boundaries of the retinal segments, the manual override function was used to manually correct the layer

segmentation algorithm on every single B-Scan. For *en face* retinal imaging and angiography, we used the Argon laser in the short wavelength range (488 nm with 500 nm barrier filter) for fundus autofluorescence (FAF) imaging and fluorescein angiography (FA) and the longer wavelength diode laser at 785 nm (barrier filter at 800 nm) for indocyanine green angiography (ICGA). Resulting data were exported as 8 bit color bitmap files and processed in Adobe Photoshop CS3 (Adobe Systems, San Jose, CA).

Electroretinography (ERG)

After anesthesia was induced and stable eye position was achieved, Ganzfeld-ERGs were recorded with a Mini-Ganzfeld-system (Roland Consult GmbH, Brandenburg, Germany). The dark-adapted (30-min adaptation) ERG protocol consisted of a stimulus intensity series (seven intensities ranging from 0.0095 to 9.5 cd * s/m^2 in 0.5 log unit steps) including the rod (0.01 cd * s/m^2), standard flash (3 cd * s/m^2) used also for evaluation of the oscillatory potentials and a high-intensity flash (10 cd * s/m^2). After 10 min of light adaptation (background light, 30 cd/m^2), photopic single flash and 30-Hz flicker responses were recorded with a stimulation intensity of 3 cd * s/m^2. All responses were amplified and band-pass filtered between 0.2 and 300 Hz. Oscillatory potentials were extracted by band-pass filtering the scotopic responses to a 3 cd * s/m^2 flash between 100 and 300 Hz. All responses were analyzed by means of a- and b-wave amplitude and implicit time. Since a set of normal values was not available, we calculated a BMD/CTRL ratio for response amplitudes at each step for further investigation of the proportional changes.

Multifocal ERGs were recorded under photopic conditions using a modified device of a HRA2 infrared fundus camera (Heidelberg Engineering, Germany) in combination with a Roland Consult multifocal ERG-system. This system allows visualization of the fundus while simultaneously stimulating the central $30°$ retinal area. Since the animals were anesthetized and artifacts (eye movements and blinking) could be avoided, a direct fundus-controlled recording and precise stimulus positioning was possible throughout the whole measurement. Furthermore, the HRA2 device also provides a correction of spherical refractive errors from -12 to $+30$ diopters without change of magnification. Although cylindrical refractive

errors were not ascertained, a sharp image of the retina could be achieved. The stimulus, presented with a built-in small black and white CRT monitor, consisted of 61 hexagonal scaled segments centered in the fovea and extending over the optic disk. Scaled stimulus pattern was chosen on the basis of high similarities of the retinal architecture to human and correct positioning of the stimulus pattern during recordings. The eccentricity of the concentric rings from the center was estimated on the basis of the 30° retinal image and stimulus pattern (i.e., from the fovea to the middle of a representative hexagon in each ring): 2°, 5°, 10° and 15° for rings 2–5, respectively. For test–retest reliability, multifocal ERGs were recorded three times on each eye, every run consisted of 8 cycles. Responses to flash stimuli were amplified and band-pass filtered between 5 and 100 Hz and recorded. An average of the responses was calculated and analyzed according to N1-P1 amplitudes and P1 implicit times of ring averages of the waveforms. Ganzfeld and multifocal ERGs were recorded using ERG-Jet contact lens electrodes (Roland Consult GmbH, Brandenburg, Germany) which were applied to the cornea with 2 % Methocel (hydroxypropyl methylcellulose, OmniVision GmbH, Germany). Despite the contact lens electrodes, a sharp image of the retina could be achieved. Both eyes were tested separately, and the ERG-Jet electrode of the contralateral (covered) eye was used as reference. Ground needle electrodes were placed under the skin of the glabella. Ganzfeld and multifocal ERG protocols were based on the ISCEV Standards [19] and were completed before fundus photography and angiography.

Histology

The animals were tranquilized with ketamine and killed with an overdose of pentobarbital (60–80 mg/kg i.v.). They were immediately perfused transcardially with 0.9 % saline, and the eyes were quickly removed prior to the perfusion with fixative. The eyes were cut open and immersion-fixed in 4 % paraformaldehyde in 0.1 M phosphate buffer (PB, pH 7.4) for 20 min at room temperature. All procedures were approved by the local animal care committee and were in accordance with the law for animal experiments issued by the German government (Tierschutzgesetz).

Following fixation, eyecups were stored in PB with 0.02 % sodium azide. A retinal piece of 3×3 mm

from the optic nerve head to the fovea was dissected from the affected eyecup and from a control eyecup, cryoprotected in graded sucrose solutions (10, 20 and 30 % in PB) and sectioned vertically (12–18 μm) with a cryostat. Immunocytochemical labeling was performed using the indirect fluorescence method. Sections were incubated overnight with primary antibodies in 3 % normal donkey serum (NDS), 1 % bovine serum albumin (BSA) and 0.5 % Triton X-100. After washing in PB, secondary antibodies were applied for 1 h. These were conjugated to either Cy3 (Dianova) or Alexa TM 488 (Invitrogen).

A rabbit polyclonal antibody against the C-terminal binding protein 2 (CtBP2, 1:5,000; Synaptic Systems, Göttingen, Germany) was used to label synaptic ribbons within the outer and inner plexiform layer, and to label photoreceptor nuclei in outer nuclear layer. ON bipolar cells were labeled with a polyclonal antibody directed against Gγ13 that was raised in rabbit (1:1,000; kind gift from Dr. R. F. Margolskee, Mount Sinai School of Medicine, New York). Glycinergic amacrine cells were labeled with a polyclonal antibody directed against the glycine transporter 1, raised in goat (1:500; Chemicon, Temecula, CA). Horizontal cells were labeled with a monoclonal mouse antibody against parvalbumin (1:10,000; Swant, Bellinzona, Switzerland).

Results

Blood chemical analysis (including blood cell count, liver, kidney, pancreas function and basic metabolic panel) of the affected animal revealed no pathological changes, a standard neurological assessment was within normal limits except for the central scotoma, and no abnormalities were noted on a high-resolution anatomical MRI study. There was no evidence for toxic effects in the animal's history. IOP measurements were carried out in both animals, showing IOP levels around the lower limit of normal values ($IOP_{BMD} = 8.5 \pm 1$ mmHg, $IOP_{CTRL} = 12.5 \pm 1.9$ mmHg).

Functional MRI

FMRI visual activation maps were measured under photopic conditions using the pRF method [9] in the left eye of the BMD animal and two controls. A comparison between the BMD animal and one of the
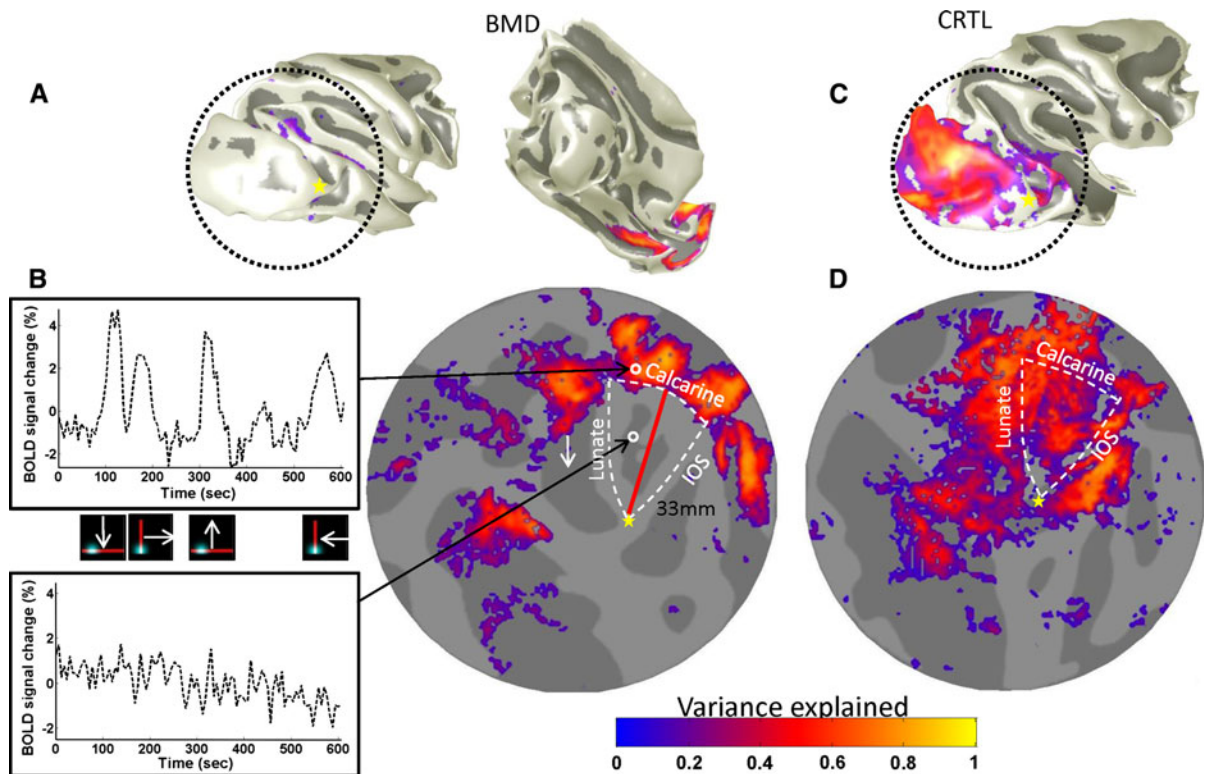
Fig. 1 Blood-oxygen-level dependence (BOLD) responses of the *BMD* and the control (CTRL) monkey. **a** Reconstructed surface representing the border of the gray and white matter of the right hemisphere of the BMD monkey with the fraction of the explained variance map overlaid thresholded at 0.15 (see "Methods"). The map was measured using a moving bar stimulus presented to the left eye of the *BMD* animal. The right eye was closed. **b** Unfolded flat map of the early visual cortex displayed in A (see "Methods"). The operculum of the monkey is outlined by the calcarine, the lunate and the inferior occipital sulcus. The two *insets* are the BOLD responses of two voxels

selected in the nondeafferented V1 and deafferented V1 of *BMD*, respectively. The cortical distance between fovea (*yellow star*) and lesion projection zone border in V1 is 33 mm for *BMD*, which agrees well with the estimated cortical distances (33 mm [11], 33.2 mm [12, 14] and 33.1 mm [13, 14]) from fovea to 10° eccentricity (the approximate radius of retinal involvement in the *BMD* subject). **c**, **d** Maps corresponding to **a**, **b**, respectively, derived from a control monkey are displayed here for comparison. The same methods, including explained variance threshold, were used. *BMD* bilateral macular dystrophy

controls is presented in Fig. 1a–d. The second control showed very similar results as the first one (not shown). The cortical surface representing the central portion of the visual field was devoid of significant visual modulation in the BMD animal. In contrast, the control animals demonstrated robust activation within the corresponding V1 area. The distance from the cortical representation of the fovea to the border where visually driven activity was first visible in area V1 was 33 mm in the BMD animal. For the control animals, the cortical distances in V1 from fovea to the approximate extent of the retinal scotoma of the BMD animal—10° of eccentricity—were measured as 33 and 32 mm. This agrees well with the estimated cortical distance that would subtend 0–10° of

eccentricity in area V1 of macaque monkeys, as determined using cortical magnification measurements from the electrophysiology literature (see "Methods").

Angiography

Prior to fluorescence angiography, we recorded fundus autofluorescence (FAF) in the control and BMD animal (supplemental Figure 1). While FAF signal in the control animal was slightly stronger, there was no distinct pattern such as a bull's-eye formation or any form of hyperfluorescence in the BMD animal. Fluorescence angiography (Fig. 2a) in the control animal displayed a regular foveal avascular zone
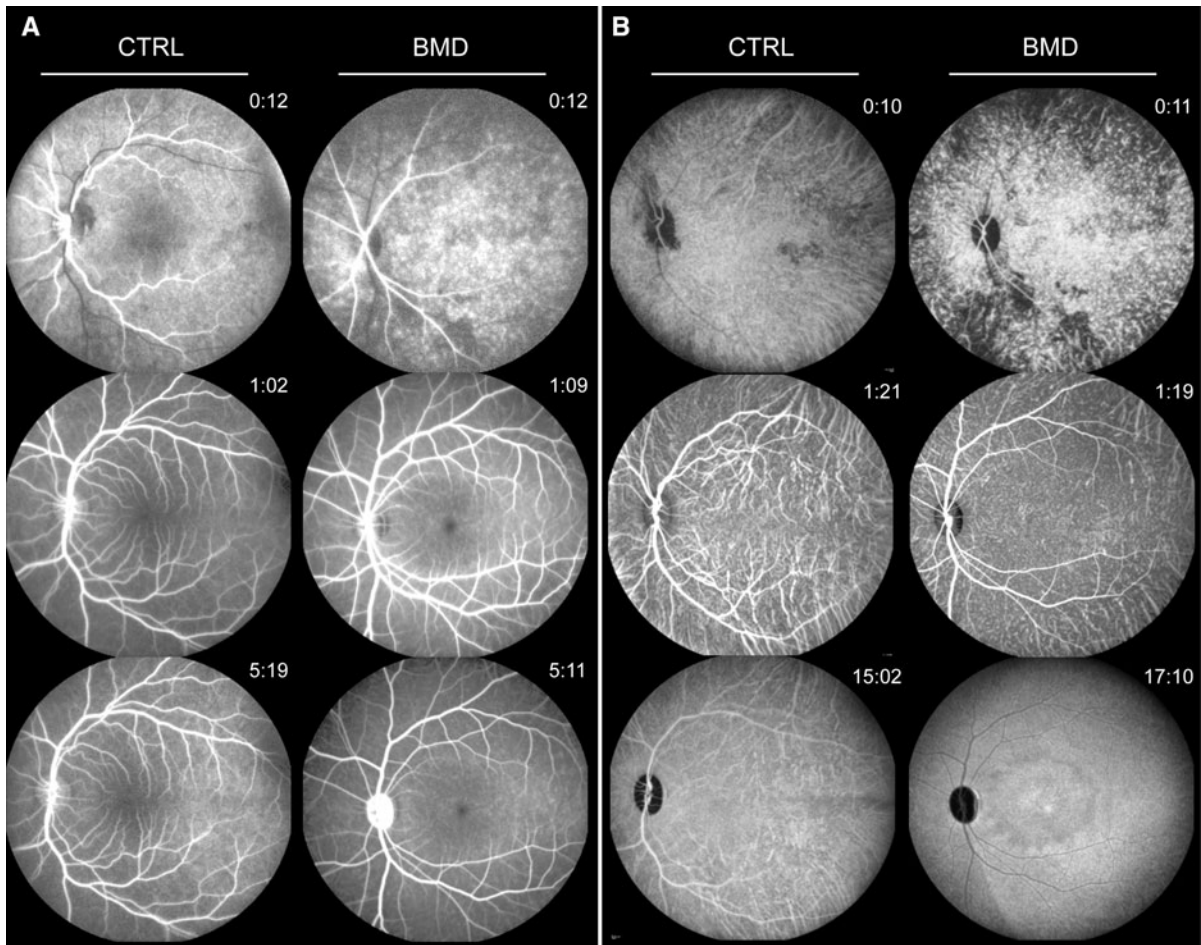
Fig. 2 Retinal angiography of CTRL and BMD monkey. Sequential recordings during fluorescein (**a**) and indocyanine green (**b**) angiography demonstrate regular timing and distribution in the CTRL animal (*left panels*), while the BMD animal (*right panels*) shows a spotty filling pattern in the early phases (*top*), an enlarged foveal avascular zone (FAZ) at the posterior pole (*middle*) and a distinct pattern of hypo- and hyperfluorescence in the central retinal region at later stages (*bottom*)

(FAZ) of 0.62 mm diameter and area of 0.32 mm^2 [20]. Likewise, systemic perfusion parameters (arm-retina time, $ART_{CTRL} = 12.4$ s) and retinal blood flow (arteriovenous passage time, $AVP_{CTRL} = 2.3$ s) in the control animal were compared well to those in healthy human subjects [21]. While perfusion characteristics were similar in the affected animal ($ART_{BMD} = 11.9$ s, $AVP_{BMD} = 2.3$ s), the diameter of the FAZ was dramatically increased to 3.73 mm diameter (8.85 mm^2 area) at baseline without signs of progression at the 1-year follow-up. Background fluorescence stemming from the choriocapillary network showed an equal distribution over the posterior pole in the control animal, while displaying a highly irregular pattern in the early phase and a central hypofluorescent area at later stages of perfusion in the affected animal. This was even more pronounced in the indocyanine green angiography (Fig. 2b), where late-phase recordings showed a concentric pattern of hyper- and hypofluorescent rings also found in some forms of macular dystrophies in humans [22].

Spectral domain optical coherence tomography

Interpolated retinal thickness profiles calculated from volume scans with 97 B-Scans at 30-μm intervals (Fig. 3) centered on the fovea revealed a total retinal thickness $TRT_{CTRL} = 303 \pm 45$ μm in the healthy
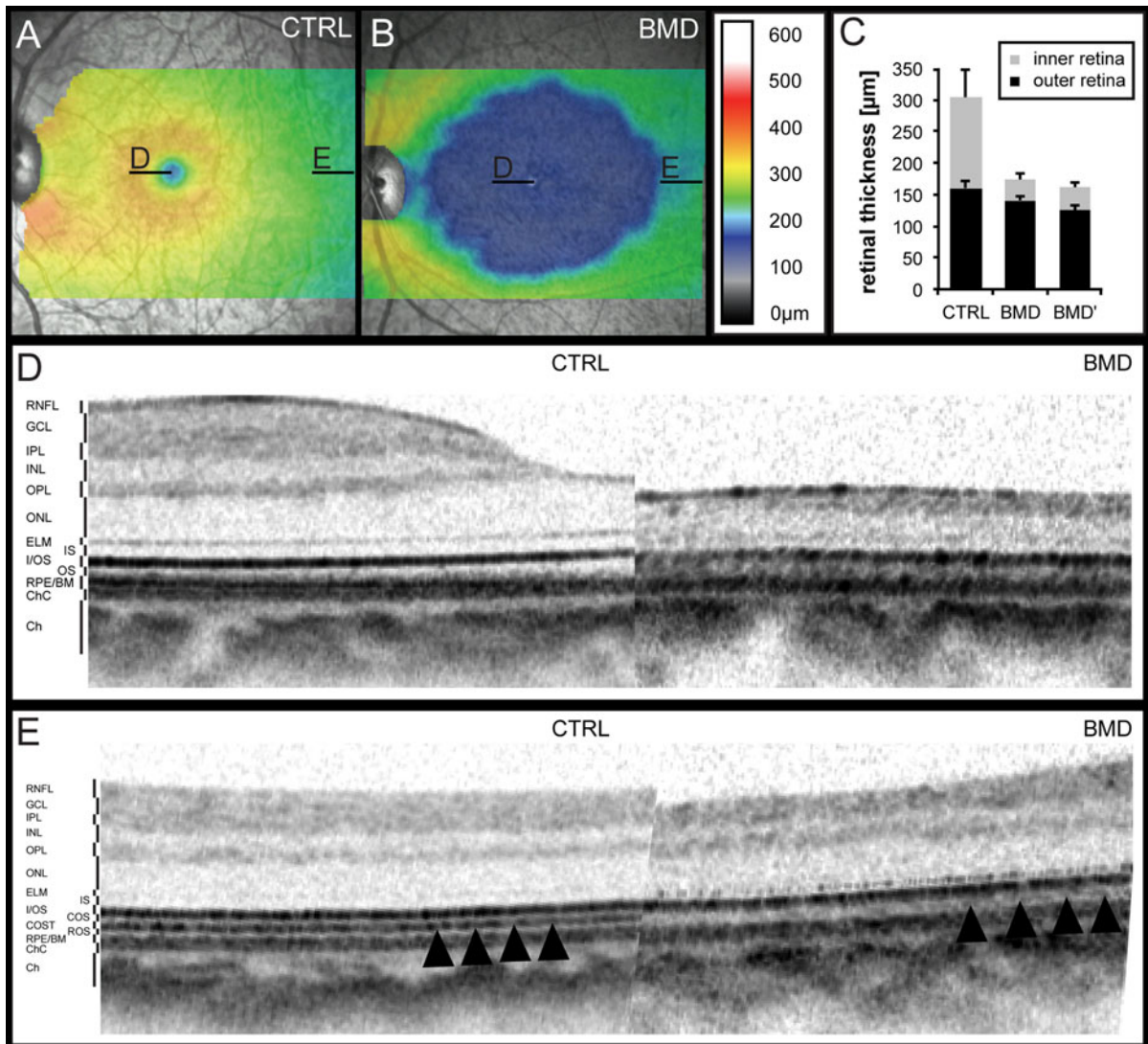
Fig. 3 Optical coherence tomography of the macular region in the CTRL and BMD monkeys. Interpolated retinal thickness profile maps centered on the fovea demonstrate the severe macular dystrophy in the BMD (**b**) compared to the CTRL (**a**) animal. Total retinal thickness is markedly reduced in BMD, with the inner retinal layers much more affected than outer retinal layers with little change at follow-up (**c**). The foveal region (**d**) in the CTRL animal (*left side*) shows the normal slope from the foveal rim toward the foveal pit. In contrast, retinal nerve fiber, ganglion cell, inner plexiform and inner nuclear layers are essentially missing in the BMD animal (*right side*), and consequently, there is no foveal rim formation. Moreover, the outer retinal signal composition features a disorganization of the inner/outer segment border (I/OS) signal in the cone-only fovea. Interestingly, while more temporal aspects of the posterior pole **e** show a second highly reflective band that is thought to correspond to the cone outer segment tips (COST, *arrowheads*) in the CTRL monkey (*left side*), the same signal only starts to appear in the BMD animal toward the periphery beyond the dystrophic center (*bottom right, arrowheads*)

control animal and TRT$_{BMD}$ = 174 ± 9 μm in the affected rhesus macaque (normal value mean = 304 μm (range 282–326 μm) as reported by Anger et al. [23]). Three-dimensional reconstruction of the retinal scans showed a near perfect rotational symmetry of the dramatic loss of central retinal tissue in BMD and the associated temporal optic atrophy (Figs. 3, 4). Horizontal radius of the atrophic area with minimal retinal thickness (center to "hard border") was 2.47 mm/2.47 mm for the right eye (baseline/
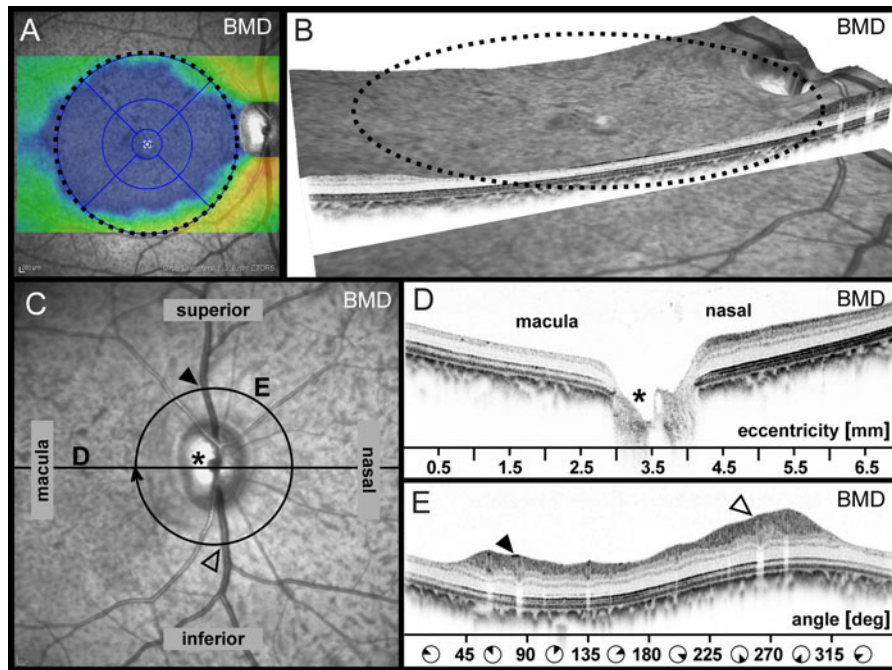
Fig. 4 The retinal thickness profile map of the right eye (**a**) and a three-dimensional reconstruction (**b**) of the retinal scans show a near perfect rotational symmetry of the dramatic loss of central retinal tissue in BMD. The horizontal cross section **d** through the optic nerve head demonstrates the dystrophic macular area with corresponding temporal optic atrophy (*asterisk*). The peripapillary ring scan **e** centered on the optic nerve head ($r = 3.4$ mm) demonstrates relatively abrupt thinning of inner retinal layers central of the vascular arcades (ca. 0–45° and 315–360°), indicating a loss primarily of the papillomacular bundle (**e**). The full and empty *arrow heads* point to the superior and inferior retinal veins correspondingly, for orientation. *Grid* in **a** indicates circular areas of 0.8, 2.4 and 4.8 mm diameter. *Dotted lines* in **a** and **b** indicate 4.8 mm eccentricity

follow-up) and 2.21 mm/2.25 mm for the left eye. The retinal lesion therefore is predicted to result in a scotoma with 10.65°/10.63° (baseline/follow-up) eccentricity for the right eye and 9.53°/9.67° for the left eye. These data correspond very well with our fMRI data on the dimensions of the recorded cortical scotoma (10°) in the left eye of the BMD animal (see above and Fig. 1).

Segmentation analysis of retinal B-scans at either the foveal center (Fig. 3d) or the temporal aspect of the posterior pole (Fig. 3e) revealed severe atrophy of inner retinal layers (inner retinal thickness, $IRT_{CTRL} = 143 \pm 45$ µm vs. $IRT_{BMD} = 33 \pm 9$ µm, Fig. 3c; normal value mean = 159 µm (range 99–209 µm) as reported by Anger et al. [23]). While the retinal nerve fiber, ganglion cell, inner plexiform and inner nuclear layers were essentially missing in the atrophic area of BMD, the dimensions of outer retina layers were surprisingly well preserved. However, detailed analysis demonstrated a disorganization of the inner/outer segment border (I/OS) signal in the cone-only fovea (Fig. 3d),

a structural aspect known to reflect photoreceptor dysfunction [24], and increased reflectivity in the otherwise hyporeflective outer segment layer. Interestingly, at the transition zone from BMD to more temporal aspects of the posterior pole, a second highly reflective band starts to emerge that is thought to arise from the cone outer segment tips (COST) (Fig. 3e). This suggests structural disintegration at the photoreceptor level in the central macula with gross inner retinal atrophy, while normal layering of the inner and outer retina can be observed peripheral of the transition zone. Conversely, the I/OS signal was equally strong throughout the posterior pole of the control animal with evidence of elongated outer segments in the central foveal region and easily detectable COST signal in the extrafoveal regions.

Horizontal B-scans through the optic nerve head (Fig. 4d) clearly showed the differences between temporal and nasal retinal morphology that underscored the site-specific pathology in BMD. Peripapillary ring scans centered on the optic nerve head
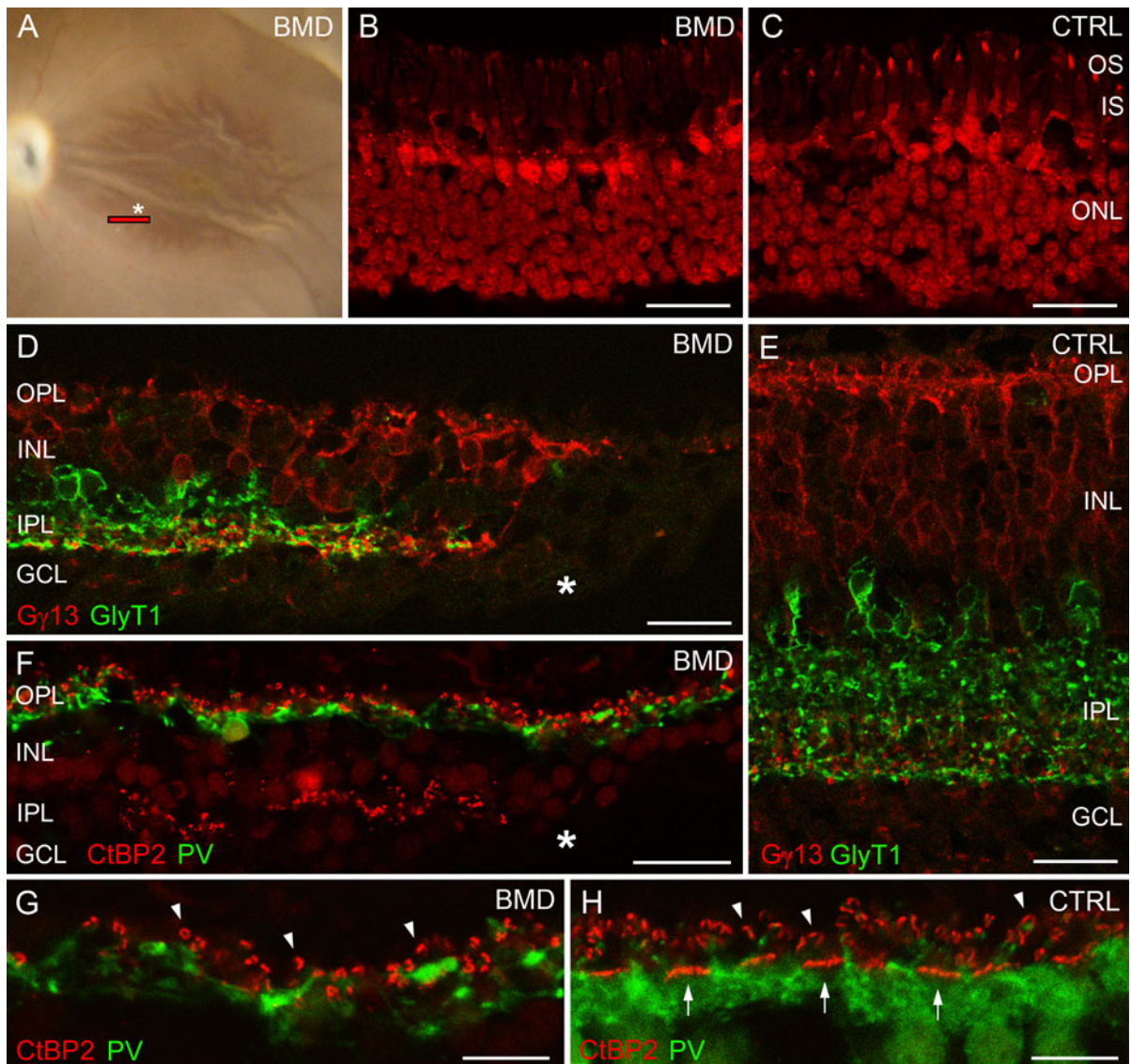
Fig. 5 Gross anatomy **a** demonstrates the atrophic aspect of the macula. Note the modest amount of *yellow* pigment appearing as macula lutea in the fovea. Note also the temporal atrophy of the optic nerve head. The *red bar* at the nasal-inferior border of the dystrophic area indicates the location from which the histological sections were taken. Labeling with CtBP2 (ribbon synapses and somata) demonstrates relatively well-preserved outer nuclear layer in the retinal region affected by MD (**b**) versus in the outer (unaffected) retina (**c**, CTRL). Staining with Gγ13 (ON bipolar cells) and GlyT1 (glycinergic amacrine cells) in the BMD **d** shows dramatic loss of inner nuclear layer neurons compared to CTRL retina (**e**) in the central atrophic areas (*asterisks*). This is also evident from parvalbumin (*horizontal* cell) and CtBP2 (ribbon synapses and somata) labeling in BMD (**f–g**) versus CTRL (**h**) sections. In the OPL of the CTRL retina, CtBP2-labeled ribbons appear as clusters of bands (*arrows*) in cone pedicles and as horseshoe-shaped structures (*arrowheads*) in rod terminals (**h**). The missing bands in the BMD OPL (**g**) indicate that cone synapses are more strongly affected than rod synapses in the BMD animal. *Scale bars* are 25 μm (**b–f**) and 10 μm (**g–h**)

(Fig. 4e) also demonstrated relatively abrupt thinning of inner retinal layers central of the vascular arcades (ca. 0–45° and 315–360°), indicating a loss primarily of the papillomacular bundle.

At follow-up after 1 year, the dimensions of the atrophic area remained essentially identical regarding the inner retinal thickness (IRT$_{baseline}$ = 33 ± 9 μm vs. IRT$_{follow-up}$ = 36 ± 9 μm), while the outer retinal

thickness showed some degree of further reduction (ORT$_{baseline}$ = 141 ± 7 μm vs. ORT$_{follow-up}$ = 125 ± 8 μm), possibly indicating a degree of continuous neurodegeneration within the original region of macular involvement.

Histology

Histologic data highlight the dramatic loss of inner retinal components such as bipolar, amacrine and horizontal cells within the affected region in the BMD animal compared to CTRL (Fig. 5) and thereby support findings in vivo. Besides structural loss of inner retinal neurons, immunohistochemical labeling shows significant loss of cone ribbon synapses within the affected area.

Electrophysiology

Dark-adapted (scotopic) Ganzfeld-ERGs revealed similar response amplitudes to brief, low-intensity flashes for the BMD and the control animals (for the 0.01 cd * s/m^2 flash 189 and 205 μV, respectively; BMD/CTRL ratio 0.92). With increasing flash intensities, the response amplitude in BMD increased less than in the control so that at the highest stimulus intensity the amplitude was significantly smaller in the BMD animal than in the control (237 and 343 μV for the 10 cd * s/m^2 stimulus, respectively; BMD/CTRL ratio 0.69). These proportional changes of response amplitudes indicated a reduced cone system contribution, since cones are known to contribute significantly to the response waveforms of bright flashes under scotopic conditions. Response implicit times of the a- and b-wave were similar in the BMD and the control animal for all flash intensities, suggesting that the surviving photoreceptors provide physiologic or near physiologic signal processing (Fig. 6).

The b/a-wave amplitude ratios of the standard flash responses were calculated to reveal differences in the contribution of the inner retina to the response waveforms, since a selective reduction in the b-wave amplitude would suggest a dysfunction of transmission
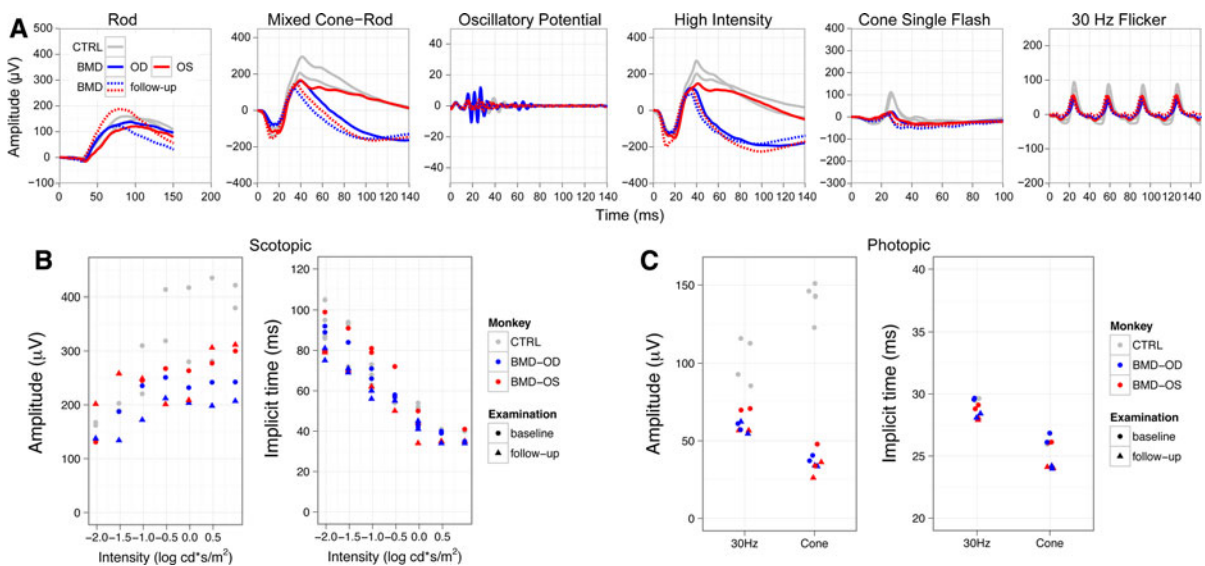
Fig. 6 Ganzfeld-ERG responses according to the ISCEV Standards in the CTRL (gray curves) and the BMD animals at baseline (blue and red lines represent the right (OD) and left eye (OS) of the BMD animal, respectively). a, panels 1–4 Scotopic recordings show a well-preserved rod photoreceptor response in the BMD retinae (panel 1, rod response). The reduction in a-wave and b-wave amplitudes at brighter stimuli (panels 2 and 4, mixed rod-cone and high-intensity responses, respectively) under scotopic conditions suggests a reduction in the total number of functioning cone photoreceptors and bipolar cells in the BMD versus the CTRL retinas, while normal implicit times suggest unchanged signal transduction characteristics for the remaining cone photoreceptors and proximal neurons (b). This pattern becomes even more evident in photopic conditions (a, panels 5–6, cone single flash and 30-Hz flicker responses, respectively) where responses of the cone photoreceptor system and its downstream signaling pathway are clearly reduced in BMD compared to CTRL (c). At 1-year follow-up (broken blue and red lines and triangles), Ganzfeld-ERG results remain essentially unchanged. ERG electrophysiology, ISCEV international society for clinical electrophysiology of vision

in the inner retina, either in the photoreceptor synapses or in the postreceptoral pathway. The constellation, where the b/a ratio is equal to or smaller than 1, is termed a negative ERG. However, both the BMD and control animal results showed similar response amplitudes and waveforms as well as b/a ratios greater unity (b/a ratio_{BMD} = 2.0, b/a ratio_{CTRL} = 2.2) on the baseline and follow-up measurements as well (b/a ratio_{BMD} = 1.9 at follow-up).

The photopic responses obtained after light adaptation showed even more reduced amplitudes in BMD compared to the control (45 and 147 μV for the 3 cd * s/m^2 photopic flash, respectively; BMD/CTRL ratio, 0.3). Implicit times again were similar for both; 30-Hz flicker responses revealed a lower magnitude, but similar phase. Even though the retinal area contributing to the photopic waveforms was obviously reduced in the BMD animal, the timing of the responses was essentially normal, suggesting again that the remaining cone system's physiological function was intact.

At follow-up after 1 year, the Ganzfeld-ERG responses obtained under scotopic and photopic adaptation were similar in amplitude, implicit time and b/a ratios, again consistent with a disease restricted to the macular area.

The multifocal ERG demonstrated reduced amplitudes at all eccentricities (ring 1–5), more pronounced in the central segment and the two adjacent rings (rings 1–3) covering a field of ca. 20° in diameter (Fig. 7). This area covered almost exactly the atrophic and largely avascular area observed in angiography and OCT imaging (Figs. 2, 3, 4). At 1-year follow-up, a similar reduction in response amplitude in the central hexagon was noticed. Implicit times at follow-up showed a prolongation, notably in rings 2–4. While small changes in amplitude may be within normal repeat variability and central variability may be attributed to worse signal-to-noise ratio, the combination with elongated implicit times could explain the slight progression (i.e., limited further reduction in the outer retinal thickness seen in the cross-sectional imaging in Fig. 3c) of the affected macular area. However, these changes in implicit time may also be within normal limits.

Discussion

Many commonly used animal models such as mice and rats lack a central retinal region with higher optical resolution due to the increased cone photoreceptor, bipolar and ganglion cell density and rarefication of retinal vasculature to further reduce optical aberration. In contrast, rhesus macaque retinal architecture shows excellent correspondence to human retinal structure, and therefore, the macaque model would be ideal for studying inherited macular degeneration [20]. Unfortunately, there is only little information in the literature regarding naturally occurring macular degeneration in nonhuman primates.

When one particular animal from our colony of rhesus macaque monkeys showed no central visual modulation in fMRI experiments (Fig. 1) combined with altered bilateral macular reflexes at the posterior pole on direct ophthalmoscopy, it underwent a thorough ophthalmologic evaluation to potentially identify an primate model of macular degeneration. Imaging data suggested normal perfusion in the periphery regarding both retinal (FA) and choroidal (ICGA) vasculature (Fig. 2). In contrast, the macula showed a drastically enlarged FAZ covering a circular area of approximately 10° in radius centered at the posterior retinal pole. Within this well-circumscribed area, the retina appeared notably thinner in comparison with the control animal. Furthermore, SD-OCT images demonstrated a disorganization of the inner/outer segment border (I/OS) signal and a severe atrophy of inner retinal layers, indicating structural changes at the level of photoreceptors and loss of more proximal neurons. This observation was supported by immunohistochemical data in retinal sections from BMD vs. CTRL animals (Fig. 5). These demonstrated a dramatic loss of bipolar, amacrine and horizontal cells in the inner nuclear layer, while the outer nuclear layer seemed relatively intact. Interestingly, cone ribbon synapses in the outer plexiform layer were much more strongly affected than rod ribbon synapses, which is in line with the reduced responses seen under photopic conditions.

SD-OCT cross sections at the edge of the dystrophic macula showed increasing signal strength in a highly reflective band thought to indicate the cone photoreceptor outer segment tips (COST), suggesting that cone density returns gradually to normal outside the affected region (Fig. 3d), where the electrophysiological responses in mfERG analysis also begin to approach control levels (Fig. 7).

The retina of a healthy macaque contains an average of 3 million cones and 61 million rods, and
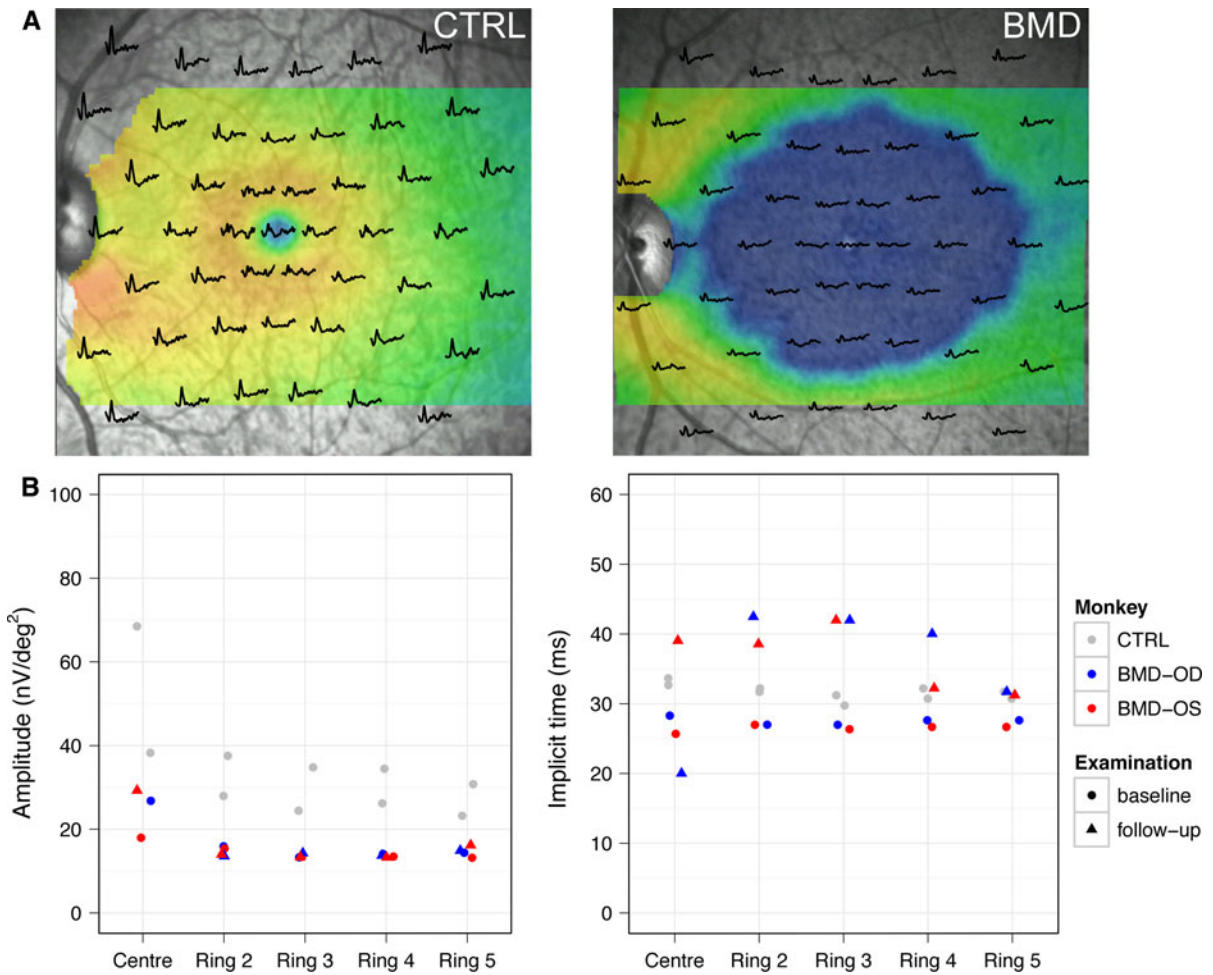
Fig. 7 MfERG response arrays of the CTRL and the BMD retinae overlaid on retinal thickness maps reveal the correlation between functional and morphological changes in the BMD animal (**a**). Ring analysis of the mfERGs **b** shows the amplitudes (*left side*) and implicit times (*right side*) for each ring in BMD and CTRL (*gray dots* show CTRL results, and *blue* and *red dots* and *triangles* represent BMD responses at baseline and at follow-up, respectively). The analysis clearly shows a reduction in amplitudes, more pronounced in the central rings. While implicit times were similar at baseline, a delay is found for ring 2–4 at 1-year follow-up. *MfERG* multifocal electroretinography

their density peaks as well as their distribution pattern correspond well with human retinal architecture [6]. Rod density is particularly high in a 15° annulus around the fovea beginning 2–3 mm from the rod-free foveola and extending to 6–8 mm toward the periphery. Cone density, on the other hand, is highest in the foveola and first decreases exponentially in the first 2 mm eccentricity followed by an almost linear peripheral decline.

Based on these anatomical properties, the observed macular disease with a dystrophic area of ca. 6 mm diameter is predicted to cause a notable reduction in cone function. This is in line with our fMRI data of the left eye in the BMD animal, confirming a central scotoma with retinotopic representation in V1 reflecting the central ca. 10° (Fig. 1). Likewise, our Ganzfeld-ERG recordings show that the cone photoreceptor system and its downstream signaling pathway are clearly affected (Fig. 6). More specifically, the reduction in a-wave and b-wave amplitudes at brighter stimuli under scotopic conditions, and the even more decreased cone responses under photopic conditions suggest the reduction in the total number of functional cone photoreceptors and bipolar cells, respectively, while the normal implicit time suggests unchanged signal transduction characteristics for the remaining

cone photoreceptors and proximal neurons in the more peripheral regions. Furthermore, multifocal ERG demonstrated reduced amplitudes more pronounced in the central three rings proving a good structure–function correlation as the bilateral macular dystrophy was limited to a central area of ca. 3 mm radius (Fig. 7). On a structural level, it is surprising to see the inner retinal layers being so selectively affected. However, while outer retinal thickness did not differ to the same amount between the affected and control animals, qualitative changes could be observed on close examination (Fig. 3). There is a clear disturbance of the highly reflective layer at the border between the inner and outer segment of photoreceptors in the outer retinal signal composition, which has been linked to photoreceptor dysfunction [24]. Extrafoveal OCT sections also showed specific attenuation of the COST signal in the dystrophic area with gradual recovery at the transitional zone, indicating structural changes at the level of the photoreceptor outer segments, where photons induce the phototransduction cascade ultimately leading to light perception.

Fortune and co-workers reported a disease phenotype in a number of rhesus macaques featuring idiopathic bilateral temporal optic atrophy (IBOA), affecting the papillomacular bundle with histologic evidence of axonal loss and gliosis limited to the temporal optic nerve. Functionally, the RNFL (retinal nerve fiber layer) loss correlated with substantial reduction in mfERG high-frequency components, while mfERG low-frequency components and all Ganzfeld-ERG amplitudes (a-wave, b-wave, oscillatory potentials or PhNR) were normal or even slightly increased [25]. The highly symmetric loss of retinal nerve fiber layer (RNFL) tissue in the papillomacular bundle of the BMD animal with its corresponding temporal atrophy of the optic nerve head compares well to this phenotype (Fig. 4). However, there are a number of striking differences to the pathology reported by Fortune. In contrast to IBOA, where the retinal nerve fiber layer/ganglion cell layer is selectively affected, in our case the inner nuclear layer is also grossly reduced in the area of atrophy, which is reflected functionally by the reduced b-wave amplitudes in the Ganzfeld-ERG (Fig. 6). Similarly, recent publications on tobacco-alcohol-induced toxic optic neuropathy in human also showed symmetric temporal optic disk pallor and RNFL loss in the papillomacular bundle, but no significant macular alterations distal of

the RNFL [26]. As secondary temporal optic atrophy is a known feature in retinal dystrophies that primarily affect the macular region [27, 28], it seems feasible that the morphological changes at the temporal optic nerve head reflect a consequence of the macular dystrophy along with its increased FAZ and rarified choroidal vasculature. However, as the pathology was already evident at the first time point of investigation, we cannot be absolutely certain about a temporal and/or causal relation.

Considering the drastic changes during development of the fovea, developmental abnormalities can be considered as potential etiologic factor for the present phenotype. All adult primate foveae possess a central avascular region known as FAZ, which is a critical requirement for foveal pit formation. Several studies indicate that the absence of FAZ (where vessels overgrow the foveal area) results in a missing foveal pit and reduced visual acuity [29]. In some cases, this foveal hypoplasia was shown to be associated with PAX6 missense mutations, a gene well known to be involved in the morphogenesis of the eye [30]. Interestingly, our case shows rather opposite changes to foveal hypoplasia, that is, a marked enlargement of the FAZ and associated atrophic appearance of the whole macular region and sequencing of the PAX6 gene showed no pathogenic mutation. If the size of the FAZ determines the geometry of the foveal indentation, the observed macular malformation might be secondary to an abnormally expanded FAZ. However, it is currently unclear which factors would be involved at what stage of such a developmental abnormality, since such macular changes have not yet been observed.

On the other hand, secondary enlargement of FAZ is a frequent finding in patients with ischemic retinal diseases such as diabetic or hypertensive retinopathy. Likewise, enlarged FAZ was also reported in patients with retinal vein occlusion or sickle cell retinopathy [31]. However, in these conditions further ischemic symptoms, like microaneurysms, bleeding, cotton-wool spots and neovascularization, are frequently seen. Such changes were not detected in our case, and the highly symmetrical macular morphology also argues against acquired diseases.

At 1-year follow-up, Ganzfeld-ERG results remained essentially unchanged, while multifocal ERGs suggested a slight progression of the disease in the central area, which corresponded with the noted changes of

outer retinal atrophy. However, otherwise there was no evidence for disease progression. Considering all observations, the pathology seen in this animal can be best described as bilateral macular dystrophy (BMD) with atrophy of the temporal optic disk. BMD targets the cone-rich macula, thereby reducing the total number of functional cone photoreceptors. The remaining cones function well (normal implicit time) with a feature that characterizes maculopathies and distinguishes them from cone dystrophies. The first ever fluorescein angiography in such a case of maculopathy in a primate revealed an enlarged FAZ, and indocyanine green angiography additionally demonstrated widespread atrophy of choriocapillary networks underneath the dystrophic macula.

The fMRI data corroborate the link between structure and function by demonstrating a corresponding central scotoma of ca. 10° eccentricity in the primary visual cortex of the affected animal [32]. This is the first extensive structural and functional characterization of a primate with profound macular degeneration exploring its potential as animal model. While the etiology of BMD in this animal has remained elusive, the advances in the field of genetic sequencing promise cost-effective whole-exome sequencing in the near future. Publication of our findings is intended to spur awareness for detecting additional potential cases of primate BMD or related macular dystrophies in other laboratories eventually leading to the identification of *Macaque* models of this disease. Also, the fact that such a dramatic retinal pathology can lead to an inconspicuous behavioral pattern points toward the need for diagnostic screening before including nonhuman primates in preclinical studies, where visual function is critical for outcome measures.

Conflict of Interest   The study sponsors had no role in study design; in the collection, analysis and interpretation of data; in the writing of the report; and in the decision to submit the paper for publication. Furthermore, the authors state that they have full control of all primary data and that they agree to allow interested parties to review their data if requested.

References

1. El-Mofty A, Gouras P, Eisner G, Balazs EA (1978) Macular degeneration in rhesus monkey (*Macaca mulatta*). Exp Eye Res 27(4):499–502
2. Dawson WW, Dawson JC, Lake KP, Gonzalez-Martinez J (2008) Maculas, monkeys, models, AMD and aging. Vision Res 48(3):360–365
3. Saperstein DA (1995) Advances in macular dystrophies. Int Ophthalmol Clin 35(4):19–35
4. Williams RA, Brody BL, Thomas RG, Kaplan RM, Brown SI (1998) The psychosocial impact of macular degeneration. Arch Ophthalmol 116(4):514–520
5. Fletcher EL, Jobling AI, Vessey KA, Luu C, Guymer RH, Baird PN (2011) Animal models of retinal disease. Prog Mol Biol Transl Sci 100:211–286
6. Wikler KC, Williams RW, Rakic P (1990) Photoreceptor mosaic: number and distribution of rods and cones in the rhesus monkey retina. J Comp Neurol 297(4):499–508
7. Logothetis NK, Guggenberger H, Peled S, Pauls J (1999) Functional imaging of the monkey brain. Nat Neurosci 2(6):555–562
8. Keliris GA, Shmuel A, Ku SP, Pfeuffer J, Oeltermann A, Steudel T, Logothetis NK (2007) Robust controlled functional MRI in alert monkeys at high magnetic field: effects of jaw and body movements. Neuroimage 36(3):550–570
9. Dumoulin SO, Wandell BA (2008) Population receptive field estimates in human visual cortex. Neuroimage 39(2):647–660
10. Wandell BA, Chial S, Backus BT (2000) Visualization and measurement of the cortical surface. J Cogn Neurosci 12(5):739–752
11. Tootell RB, Switkes E, Silverman MS, Hamilton SL (1988) Functional anatomy of macaque striate cortex. II. Retinotopic organization. J Neurosci 8(5):1531–1568
12. Van Essen DC, Newsome WT, Maunsell JH (1984) The visual field representation in striate cortex of the macaque monkey: asymmetries, anisotropies, and individual variability. Vision Res 24(5):429–448
13. LeVay S, Connolly M, Houde J, Van Essen DC (1985) The complete pattern of ocular dominance stripes in the striate cortex and visual field of the macaque monkey. J Neurosci 5(2):486–501
14. Dow BM, Vautin RG, Bauer R (1985) The mapping of visual space onto foveal striate cortex in the macaque monkey. J Neurosci 5(4):890–902
15. Fischer MD, Huber G, Beck SC, Tanimoto N, Muehlfriedel R, Fahl E, Grimm C, Wenzel A, Reme CE, van de Pavert SA, Wijnholds J, Pacal M, Bremner R, Seeliger MW (2009) Noninvasive, in vivo assessment of mouse retinal structure using optical coherence tomography. PLoS One 4(10):e7507
16. Huber G, Beck SC, Grimm C, Sahaboglu-Tekgoz A, Paquet-Durand F, Wenzel A, Humphries P, Redmond TM, Seeliger MW, Fischer MD (2009) Spectral domain optical coherence tomography in mouse models of retinal degeneration. Invest Ophthalmol Vis Sci 50(12):5888–5895
17. Huber G, Heynen S, Imsand C, vom Hagen F, Muehlfriedel R, Tanimoto N, Feng Y, Hammes HP, Grimm C, Peichl L,

Seeliger MW, Beck SC (2010) Novel rodent models for macular research. PLoS One 5(10):e13403

18. Helb HM, Charbel Issa P, Fleckenstein M, Schmitz-Valckenberg S, Scholl HP, Meyer CH, Eter N, Holz FG (2010) Clinical evaluation of simultaneous confocal scanning laser ophthalmoscopy imaging combined with high-resolution, spectral-domain optical coherence tomography. Acta Ophthalmol 88(8):842–849

19. Marmor MF, Fulton AB, Holder GE, Miyake Y, Brigell M, Bach M (2009) ISCEV Standard for full-field clinical electroretinography (2008 update). Doc Ophthalmol 118(1): 69–77

20. Kong X, Wang K, Sun X, Witt RE (2010) Comparative study of the retinal vessel anatomy of rhesus monkeys and humans. Clin Exp Ophthalmol 38(6):629–634

21. Bertram B, Wolf S, Fiehofer S, Schulte K, Arend O, Reim M (1991) Retinal circulation times in diabetes mellitus type 1. Br J Ophthalmol 75(8):462–465

22. Walter P, Mazinani B (2010) Macular dystrophies–hereditary macular degenerations. Klin Monatsbl Augenh 227(1): R1–R14

23. Anger EM, Unterhuber A, Hermann B, Sattmann H, Schubert C, Morgan JE, Cowey A, Ahnelt PK, Drexler W (2004) Ultrahigh resolution optical coherence tomography of the monkey fovea. Identification of retinal sublayers by correlation with semithin histology sections. Exp Eye Res 78(6): 1117–1125

24. Fischer MD, Fleischhauer JC, Gillies MC, Sutter FK, Helbig H, Barthelmes D (2008) A new method to monitor visual field defects caused by photoreceptor degeneration by quantitative optical coherence tomography. Invest Ophthalmol Vis Sci 49(8):3617–3621

25. Fortune B, Wang L, Bui BV, Burgoyne CF, Cioffi GA (2005) Idiopathic bilateral optic atrophy in the rhesus macaque. Invest Ophthalmol Vis Sci 46(11):3943–3956

26. Moura FC, Monteiro ML (2010) Evaluation of retinal nerve fiber layer thickness measurements using optical coherence tomography in patients with tobacco-alcohol-induced toxic optic neuropathy. Indian J Ophthalmol 58(2):143–146

27. Newman NM, Stevens RA, Heckenlively JR (1987) Nerve fibre layer loss in diseases of the outer retinal layer. Brit J Ophthalmol 71(1):21–26

28. Newman NJ (1993) Optic disc pallor: a false localizing sign. Surv Ophthalmol 37(4):273–282

29. Provis JM, Hendrickson AE (2008) The foveal avascular region of developing human retina. Arch Ophthalmol 126(4):507–511

30. Azuma N, Nishina S, Yanagisawa H, Okuyama T, Yamada M (1996) PAX6 missense mutation in isolated foveal hypoplasia. Nat Genet 13(2):141–142

31. Parodi MB, Visintin F, Della Rupe P, Ravalico G (1995) Foveal avascular zone in macular branch retinal vein occlusion. Int Ophthalmol 19(1):25–28

32. Drasdo N, Fowler CW (1974) Non-linear projection of the retinal image in a wide-angle schematic eye. Brit J Ophthalmol 58(8):709–714

NEUROSYSTEMS

Visual cortex organisation in a macaque monkey with macular degeneration

Yibin Shao,[1]* Georgios A. Keliris,[1,2]* Amalia Papanikolaou,[1] M. Dominik Fischer,[3,4] Ditta Zobor,[3] Herbert Jägle,[5] Nikos K. Logothetis[1,6] and Stelios M. Smirnakis[7]

[1]Max-Planck Institute for Biological Cybernetics, 72076 Tübingen, Germany
[2]Bernstein Center for Computational Neuroscience, Tübingen, Germany
[3]Institute for Ophthalmic Research, Centre for Ophthalmology, Tübingen, Germany
[4]Nuffield Laboratory of Ophthalmology, Department of Clinical Neurosciences, University of Oxford, Oxford, UK
[5]University Eye Clinic, University of Regensburg, Regensburg, Germany
[6]Division of Imaging Science and Biomedical Engineering, University of Manchester, Manchester, UK
[7]Department of Neuroscience and Neurology, Baylor College of Medicine, Houston, TX, USA

Abstract

The visual field is retinotopically represented in early visual areas. It has been suggested that when adult primary visual cortex (V1) is deprived of normal retinal input it is capable of large-scale reorganisation, with neurons inside the lesion projection zone (LPZ) being visually driven by inputs from intact retinal regions. Early functional magnetic resonance imaging (fMRI) studies in humans with macular degeneration (MD) report > 1 cm spread of activity inside the LPZ border, whereas recent results report no shift of the LPZ border. Here, we used fMRI population receptive field measurements to study, for the first time, the visual cortex organisation of one macaque monkey with MD and to compare it with normal controls. Our results showed that the border of the V1 LPZ remained stable, suggesting that the deafferented area V1 zone of the MD animal has limited capacity for reorganisation. Interestingly, the pRF size of non-deafferented V1 voxels increased slightly (~20% on average), although this effect appears weaker than that in previous single-unit recording reports. Area V2 also showed limited reorganisation. Remarkably, area V5/MT of the MD animal showed extensive activation compared to controls stimulated over the part of the visual field that was spared in the MD animal. Furthermore, population receptive field size distributions differed markedly in area V5/MT of the MD animal. Taken together, these results suggest that V5/MT has a higher potential for reorganisation after MD than earlier visual cortex.

Introduction

Early visual areas have a topographically precise, retinotopic, representation of the visual field (Van Essen & Maunsell, 1983; Tootell *et al.*, 1988; Brewer *et al.*, 2002; Gattass *et al.*, 2005; Wandell *et al.*, 2007). These maps remain stable over time in healthy adults but are thought to be plastic following injury of the visual pathways (Kaas *et al.*, 1990; Heinen & Skavenski, 1991; Gilbert & Wiesel, 1992; Chino *et al.*, 1995; Morland *et al.*, 2001; Baker, 2005; Giannikopoulos, 2006; Baker *et al.*, 2008; Schumacher *et al.*, 2008; Dilks *et al.*, 2009; Levin *et al.*, 2010). Understanding the capacity of the visual system for reorganisation following injury is an important step in the long-term effort to design treatments aimed at enhancing the ability of the visual system to recover after injury.

The term 'reorganisation' is difficult to define precisely and has sometimes been used loosely in the literature. To avoid confusion here, we adopt similar conventions as Wandell & Smirnakis (2009) and use the term reorganisation to refer to changes that occur over a long period of time and generally require the generation of new anatomical connections or, at least, a permanent change of strength in existing connections. This is in contrast to adaptive processes, which typically operate over a shorter time scale, tracking changes in input statistics. We note that the time scales over which reorganisation vs. adaptive processes operate overlap, and it is often difficult from functional magnetic resonance imaging (fMRI) to draw a sharp distinction between the two.

Several groups have studied the capacity of the visual cortex for reorganisation following retinal lesions, producing controversial results. The majority of electrophysiology studies after homonymous retinal lesions in adult cats and macaques reported that area V1 exhibits a considerable degree of plasticity into adulthood (Kaas *et al.*, 1990; Heinen & Skavenski, 1991; Gilbert & Wiesel, 1992; Giannikopoulos, 2006; Gilbert & Li, 2012). However, other studies using cytochrome oxidase (Horton & Hocking, 1998), electrophysiology (Murakami *et al.*, 1997) and fMRI (Smirnakis *et al.*, 2005) have suggested that post-lesion responses inside the V1 lesion projection zone (LPZ) are weak or absent.

Correspondence: Georgios A. Keliris, PhD, as above.
E-mail: georgios.keliris@tuebingen.mpg.de

*Y.S. and G.A.K. contributed equally to this work.

Several groups have moved beyond experimentally induced retinal lesions to study visual cortex reorganisation in a human retinal disease state called macular degeneration (MD). MD is a common cause of human visual impairment, and typically damages the central retina, gradually eliminating the normal retinal input to a large, central, region of the visual cortex. Several fMRI studies have suggested that human primary visual cortex, deprived of its normal retinal input by MD, undergoes large-scale reorganisation spanning centimetres of cortical space (Baker, 2005; Baker *et al.*, 2008; Schumacher *et al.*, 2008; Dilks *et al.*, 2009). In contrast, the initial report (Sunness *et al.*, 2004) found large-scale reorganisation in V1 to be absent. The largest human fMRI study surveying MD patients to date (Baseler *et al.*, 2011) has also reported a lack of large-scale reorganisation in V1. Wandell & Smirnakis (2009) recently reviewed some of these results in human and animal literature, pointing out that there are numerous inconsistencies still waiting to be resolved.

One difficulty is comparing results from the animal literature, which study cortical reorganisation following experimentally induced retinal lesions, with results from the human literature studying subjects with MD. Acute retinal lesions are not necessarily equivalent to lesions induced by a chronic process such as MD. A study of visual cortex reorganisation in animals suffering from MD can help bridge this gap. Here we use fMRI population receptive field measurements (Dumoulin & Wandell, 2008) to study cortical reorganisation in a macaque monkey suffering from a chronic MD condition approximating human juvenile MD. We compare our results with both the human fMRI and the macaque fMRI and electrophysiology literature.

Materials and methods

Subjects

A male monkey with a binocular central retinal lesion of ~10°(left eye) and ~11° (right eye) radius due to juvenile MD, weighing 9 kg (Dominik Fischer *et al.*, 2012), and two healthy adult monkeys (C1 and C2), one male and one female, weighing 9 and 6 kg respectively, were used for these experiments. All sessions were performed with great care to ensure the well-being of the animals, were approved by the local authorities (Regierungspraesidium) and were in full compliance with the guidelines of the European Community (EUVD 86/609/EEC) for the care and use of laboratory animals.

The monkeys were anesthetised during the fMRI experiments. Details of the anesthesia protocol have been given previously (Logothetis *et al.*, 1999). Briefly, the animals were premedicated with glycopyrolate [0.01 mg/kg, intramuscular (IM)] and ketamine (15 mg/kg, IM), and then deep anesthesia was induced with fentanyl (3 μg/kg), thiopental (5 mg/kg) and succinyl chloride (3 mg/kg). Anesthesia was maintained with remifentanyl (0.5–2 μg/kg/min) under paralysis with mivacurium chloride (3–6 mg/kg/h) to ensure the suppression of eye movements. Heart rate and blood oxygen saturation were monitored continuously with a pulse-oxymeter. Body temperature was kept constant at 37–38° Celsius.

Stimuli

Visual stimuli were displayed at a resolution of 800 × 600 pixels with a 60-Hz frame rate, using a custom-made fibre-optic projection system with mean luminance of ~100 cd/m². Stimuli were centred on the approximate location of the fovea (centre of the lesion) by using a modified fundus camera (Zeiss RC250). Animal eyes were fitted with appropriate contact lenses to ensure the stimulus remained in focus. Monocular stimuli were presented in the left eye for the MD animal and the controls. The field of view was 30° horizontal × 23° vertical visual angle. The stimulus consisted of a bar aperture with a width of 2° and a length equal to the field of view moving by 1° per volume acquisition (6 s) passing over a rotating polar checkerboard sequentially in four different directions (top-to-bottom, left-to-right, bottom-to-top and right-to-left). The bars were presented continuously with no gap. The same moving bar stimuli were presented to the MD monkey and to the healthy controls. Outside the bar aperture an isoluminant gray background was presented. One important control condition involved presenting the same moving bar stimuli to healthy animals while occluding the central part of the visual field with a black [RGB color index = (0 0 0)] disk of 10° radius. We refer to this as the 'artificial scotoma' (AS) condition and it was designed *a priori* (before the fMRI experiments) to match the size of the lesion in the left eye of the MD animal, which was used for fMRI imaging. This control allowed us to probe whether changes observed in the fMRI signal pattern in area V1 could potentially represent a short-term effect induced because of the absence of central visual stimulation, as opposed to long-term cortical reorganisation. As we reported earlier (Dominik Fischer *et al.*, 2012), the radius of MD lesion inside which the inner nuclear layer thickness is destroyed is 9.6° (2.23 mm). The size of the artificial scotoma was taken to extend 0.4° further, corresponding to the point at the MD lesion border where > 75% of the thickness of the inner retina has been destroyed. Note that inner nuclear layer thickness returns to normal at 11.2°, so the full extent of the 'soft' border, i.e. the region of the border where the lesion is incomplete and may therefore transmit some information to the cortex, ranged from 9.6 to 11.2° (i.e. size of the lesion border is 1.6°).

Data acquisition

FMRI experiments were performed on a 4.7-T vertical scanner (Bruker Biospec, Bruker Biospin GmbH, Ettlingen, Germany). Multislice fMRI was performed by the use of eight segmented gradient-recalled echo-planar imaging (EPI). Volumes of 17 slices of 1 × 1 × 2 mm³ were collected, each with a field of view (FOV) of 128 × 128 mm on a 128 × 128 matrix and 2-mm slice thickness, flip angle (FA) 40°, echo time (TE) 20 ms and a repetition time (TR) of 750 ms per segment resulting in a volume acquisition time of 6 s. For anatomical measurements we used a FLASH sequence with the same FOV 128 × 128 mm², matrix 256 × 256, slice thickness 2 mm, FA 70°, TE 10 ms and TR 2000 ms. A high-resolution 3-D-MDEFT anatomical scan with an isotropic resolution of 0.5 mm was acquired for co-registration with the FLASH and EPI images. For more details on the fMRI methods see Logothetis *et al.* (1999); Keliris *et al.* (2007). Each fMRI scan included two repetitions of the stimuli (204 volumes per scan) and we acquired 5–7 scans per session.

Data analysis

The expected V1 LPZ of the retinal lesion was calculated from the ^{14}c-2-deoxy-d-glucose staining retinotopic organisation maps (Tootell *et al.*, 1988), and from electrophysiological cortical magnification measurements [$M_1(r) = 13r^{-1.22}$; Van Essen *et al.*, 1984; or $M_2(r) = 15.7(r + 1.62)^{-1}$; LeVay *et al.*, 1985;], where r is the eccentricity from the centre of the visual field, and M is the magnification factor in mm/°). By integrating the magnification factor equation, the radius D from eccentricity I to eccentricity E can be calculated. Cortical distance in the fovea (from 0 to 1° eccentricity)

was estimated using a different equation, more accurate for the central visual field: $D_f(r) = 7\text{In}(r + 0.33)$ (Dow *et al.*, 1985).

FMRI data were reconstructed and imported into a MATLAB-based toolbox (mrVista; http://white.stanford.edu/software/) (Amano *et al.*, 2009; Levin *et al.*, 2010). The gray–white matter boundary was manually segmented using itkGray from the high-resolution 3-D-MDEFT anatomical images, and 3-D cortical surface and flat mesh models were created and realigned with the functional data by using mrMesh/mrVista (Wandell *et al.*, 2000). Data were analysed by using the voxel-based population receptive field (pRF) analysis method described by Dumoulin & Wandell (2008). We note that the pRF represents the sum response of a large population of neurons within a voxel and it is dependent on the size and the position scatter of the individual receptive fields (see also Haak *et al.*, 2012). Briefly, the activity of each voxel was fitted to a two-dimensional Gaussian function with three parameters (the visual field spatial coordinates x, y reflecting the centre of the pRF and the SD reflecting the pRF size). Explained variance (EV) maps (the fraction of the time series that can be explained by the model) were drawn in order to estimate the noise level and set the threshold. We set the threshold of the EV fraction to be 0.15 for the MD and first control monkey as in previous studies (Levin *et al.*, 2010; Baseler *et al.*, 2011). The noise level of the second control monkey was found to be slightly higher (Fig. 3) and we chose the threshold to be 0.2 (2 SD above the mean of the EV level of a selected non-visually responsive region of interest). After the pRF model fitting, for each voxel above the threshold we got the estimated position of the centre and the size of the pRF. Three types of retinotopic maps were then plotted: the eccentricity map, the polar angle map and the pRF size map. Visual areas were defined by horizontal and vertical meridians of the angle maps and were found to respect anatomical boundaries.

Results

Characterisation of the retinal lesion

The MD monkey was identified in the colony of the Max Planck Institute for Biological Cybernetics, Tuebingen, Germany, after an fMRI experiment that showed absence of activation in the occipital gyrus. The animal was subsequently examined ophthalmologically and diagnosed to have a chronic MD condition that approximates human juvenile MD (Dominik Fischer *et al.*, 2012). Optical coherence tomography (OCT) and multifocal electroretinogram (ERG) were used to characterise the retinal lesion of the MD monkey (Fig. 1). Figure 1a shows the retinal thickness map calculated from the OCT of the MD and one control monkey; ERG results are superimposed. The total retinal thickness is markedly reduced in the MD monkey compared with the control. The retina of the left eye of the MD animal is greatly thinned in a central region of 2.23 mm radius, representing a large central visual field scotoma with a soft border, where the inner retina is between completely destroyed and normal (see figs 3 and 5d in Dominik Fischer *et al.*, 2012). We measured that this yields a near-symmetric visual field loss of 9.6° radius on average with a soft border of 1.6° (Dominik Fischer *et al.*, 2012; see also Drasdo & Fowler, 1974). Furthermore, multifocal ERG responses were markedly reduced within the scotoma of the MD animal in contrast to the control. Figure 1b shows the optical coherence tomography of the layers of the foveal retina of the MD and the control monkey. The photoreceptor layer of the retina of the MD animal is relatively preserved while the retinal nerve fibre, ganglion cell layer, inner plexiform and inner nuclear layers are destroyed. This was confirmed by retinal histology post-mortem. A detailed account of the retinal pathology of this animal is described elsewhere (Dominik Fischer *et al.*, 2012). Behavioural data from the MD animal confirmed the existence of the central scotoma, but unfortunately the animal had to be killed for health reasons unrelated to this experiment before the entire scotoma border could be mapped in detail behaviourally. We stress that this does not affect our analysis here, as the anatomical borders of the retinal lesion and how they correspond to the visual field have been measured precisely by ophtalmoscopy and confirmed by histology (Dominik Fischer *et al.*, 2012). Specifically, no spared islands were found inside the area of the retinal lesion, and the extent of the lesion border was confirmed histologically.

Visual modulation: extent of the retinal lesion projection zone

Visual cortical responses were measured during anesthetised fMRI for both the MD and two control animals (see Materials and methods). Note that the normal central (~10° radius) retinal input is eliminated in the MD animal.

Statistical parametric maps (SPMs) of visual cortical activity were estimated from the blood oxygenation level dependent (BOLD) responses and were overlaid on the reconstructed gray–white matter surface meshes of each animal. Figure 2a and b presents two snapshots of such SPMs overlaid onto the right hemisphere of the MD animal. As shown in Fig. 2b the operculum of the MD animal is devoid of any statistically significant activation, in contrast to the control animal (Fig. 2c). We used the isotropic pRF model to estimate the centre and size of the receptive field voxel by voxel by fitting the model to the responses elicited at each voxel from the moving bar stimulus (Fig. 2a). Figure 2a illustrates the optimal pRF of a voxel in peripheral V1, outside the LPZ, showing that the corresponding, predicted, BOLD time series (blue line) matches very well with the measured averaged BOLD time series (black line). As demonstrated by the small subpanels over the time-course in Fig. 2a, whenever the stimulus passed over the estimated receptive field location (small top panels, Fig. 2a) a peak response appeared in the time series. On the other hand, the BOLD time series of voxels lying within the LPZ were not modulated by the stimulus at any location, remaining at baseline levels (Fig. 2b). For such voxels, the pRF model does not explain a significant proportion of the BOLD time series variance, indicating that the voxel does not get significantly modulated by the stimulus.

In an attempt to gain further insight about the extent of the retinal lesion projection zone in the visual cortex of the MD animal, we compared the EV SPMs of the MD and two control animals with a 10° radius AS (C1AS and C2AS) on the unfolded cortical surfaces (see Materials and methods). It is important to note that for this comparison to be fair we selected monkeys whose brain size was similar to the MD animal. Specifically, for the first control the average distance from fovea to the calcarine fissure was the same as in the MD animal, and for the second control 1 mm larger. Maps of the MD and control animals are shown in Fig. 3.

Given that the shape of the retinal scotoma is approximately symmetric, the extent of the LPZ can be quantified by measuring the average distance from foveal V1 to the border of the LPZ, and then comparing this with the distance estimated from systematic electrophysiological experiments on the same species. We estimated the cortical distances from fovea to 10° eccentricity in macaque using previous reports to range from 33 mm (Tootell *et al.*, 1988) to 33.2 mm (Van Essen *et al.*, 1984; Dow *et al.*, 1985) and 33.1 mm *(Dow et al., 1985; LeVay et al., 1985)*. The cortical distances
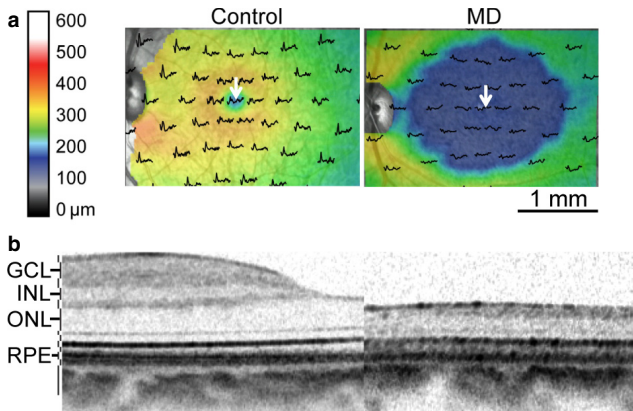
FIG. 1. The pathophysiology of the retinal lesion of the MD monkey. (a) Interpolated OCT retinal thickness maps of MD and one control monkey. The multifocal ERG results are superimposed on the retinal thickness maps. The retina of the MD animal is greatly thinned in a central region of 2.2 mm radius and yields a visual field loss of 9.6° radius. (b) OCT of the MD (right) and the control monkey retina (left) from the foveal rim towards the foveal pit (indicated by the white arrows in a). GCL, ganglion cell layer; INL, inner nuclear layer; ONL, outer nuclear layer; RPE, retinal pigment epithelium. Panels a and b were reproduced with kind permission from Springer Science+Business Media B.V. from parts of figs 3 and 7 in Dominik Fischer *et al.*, 2012.

between the fovea and the border of the V1 LPZ for the MD monkey and the border of the artificial scotoma projection zone (ASPZ) for the two control monkeys were measured at various polar angles, and found to be within the range 32–34 mm (samples along the hor-

FIG. 3. Fraction of EV in the visual cortex of the MD monkey vs. two controls under the AS condition. (a) Unfolded flat map of the early visual cortex of the right hemisphere of the MD animal. The operculum of the monkey is outlined by the calcarine sulcus (CS), the lunate sulcus (LuS) and the inferior occipital sulcus (IoS). The cortical distance between fovea (yellow star) and the LPZ border in V1 is ~33 mm for both the MD monkey and for the control monkeys with a 10° radius AS (c and e), which agrees well with the retinotopically projected cortical distance derived from the extent of the retinal lesion (see text). (b) Percentage EV as a function of eccentricity in V1 (red lines) and V2 (green lines) for the MD monkey and (d and f) control monkeys under the AS condition. The boundaries of the LPZ border (MD monkey) are illustrated by the dashed lines and of the ASPZ border (control monkey under the AS condition) by the dotted lines.
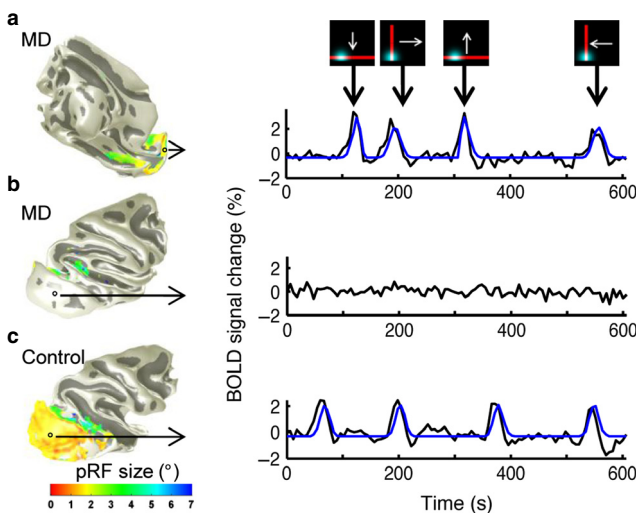

FIG. 2. Comparing BOLD responses from the MD animal and one control monkey. (a) PRF size map obtained with the bar stimuli overlaid on the inflated gray–white matter surface of the posterior right hemisphere of the MD macaque. The estimated pRF and time series for one selected voxel in the non-deafferented V1 are illustrated. The predicted time series shown in blue matches very well with the actual average BOLD time series in black. Insets on top show the position of the bars that generated the BOLD signal peaks shown below. (b) Average BOLD time series of a voxel inside the deafferented part of the MD monkey V1. Note that there is no significant modulation by the visual stimulus at this position. This results in a large area devoid of visually driven activity in central V1 of the MD monkey that corresponds to the lesion projection zone of the retinal lesion (see Fig. 3). This can be contrasted with (c) the PRF size map on the operculum of a control monkey.

izontal meridians are shown in Fig. 3); this is also consistent with the distances estimated from the literature. Importantly, across the border of the LPZ (or the ASPZ) the fraction of EV rises sharply (Fig. 3a, c and e). The result is that the LPZ or ASPZ border does not shift much due to the choice of threshold, and the size of the LPZ and ASPZ does not change much as a result of a reasonable threshold choice. To investigate this further we plotted how the fraction of EV in area V1 changes as a function of eccentricity. For both the MD and the control animals with AS, EV changes rapidly, as shown by the steep slopes of the curves (Fig. 3b, d and f). The boundaries of the LPZ and ASPZ borders are illustrated by the dashed and dotted lines for the MD monkey and two control monkeys with AS, respectively. Compared with the control monkeys, the V1 LPZ border of the MD monkey spreads ~ 0.5° further towards the scotoma (8.5–9° eccentricity, corresponding to ~0.5 mm on the cortical surface). This difference could be explained by taking into account that the extent of the absolute retinal lesion (inner nuclear layer thickness ~0) was 9.6° vs. the 10° AS, and suggests

that even the part of the soft lesion border with 75% inner nuclear layer damage can activate area V1. Alternatively, this could represent a minimal change of the V1 LPZ border by ~0.5 mm. Overall, our results suggest that the V1 LPZ border does not shift appreciably on the order of 1 mm. Voxel histograms of the fraction of EV were similar inside the V1 LPZ and the ASPZ, were commensurate with histograms obtained from non-visually responsive regions, and were well separated from histograms obtained outside the LPZ (ASPZ). Area V2 showed similar trends as V1 (Fig. 3b and d), suggesting that the border of the LPZ in area V2 also did not shift appreciably in this situation.

Retinotopic representation

Although our results argue against a shift of the V1 LPZ border, the size and retinotopic location of the pRFs in the non-deafferented peripheral areas could still change as a result of chronic loss of input. We first compared the locations of the pRFs by plotting the retinotopic angle and eccentricity maps on the visual cortex. Figure 4 shows the thresholded maps of the MD animal and two controls with and without AS and projected on the unfolded and flattened white–grey matter surface. The eccentricity map of the MD monkey showed a similar concentric structure in early visual areas as the maps of the controls. In addition, the positions of the horizontal and vertical meridian which can be seen in the angular maps matched the known anatomical boundaries between areas. Furthermore, there was no obvious distortion in the angular maps of the MD monkey outside the region of the LPZ and the retinotopic structure of non-deafferented early visual cortex remained unchanged.

In contrast to early visual areas V1 (N = 1584, 1499, 1395 significantly activated voxels, counted on anatomical scans, for MD, C1AS and C2AS respectively) and V2 (N = 1417, 1324, 1268), area V5/MT of the MD monkey showed more extensive activation than the control monkeys with AS (N = 561, 152, 162). The area of V5/MT that was activated in the MD monkey was similar to the extent of V5/MT activity seen in the control monkeys under full visual field stimulation (N = 612, 722). These suggest that marked reorganisation occurred in area V5/MT of the MD monkey. Nonspecific changes in signal-to-noise ratios (SNR), defined here as the mean intensity of the voxel divided by the SD over time, cannot explain these observations because the SNRs among the scans for the MD and control monkeys were similar in area V1 (1.9, 1.9, 1.9; median logarithm of SNRs for MD, C1 and C2 respectively), V2 (1.9, 2.0, 1.8) and V5/MT (1.9, 1.9, 1.8). Other extrastriate areas (e.g. area V3/V3A) also appear to be upregulated in the MD animal (see Figs 3 and 4), but more data would be needed to make a definite statement here.

pRF size analysis

An important piece of information provided by the pRF method is the pRF size. The pRF size map for the MD and control monkeys are presented in Fig. 4 bottom panels overlaid on the flattened cortical mesh. pRF sizes in area V5/MT were smaller for the MD animal than the controls with a 10° AS. The change in pRF size together with the expansion of the activated area in V5/MT of the MD monkey provide converging evidence for substantial reorganisation in this area.
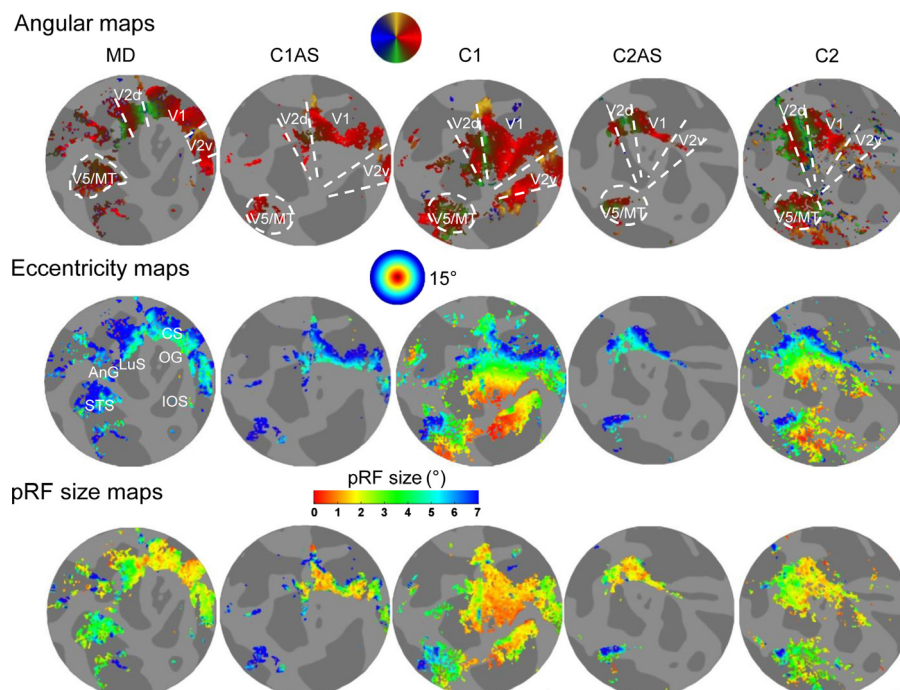
FIG. 4. Retinotopic maps derived via population receptive field analysis. Angular, eccentricity and pRF size maps of the MD monkey and two control monkeys with and without AS. The positions of several visual areas and major gyri and sulci are labeled: occipital gyrus (OG), lunate sulcus (LuS), superior temporal sulcus (STS), calcarine (CS), inferior occipital sulcus (IOS) and angular gyrus (AnG). There is no obvious distortion in the retinotopic maps of the MD monkey in the non-deafferentted regions of the early visual areas. Note, however, that the situation is different for area V5/MT. (i) The spatial extent of visually driven activation of the V5/MT complex in the MD animal (left column) is much larger than that observed in the control with the AS (middle column) and approximates the extent of V5/MT activation seen in the control animal under full field stimulation (right column). (ii) V5/MT activity in the MD animal arises from voxels whose pRF centres have phase values that correspond to the region of the intact retina (blue/cyan color, left column eccentricity map). Most of these pRFs appear to be ectopic, as they correspond to regions of area V5/MT that would ordinarily be activated by pRFs centred at different eccentricities (compare with eccentricity map, right column).

Importantly, the pRF features of controls stimulated under the AS condition remained unchanged compared with normal (no artificial scotoma) visual stimulation conditions outside the ASPZ in areas V1, V2 and V5/MT (Fig. 5), in agreement with previous reports (Baseler *et al.*, 2011; Haak *et al.*, 2012).

In order to quantitatively measure the changes that occur in the receptive field maps between the MD and control monkeys with AS, we measured pRF centre and size distributions in different visual areas (Figs 6a and 7a). As the shape of the retinal lesion of the MD monkey was nearly circular, the borders of the LPZ in visual cortical areas were nearly isoeccentric, and the pRF centre distributions could be characterised by plotting the histogram of voxels within different eccentricity bins.

Assuming reorganisation happens, one would expect that neurons close to the border of the LPZ should respond to input from the intact retina located adjacent to the lesion. In this case, the number of voxels with receptive fields at eccentricities near and a little beyond the eccentricity of the LPZ border would increase. This was not what we found in area V1; instead, the distribution of the voxels as a function of eccentricity followed a similar pattern for both the MD and the control monkeys with AS (Fig. 6a, left panel). Looking at Fig 6a one might think it possible that there is a slight difference in the histogram profiles around eccentricities 10–12°, but this could be accounted for by the tapered nature of the MD lesion border (~1.6°) and cannot be regarded as definite.

In contrast, the pRF size distribution in area V1 of the MD monkey was clearly shifted towards larger pRF sizes (Fig. 6a, right panel). We plotted the pRF size as a function of eccentricity in V1 of the MD and control monkeys with AS. Our results illustrate that pRF size in area V1 of the MD animal increased linearly with eccentricity as in the controls, and that the pRF sizes in the MD animal were larger than the controls with AS for all eccentricities (Fig. 6b). This result cannot be explained by 'ectopic' voxels

located inside the LPZ but suggests a rather systematic expansion in pRF sizes close to but outside the LPZ border. Although there is a trend for the effect to be smaller at higher eccentricities (Fig. 6b) this nevertheless suggests that pRF expansion extends to voxels which are considerably distant (~3–5mm) from the LPZ border, towards normal non-deafferented cortex.

PRF sizes in area V2 remained similar in the MD animal and in the controls with the AS (Fig. 6c), and the LPZ border was not found to be shifted (Fig. 3b, d and f), suggesting limited reorganisation in area V2 similarly to V1.

Remarkably, the number of visually modulated voxels in area V5/MT of the MD monkey was similar with that of the control animal under full-field stimulation but much higher than the control with an AS (Fig. 7a, see also Fig. 4). This suggests that visually driven activity occurs in most voxels of area V5/MT in the MD animal, but only in a fraction of the area V5/MT voxels in the controls with an AS. Specifically, there were more voxels activated as well as a larger fraction of voxels with small pRF sizes in the MD animal. The number of voxels activated in V5/MT of the two control animals under the AS condition was very small and therefore a direct comparison with the MD was very noisy. Alternatively, we plotted the pRF size as a function of eccentricity in area V5/MT of the MD and compared it with the control monkeys with full-field stimulation (note that as we show in Fig. 5 there was no significant difference between the pRF sizes in controls and controls with AS). Our results illustrate that the pRF sizes in area V5/MT of the MD animal increased linearly with eccentricity as in the controls (Fig. 7b). Importantly, the pRF sizes in the MD animal were smaller than the controls for all eccentricities.

Discussion

Several studies have reported substantial reorganisation in the primary visual cortex of cat and monkey following retinal lesions (Kaas *et al.*, 1990; Heinen & Skavenski, 1991; Gilbert & Wiesel, 1992; Giannikopoulos, 2006) while others have reported minimal, if any, changes (Murakami *et al.*, 1997; Horton & Hocking, 1998; Smirnakis *et al.*, 2005). Similarly, several human fMRI studies in MD patients have suggested that human primary visual cortex undergoes large-scale reorganisation (Baker, 2005; Baker *et al.*, 2008; Schumacher *et al.*, 2008; Dilks *et al.*, 2009), but others claim the reverse (Sunness *et al.*, 2004; Baseler *et al.*, 2011) or qualify the reported reorganisation as being dependent on top-down feedback (Masuda *et al.*, 2008). Recently, Wandell & Smirnakis (2009) reviewed the capacity of the primary visual cortex for reorganisation following retinal lesions, underscoring the existence of multiple points of controversy.

One reason for some of the differences noted in the literature may be that human studies involve subjects with MD while animal studies involve induced retinal lesions. Here we were given the opportunity to study a macaque with MD that was identified in the colony of the Max Planck Institute for Biological Cybernetics. We used fMRI to measure population receptive field characteristics in the monkey suffering from MD and made direct comparisons with results obtained from healthy macaques with similar area V1 size, which were presented with partially occluded central visual field stimuli that simulated the MD visual field deficit (this is referred to as the AS stimulation condition).

We found no significant shift of the LPZ border, suggesting no large-scale remapping occurs in area V1 of the MD animal. This is in contrast to previous reports (Kaas *et al.*, 1990; Heinen & Skavenski, 1991; Gilbert & Wiesel, 1992; Chino *et al.*, 1995; Giannikopoulos,
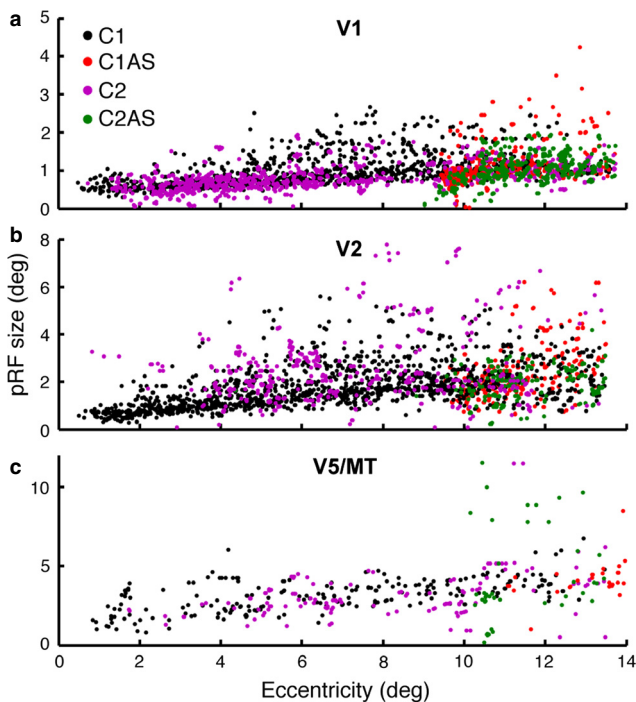

Fig. 5. Scatter plots of pRF size vs. eccentricity in voxels of control monkeys with and without artificial scotoma. (a) Area V1, (b) area V2 and (c) area V5/MT. pRF size estimates outside the ASPZ for the AS condition are similar to the controls under full-field stimulation.
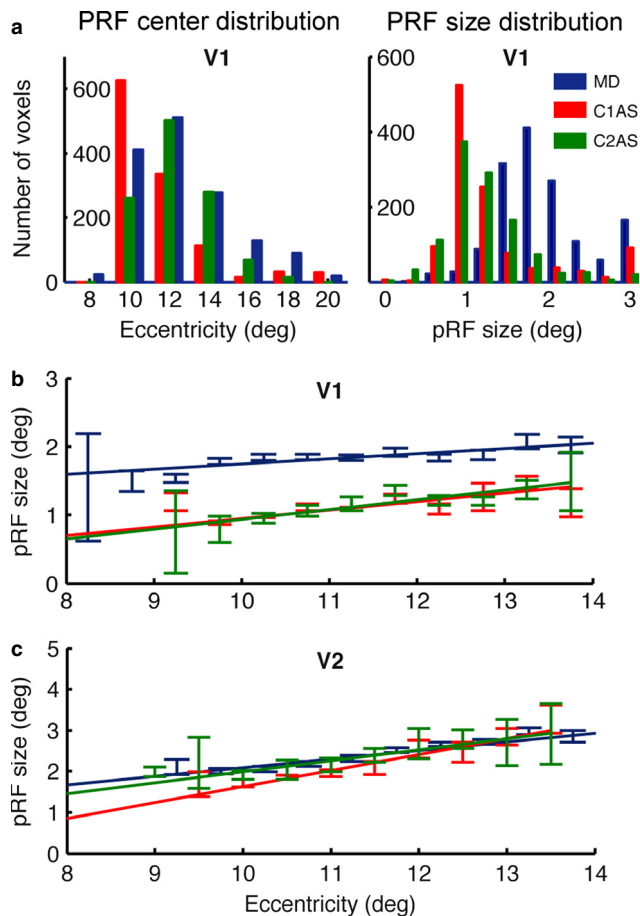
FIG. 6. Population receptive field analysis in area V1. (a) Distribution of the pRF centres as a function of eccentricity (left panel) and size (right panel) in the MD monkey and in control monkeys with AS. The distribution of pRF centres as a function of eccentricity away from the area V1 LPZ border are similar between the MD animal and the AS control, though a slight (1–2°) shift towards slightly higher eccentricities cannot be excluded for pRFs lying right outside the LPZ border (see also Discussion). A more pronounced change is seen when examining pRF sizes. The distribution of pRF sizes is clearly shifted towards larger values in the MD animal (right panels). (b) pRF size in area V1 as a function of eccentricity for the MD animal and two control monkeys under the AS condition. The slopes (S) of the functions are labelled. PRF size in area V1 of the MD animal increased linearly with eccentricity as in the AS controls, but remained larger than the controls for all eccentricities examined (~9–14°). The slope of the curves is different so that the size difference gap decreases with increasing eccentricity, i.e. as one moves away from the border of the LPZ. (c) pRF size in area V2 as a function of eccentricity for the MD animal and two control monkeys under the AS condition.
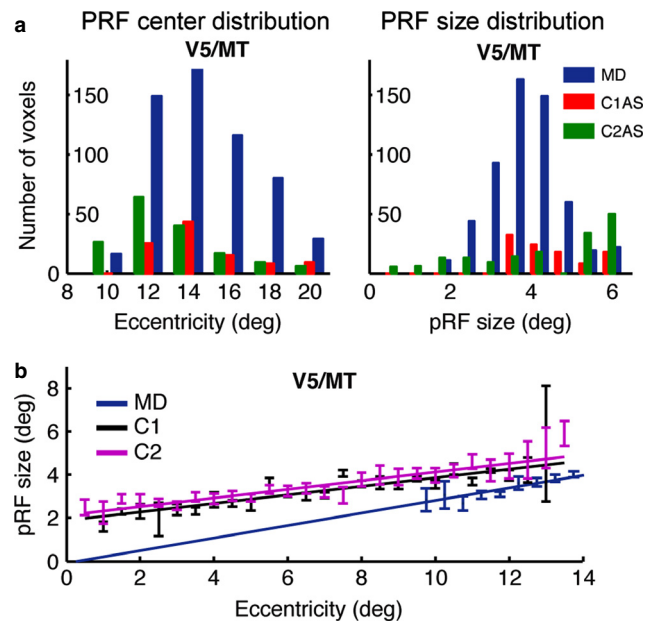
FIG. 7. pRF analysis in area V5/MT. (a) Distribution of the pRF centres as a function of eccentricity (left panel) and size (right panel) in the MD monkey and in control monkeys with AS. Note that the number of visually modulated voxels in area V5/MT of the MD monkey is much higher than in the AS control (see also Fig. 4). There is also a larger fraction of voxels with small pRF sizes in the MD animal. (b) pRF size in area V1 as a function of eccentricity for the MD animal and two control monkeys. Note that as the number of voxels activated in V5/MT under the AS condition in the two control animals was very small we have used the controls under full-field stimulation for the comparison.

2006) which reported the existence of ectopic receptive fields inside the LPZ and over a large range of distances up to 5 mm. The position of the LPZ border in the MD animal was within ~0.5 mm of the position of the 10° AS projection zone border obtained from control animals (Fig. 3). Even the observed ~0.5 mm shift can be explained without having to resort to cortical reorganisation: As the 'hard' border of the MD lesion was 9.6°, the difference between LPZ and ASPZ borders can be fully explained if the tapering part of the retinal lesion border is capable of transmitting functional information to area V1. These results are in agreement with a previous study in macaque monkeys following retinal lesions induced by laser photocoagulation (Smirnakis *et al.*, 2005) and with recent fMRI results in human MD patients (Baseler *et al.*, 2011). In contrast to Baseler *et al.* (2011; note the differences in preparation and species), we found that there

were very few voxels with significant visual modulation inside the V1 LPZ of the MD monkey or inside the ASPZ of the control monkeys (Fig. 3). The sampling rates in V1 LPZ were 0.7%, 1.2% and 1.8% for the MD, C1AS and C2AS respectively. Visual inspection of the pRFs inside the LPZ/ASPZ that had the highest EV revealed that they were noisy and not representative. This difference might reflect the differences in the AS mask luminance. In our experiments, the AS mask luminance was set to black [RGB = (0 0 0)], in comparison with some previous studies using grey background luminance (Baseler *et al.*, 2011; Haak *et al.*, 2012). Other factors (such as anesthesia) might also play a role.

A possible explanation for the differences between studies reporting large-scale reorganisation (Baker, 2005; Baker *et al.*, 2008; Schumacher *et al.*, 2008) and other studies including ours (Sunness *et al.*, 2004; Baseler *et al.*, 2011) that do not, might be the employment of a behavioural task; subjects in studies reporting large-scale reorganisation typically performed a one-back memory task (Baker, 2005). A recent report demonstrated visual responsiveness inside the V1 LPZ of MD patients only when the subject performed a stimulus-related judgment as opposed to passive viewing (Masuda *et al.*, 2008). They proposed that responses inside the LPZ are driven by feedback from extrastriate visual cortex elicited by the demands of the stimulus-related judgment task (Masuda *et al.*, 2008). Feedback signals from extrastriate cortex (e.g. V5/MT) can influence V1 (Zeki & Shipp, 1988; Angelucci *et al.*, 2002; Harrison *et al.*, 2007). It would have been desirable to measure the cortical response and pRF features while the MD monkey performed a stimulus-related judgment task, compared to the experiments under anesthesia. Unfortunately, this turned out to be impossible because the animal had to be killed for reasons unrelated to these experiments.

The distribution of pRF centres as a function of eccentricity outside the LPZ (ASPZ) was roughly similar between the MD animal and controls with the AS (Fig. 6a, left panel). However, we found that pRF sizes in the non-deafferented V1 region, i.e. outside the LPZ border, were on average ~20% larger in the MD monkey. PRF size measurements reflect both the receptive field size of individual units inside a voxel and their scatter. The neuronal receptive field and scatter have been reported to co-vary (Hubel & Wiesel, 1974). A recent study by Haak et al. (2012) investigated how the pRFs change under AS conditions presented to human subjects and found that pRFs near the border of the AS tend to increase in size (see also Wandell & Smirnakis, 2009). They speculate that the removal of input for voxels inside and near the border of the AS is likely to preferably affect the neurons with small RFs while neurons with larger RFs can still be stimulated by locations outside the AS biasing thus the pRF measurements to larger values. The 20% increase in pRF size we measured is likely to reflect at least partially a similar mechanism. Alternatively, single-neuron RFs could indeed become larger but this effect is potentially overestimated in the pRF measurements. Although the enlargement of pRFs qualitatively agrees with prior electrophysiology studies reporting single- and multi-unit receptive field increases near the border of the lesion projection zone (Gilbert & Wiesel, 1992), it is quantitatively very different: Gilbert & Wiesel (1992) reported a several-fold receptive field size increase over a period of 2 months, whereas the increase we saw is much less pronounced. The ~20% increase in pRF size we report here is more in agreement with other reports (Chino et al., 1995), and could potentially be explained by changes in the balance between excitation and inhibition (Hubel & Wiesel, 1959; Cavanaugh, 2002) induced by deafferentiation. For example, inhibitory inputs arising inside the LPZ may be weakened by deafferentiation (Hendry & Jones, 1986; Rosier et al., 1995; Arckens et al., 1998; Wade & Rowland, 2010), releasing from inhibition units lying outside the LPZ border. PRFs corresponding to voxels lying outside the LPZ would then increase in size. This hypothesis is supported by the observation that the increase in pRF size was greater close to the LPZ border than at higher eccentricities (Fig. 6b). PRF size might also change as a result of altered top-down feedback to area V1 from higher areas. This explanation is less likely, however, as our experiments were performed under anesthesia.

Area V2 also showed limited reorganisation indicated by the stable V2 LPZ border (Fig. 3), and similar pRF sizes outside the V2 LPZ in the MD animal and in controls with the AS (Fig. 6c).

The more striking finding in our study was the large extent of activation seen in area V5/MT of the MD monkey in comparison with control monkeys stimulated with the AS. Earlier reports suggested that functional responses and inter-hemispheric connectivity of human area MT appeared to be relatively unaffected by long periods of deprivation of structured visual input (Fine et al., 2003; Levin et al., 2010). To the best of our knowledge, V5/MT upregulation in subjects with MD has not been reported before, though it is suggested by figures presented in several studies (Baker, 2005; Baker et al., 2008; see fig. 3 in these references). Analysis of the distribution of pRF centre locations in area V5/MT of the MD vs. the control animals revealed that many more voxels in area V5/MT of the MD animal respond to inputs from intact, peripheral retina. Some of these voxels are probably from inside the LPZ given that the size of V5/MT activated in the MD animal (both in number of voxels and anatomically) was similar to the extent of V5/MT activity seen in the control animals under full visual field stimulation and much larger than the activity in controls with AS. Neurons in area V5/MT normally have large, overlapping receptive fields receiving

inputs from multiple units with smaller receptive fields in area V1 (Hubel & Wiesel, 1974; Albright & Desimone, 1987). Following central V1 deafferentiation many V5/MT cells lose only part of their input, preserving the connections that lie outside the area V1 LPZ. These connections are likely to be weak initially, explaining why areas V5/MT of control monkeys are poorly activated under the AS condition (Fig. 4). Over time, however, the surviving connections apparently get strengthened and become capable of driving the significant, though ectopic, extent of visual modulation we observed in area V5/MT of the MD animal (Fig. 7a). This hypothesis is consistent with the fact that area V5/MT pRF sizes in the MD monkey are on average smaller than in controls under the AS condition. One way this may come about is if, over time, deafferented regions of area V5/MT become capable of being visually modulated by stimuli presented outside the retinal lesion but these reorganised, ectopic, pRFs never return to their original size. The relatively slow, chronic progression of MD probably contributes to the large-scale reorganisation that is observed.

In summary, our results in this macaque subject with MD suggest that area V1 shows at best limited reorganisation: (i) the LPZ border did not shift, and (ii) only a modest, 20% on average, pRF size change was observed outside the LPZ border. Area V2 also shows limited reorganisation. In contrast, extrastriate area V5/MT shows considerably more capacity for reorganisation: visually modulated ectopic pRFs in the MD animal cover a cortical area much larger than expected from AS controls. Area V5/MT could therefore potentially serve as the source of relatively strong feedback inside the area V1 LPZ.

Abbreviations

AS, artificial scotoma; ASPZ, artificial scotoma projection zone; BOLD, blood oxygenation level-dependent; ERG, electroretinogram; EV, explained variance; fMRI, functional magnetic resonance imaging; LPZ, lesion projection zone; MD, macular degeneration; OCT, optical coherence tomography; pRF, population receptive field.

References

Albright, T.D. & Desimone, R. (1987) Local precision of visuotopic organization in the middle temporal area (MT) of the macaque. *Exp. Brain Res.*, **65**, 582–592.

Amano, K., Wandell, B.A. & Dumoulin, S.O. (2009) Visual field maps, population receptive field sizes, and visual field coverage in the human MT+ complex. *J. Neurophysiol.*, **102**, 2704–2718.

Angelucci, A., Levitt, J.B., Walton, E.J., Hupe, J.M., Bullier, J. & Lund, J.S. (2002) Circuits for local and global signal integration in primary visual cortex. *J. Neurosci.*, **22**, 8633–8646.

Arckens, L., Eysel, U.T., Vanderhaeghen, J.J., Orban, G.A. & Vandesande, F. (1998) Effect of sensory deafferentation on the GABAergic circuitry of the adult cat visual system. *Neuroscience*, **83**, 381–391.

Baker, C.I. (2005) Reorganization of visual processing in macular degeneration. *J. Neurosci.*, **25**, 614–618.

Baker, C.I., Dilks, D.D., Peli, E. & Kanwisher, N. (2008) Reorganization of visual processing in macular degeneration: replication and clues about the role of foveal loss. *Vision Res.*, **48**, 1910–1919.

Baseler, H.A., Gouws, A., Haak, K.V., Racey, C., Crossland, M.D., Tufail, A., Rubin, G.S., Cornelissen, F.W. & Morland, A.B. (2011) Large-scale

remapping of visual cortex is absent in adult humans with macular degeneration. *Nat. Neurosci.*, **14**, 649–655.

Brewer, A.A., Press, W.A., Logothetis, N.K. & Wandell, B.A. (2002) Visual areas in macaque cortex measured using functional magnetic resonance imaging. *J. Neurosci.*, **22**, 10416–10426.

Cavanaugh, J.R. (2002) Nature and interaction of signals from the receptive field center and surround in macaque V1 neurons. *J. Neurophysiol.*, **88**, 2530–2546.

Chino, Y.M., Smith, E.L., Kaas, J.H., Sasaki, Y. & Cheng, H. (1995) Receptive-field properties of deafferentated visual cortical-neurons after topographic map reorganization in adult cats. *J. Neurosci.*, **15**, 2417–2433.

Dilks, D.D., Baker, C.I., Peli, E. & Kanwisher, N. (2009) Reorganization of visual processing in macular degeneration is not specific to the "preferred retinal locus". *J. Neurosci.*, **29**, 2768–2773.

Dominik Fischer, M., Zobor, D., Keliris, G.A., Shao, Y., Seeliger, M.W., Haverkamp, S., Jagle, H., Logothetis, N.K. & Smirnakis, S.M. (2012) Detailed functional and structural characterization of a macular lesion in a rhesus macaque. *Doc. Ophthalmol.*, **125**, 179–194.

Dow, B.M., Vautin, R.G. & Bauer, R. (1985) The mapping of visual space onto foveal striate cortex in the macaque monkey. *J. Neurosci.*, **5**, 890–902.

Drasdo, N. & Fowler, C.W. (1974) Non-linear projection of the retinal image in a wide-angle schematic eye. *Brit. J. Ophthalmol.*, **58**, 709–714.

Dumoulin, S.O. & Wandell, B.A. (2008) Population receptive field estimates in human visual cortex. *NeuroImage*, **39**, 647–660.

Fine, I., Wade, A.R., Brewer, A.A., May, M.G., Goodman, D.F., Boynton, G.M., Wandell, B.A. & MacLeod, D.I. (2003) Long-term deprivation affects visual perception and cortex. *Nat. Neurosci.*, **6**, 915–916.

Gattass, R., Nascimento-Silva, S., Soares, J.G.M., Lima, B., Jansen, A.K., Diogo, A.C.M., Farias, M.F., Botelho, M.M.E.P., Mariani, O.S., Azzi, J. & Fiorani, M. (2005) Cortical visual areas in monkeys: location, topography, connections, columns, plasticity and cortical dynamics. *Philos. T. Roy. Soc. B.*, **360**, 709–731.

Giannikopoulos, D.V. (2006) Dynamics and specificity of cortical map reorganization after retinal lesions. *Proc. Natl. Acad. Sci.*, **103**, 10805–10810.

Gilbert, C.D. & Li, W. (2012) Adult visual cortical plasticity. *Neuron*, **75**, 250–264.

Gilbert, C.D. & Wiesel, T.N. (1992) Receptive-field dynamics in adult primary visual-cortex. *Nature*, **356**, 150–152.

Haak, K.V., Cornelissen, F.W. & Morland, A.B. (2012) Population receptive field dynamics in human visual cortex. *Plos One*, **7**, e37686.

Harrison, L.M., Stephan, K.E., Rees, G. & Friston, K.J. (2007) Extra-classical receptive field effects measured in striate cortex with fMRI. *Neuro-Image*, **34**, 1199–1208.

Heinen, S.J. & Skavenski, A.A. (1991) Recovery of visual responses in foveal V1 neurons following bilateral foveal lesions in adult monkey. *Exp. Brain Res.*, **83**, 670–674.

Hendry, S.H. & Jones, E.G. (1986) Reduction in number of immunostained GABAergic neurones in deprived-eye dominance columns of monkey area 17. *Nature*, **320**, 750–753.

Horton, J.C. & Hocking, D.R. (1998) Monocular core zones and binocular border strips in primate striate cortex revealed by the contrasting effects of enucleation, eyelid suture, and retinal laser lesions on cytochrome oxidase activity. *J. Neurosci.*, **18**, 5433–5455.

Hubel, D.H. & Wiesel, T.N. (1959) Receptive fields of single neurones in the cat's striate cortex. *J. Physiol.*, **148**, 574–591.

Hubel, D.H. & Wiesel, T.N. (1974) Uniformity of monkey striate cortex: a parallel relationship between field size, scatter, and magnification factor. *J. Comp. Neurol.*, **158**, 295–305.

Kaas, J.H., Krubitzer, L.A., Chino, Y.M., Langston, A.L., Polley, E.H. & Blair, N. (1990) Reorganization of retinotopic cortical maps in adult mammals after lesions of the retina. *Science*, **248**, 229–231.

Keliris, G.A., Shmuel, A., Ku, S.P., Pfeuffer, J., Oeltermann, A., Steudel, T. & Logothetis, N.K. (2007) Robust controlled functional MRI in alert monkeys at high magnetic field: effects of jaw and body movements. *Neuro-Image*, **36**, 550–570.

LeVay, S., Connolly, M., Houde, J. & Van Essen, D.C. (1985) The complete pattern of ocular dominance stripes in the striate cortex and visual field of the macaque monkey. *J. Neurosci.*, **5**, 486–501.

Levin, N., Dumoulin, S.O., Winawer, J., Dougherty, R.F. & Wandell, B.A. (2010) Cortical maps and white matter tracts following long period of visual deprivation and retinal image restoration. *Neuron*, **65**, 21–31.

Logothetis, N.K., Guggenberger, H., Peled, S. & Pauls, J. (1999) Functional imaging of the monkey brain. *Nat. Neurosci.*, **2**, 555–562.

Masuda, Y., Dumoulin, S.O., Nakadomari, S. & Wandell, B.A. (2008) V1 projection zone signals in human macular degeneration depend on task, not stimulus. *Cereb. Cortex*, **18**, 2483–2493.

Morland, A.B., Baseler, H.A., Hoffmann, M.B., Sharpe, L.T. & Wandell, B.A. (2001) Abnormal retinotopic representations in human visual cortex revealed by fMRI. *Acta Psychol. (Amst)*, **107**, 229–247.

Murakami, I., Komatsu, H. & Kinoshita, M. (1997) Perceptual filling-in at the scotoma following a monocular retinal lesion in the monkey. *Visual Neurosci.*, **14**, 89–101.

Rosier, A.M., Arckens, L., Demeulemeester, H., Orban, G.A., Eysel, U.T., Wu, Y.J. & Vandesande, F. (1995) Effect of sensory deafferentation on immunoreactivity of Gabaergic cells and on Gaba receptors in the adult cat visual-cortex. *J. Comp. Neurol.*, **359**, 476–489.

Schumacher, E.H., Jacko, J.A., Primo, S.A., Main, K.L., Moloney, K.P., Kinzel, E.N. & Ginn, J. (2008) Reorganization of visual processing is related to eccentric viewing in patients with macular degeneration. *Restor. Neurol. Neuros.*, **26**, 391–402.

Smirnakis, S.M., Brewer, A.A., Schmid, M.C., Tolias, A.S., Schüz, A., Augath, M., Inhoffen, W., Wandell, B.A. & Logothetis, N.K. (2005) Lack of long-term cortical reorganization after macaque retinal lesions. *Nature*, **435**, 300–307.

Sunness, J.S., Liu, T. & Yantis, S. (2004) Retinotopic mapping of the visual cortex using functional magnetic resonance imaging in a patient with central scotomas from atrophic macular degeneration. *Ophthalmology*, **111**, 1595–1598.

Tootell, R.B., Switkes, E., Silverman, M.S. & Hamilton, S.L. (1988) Functional anatomy of macaque striate cortex. II. Retinotopic organization. *J. Neurosci.*, **8**, 1531–1568.

Van Essen, D.C. & Maunsell, J.H.R. (1983) Hierarchical organization and functional streams in the visual-cortex. *Trends Neurosci.*, **6**, 370–375.

Van Essen, D.C., Newsome, W.T. & Maunsell, J.H. (1984) The visual field representation in striate cortex of the macaque monkey: asymmetries, anisotropies, and individual variability. *Vision Res.*, **24**, 429–448.

Wade, A.R. & Rowland, J. (2010) Early suppressive mechanisms and the negative blood oxygenation level-dependent response in human visual cortex. *J. Neurosci.*, **30**, 5008–5019.

Wandell, B.A. & Smirnakis, S.M. (2009) Plasticity and stability of visual field maps in adult primary visual cortex. *Nat. Rev. Neurosci.*, **10**, 873–884.

Wandell, B.A., Chial, S. & Backus, B.T. (2000) Visualization and measurement of the cortical surface. *J. Cognitive Neurosci.*, **12**, 739–752.

Wandell, B.A., Dumoulin, S.O. & Brewer, A.A. (2007) Visual field maps in human cortex. *Neuron*, **56**, 366–383.

Zeki, S. & Shipp, S. (1988) The functional logic of cortical connections. *Nature*, **335**, 311–317.

Macaque area V2/V3 reorganization following homonymous retinal lesions

Yibin Shao[1], Georgios A. Keliris[1,2,3], Michael C. Schmid[4], Mark Augath[5], Nikos K. Logothetis[1,6], Stelios M. Smirnakis[7]

[1]Max-Planck Institute for Biological Cybernetics, Tübingen, Germany, [2]Bernstein Center for Computational Neuroscience, Tübingen, Germany, [3]BioImaging Laboratory, University of Antwerp, Antwerp, Belgium, [4]Ernst Strüngmann Institute (ESI) for Neuroscience in Cooperation with Max Planck Society, Frankfurt, Germany, [5]Institute for Biomedical Engineering, ETH Zurich, Switzerland, [6]Division of Imaging Science and Biomedical Engineering, University of Manchester, United Kingdom, [7]Baylor College of Medicine, Department of Neuroscience and Neurology, One Baylor Plaza, Houston TX, USA.

Corresponding author: Georgios A. Keliris

Max Planck Institute for Biological Cybernetics

Spemannstrasse 38, 72076, Tuebingen, Germany

georgios.keliris@tuebingen.mpg.de

Running title: Reorganization of V2/V3 after retinal lesions

Abstract

In the adult visual system, topographic reorganization of the primary visual cortex (V1) after retinal lesions has been extensively investigated. In contrast, the plasticity of higher-order/extrastriate areas following retinal lesions is less well studied. Here, we used fMRI to study reorganization of visual areas V2/V3 following the induction of permanent, binocular, homonymous retinal lesions in 4 adult macaque monkeys. We found that a few hours after the lesion, ~50% of the area V2/V3 lesion projection zone (LPZ) could already be modulated by visual stimuli. Furthermore, ~70% of the voxels that did not show visual modulation on the day of the lesion could be visually modulated 2 weeks later, and the mean modulation strength remained approximately stable thereafter for the duration of our observations (4-5 months). The distribution of eccentricities of visually modulated voxels inside the V2/V3 LPZ spanned a wider range post-lesion than pre-lesion, suggesting that neurons inside the LPZ reorganize by receiving input either from the foveal or the peripheral border of the LPZ, depending on proximity. Overall, we conclude that area V2/V3 of adult rhesus macaques displays a significant capacity for topographic reorganization following retinal lesions markedly exceeding the corresponding capacity of area V1.

Introduction

Understanding the detailed capacity of the adult visual system for plasticity is important as it may inform the design of rehabilitative treatments aiming to enhance visual recovery after injury.

Complete homonymous retinal injury eliminates the sensory input to retinotopically corresponding regions of visual cortex. Since the 1990s several studies have focused on the reorganization of the primary visual cortex (V1) after homonymous retinal lesions, producing in part conflicting results. Several studies reported substantial reorganization in the primary visual cortex of cats and monkeys following retinal lesions (Calford and others 2000; Giannikopoulos 2006; Gilbert and Li 2012; Gilbert and Wiesel 1992; Heinen and Skavenski 1991; Kaas and others 1990). Other reports however found minimal, if any, topographic changes (Horton and Hocking 1998; Murakami and others 1997; Smirnakis and others 2005). In a recent review, Wandell and Smirnakis (Wandell and Smirnakis 2009) suggested that electrophysiological recording selection bias influences receptive field assessment, largely explaining the disparity of the results. Similarly, several human fMRI case reports of patients with macular degeneration, suggest that human primary visual cortex undergoes large-scale reorganization (Baker 2005; Baker and others 2008; Dilks and others 2009; Schumacher and others 2008). Other studies however (Baseler and others 2011; Sunness and others 2004), including a recent comprehensive report on 16 patients (Baseler and others 2011), find no significant reorganization, or qualify the reported reorganization as being the result of task-dependent extra-retinal top-down feedback (Masuda and others 2008). For a

comprehensive review on the capacity of V1 for reorganization following retinal lesions see (Wandell and Smirnakis 2009). Overall, the weight of recent evidence (but see (Gilbert and Li 2012) for a dissenting view) suggests that minimal, if any, feed-forward reorganization occurs in the primary visual cortex of cats or primates following retinal lesions. However, much less is known about the capacity of extrastriate cortex for reorganization following retinal lesions, and this is the question we tackle in this work.

Visual responsiveness of areas V2/V3 is often thought to depend entirely on V1 input. This is largely based on the finding that transient inactivation of area V1 by cooling immediately eliminates more than 95% of visually driven activity seen in retinotopically corresponding locations of areas V2/V3 (Girard and Bullier 1989; Girard and others 1991; Schiller and Malpeli 1977). However, there is evidence that extrastriate cortex has the capacity to reorganize over longer time scales (weeks-months) following permanent area V1 aspiration lesions: a recent macaque study suggested that in the case of chronic V1 lesions visually driven BOLD responses can be elicited inside the lesion projection zone of areas V2 and V3 (Schmid and others 2009). Furthermore, it was recently shown that this persistent activity as well as the monkeys' residual visually based detection performance ("blindsight"), are mediated by inputs from the lateral geniculate nucleus (Schmid and others 2010). An fMRI study in a human subject with hemianopia following area V1 injury also reports that visually driven activity persists in areas V2, V3 and V3A, arguing that this is likely the result of cortical reorganization (Baseler and others 1999).

Although literature suggests that extrastriate cortex has the capacity for reorganization after V1 lesions, the question of what happens after retinal lesions remains open. It is

possible that extrastriate cortex has different capacity for reorganization depending on the mechanism of de-afferentiation (retina vs V1). For one, subcortical pathways are thought to mediate the activity of areas V2 and V3 in the absence of V1 input (Schmid and others 2010; Schmid and others 2009), but input to these pathways is silenced in the case of retinal lesions. Reports from the literature of "filling-in" studies suggest that in higher areas, under the right conditions, visual responses can be seen in cortical locations that are far away from the visual stimulus. For example, De Weerd et. al. showed that the responses of extrastriate V2/V3 neurons whose receptive fields are contained inside an area devoid of visual stimulation (artificial scotoma) increase within seconds to reach a level comparable to that elicited by direct visual stimulation (De Weerd and others 1995). Activation and perhaps enhancement of these pathways may be able to support reorganization.

In a recent case study on a juvenile macaque monkey with congenital dense bilateral macular degeneration (Shao and others 2013), we reported that extensive reorganization was seen in area V5/MT. Here, we extend these results by using fMRI to study whether areas V2/V3 reorganize following bilateral homonymous retinal lesions induced by photocoagulation in adult macaques. The substantial topographic reorganization of V2/V3 demonstrated here is markedly different from previous findings in V1 of the same animals, which showed minimal, if any, reorganization following retinal lesions (Smirnakis and others 2005). We argue that, in contrast to area V1, significant reorganization occurs in area V2/V3 under these conditions.

Materials and Methods

Subjects

Four healthy adult Macaca mulatta (M1, M2, M3 and M4) were used for these experiments. The experimental and surgical procedures were performed with care, in full compliance with the German Law for the Protection of Animals, the European Community guidelines for the care and use of laboratory animals (EUVS 86/609/EEC), and the recommendations of the Weatherall report for the use of non-human primates in research. The regional authorities (Regierungspräsidium Tübingen) approved our experimental protocol and the institutional representatives for animal protection supervised all procedures.

The monkeys were anesthetized during the fMRI experiments. Details on the anesthesia protocol have been given previously (Logothetis and others 1999). Briefly, the animals were intubated after induction with fentanyl (31 µg/kg), thiopental (5 mg/kg) and succinylcholine chloride (3mg/kg); anesthesia was maintained with isoflurane (M2 and M4) or remifentanyl (0.5-2 µg/kg/min, M1 and M3). Mivacurium chloride (5–7mg/kg/ h) was used after induction to ensure the suppression of eye movements. Heart rate and blood oxygen saturation were monitored continuously with a pulse-oxymeter. Body temperature was kept at 38-39°.

Homonymous retinal lesions were induced by using a photocoagulation laser (NIDEKGYC-2000; 532nm) under general anesthesia (Fig. 1A) as described in Smirnakis *et al.*, 2005 (Smirnakis and others 2005). Histological results confirmed that the photoreceptor and bipolar cell layers as well as most of the ganglion cell layer of the extrafoveal retina were destroyed (Fig. 1B). Histological confirmation was obtained in two of the four animals. Animal fundi were photographed in each experimental session,

and we confirmed that all lesions remained stable throughout the course of the experiments (see Smirnakis et al., 2005 for the details).

Figure 1

Stimulus

Stimuli were presented monocularly, at resolution of 640 × 480 pixels with a 60 Hz frame rate using an SVGA fibre-optic system (AVOTEC). Stimuli were centered on the fovea by using a modified fundus camera. Animals were fitted appropriate lenses to ensure the stimulus remained in focus. Standard expanding ring stimuli (outer radius expanded from either 0.3° or 0.9° to 6.9° in steps of 0.6°, i.e. 12 or 11 annuli, frame interval, 6sec) and rotating wedge (90° wedges rotated in steps of 30°, i.e. 12 annuli, frame interval, 6sec) were presented to the subjects monocularly, always in the same eye for each animal. The full retinotopic maps were obtained pre-lesion but after lesioning only the eccentricity maps were followed. The first measurement was obtained on the day of the lesion. The earliest subsequent measurement was obtained 14 days later to comply with the accepted animal protocol.

One important control condition involved presenting the same expanding ring stimuli to the subjects and at the same time occluding a region in the normal half of the visual field. This region was designed to mirror the approximate location of the retinal lesion. We refer to this as the "artificial scotoma" (AS) condition. For all four subjects, the ASs were centered at (3.7°, 0) or (-3.7°, 0), on the opposite side of the scotoma resulting from the retinal lesion, and had a diameter of 3.7°.

FMRI experiments were performed on a 4.7T vertical scanner (Bruker Biospec, Bruker Biospin GmbH, Ettlingen, Germany). Multi-slice fMRI was performed by the use of 8 segmented gradient-recalled echo-planar imaging (EPI). The acquisition parameters were TE = 20 ms, TR = 750 or 805 ms, flip angle = 40°. Either 15 or 17 axial slices were collected at $1 \times 1\text{mm}^2$ in-plane resolution and 2-mm thickness. A full-brain anatomical scan was acquired before lesioning at $0.5 \times 0.5 \times 0.5\text{mm}^3$ resolution for co-registration with the EPI images by using an MDEFT sequence (Keliris and others 2007; Logothetis and others 1999).

Data analysis

FMRI data were reconstructed and imported into a MATLAB based toolbox (mrVista; http://white. stanford.edu/software/) (Amano and others 2009; Levin and others 2010). The gray-white matter boundary was manually segmented using itkGray from the high resolution 3D-MDEFT anatomical images, and 3D cortical surface and flat mesh models were created and realigned with the functional data by using mrMesh/mrVista (Wandell and others 2000).

In a typical experiment 5 to 10 repeats of the expanding ring and rotating wedge stimulation paradigm were performed and the average BOLD signal time course was generated. To obtain the retinotopic maps we have used the travelling wave method (Engel and others 1997). The strength of the visual modulation was assessed using the measure of coherence, computed with the expanding ring stimuli. Coherence is defined as the Fourier amplitude of the BOLD signal at the stimulus presentation frequency (12 or 11 in our experiments) divided by the square root of the power over a range (12 for

this analysis) of nearby frequencies (Smirnakis and others 2005). The retinotopic maps were then fitted into a template of expected eccentricity and angle maps (atlas fitting) (Dougherty and others 2003). During this procedure, the four sides of the visual field map, from fovea to periphery and from upper to lower vertical meridian were defined manually by simultaneously looking at angle and eccentricity maps, and were found to obey expected anatomical landmarks. For example, the dorsal V1/V2 border was confirmed to lay ~2mm from the lip of the lunate, the ventral V1/V2 border along the inferior occipital sulcus (Brewer and others 2002), and the dorsal V2/V3 boundary at the bottom of the lunate sulcus. The calcarine sulcus was at ~6.5^0 eccentricity as reported in (Gattass and others 2005). The fitting algorithm deforms these templates to match the eccentricity and angle data, allowing local deformations but no tears or folds in the atlas. The atlas with the least error compared with the data was generated, following (Dougherty and others 2003). Visual inspection confirmed no major errors.

Results

Defining the area V2/V3 lesion projection zone (LPZ)

Before lesioning the retina, retinotopic maps were measured using standard expanding rings and rotating wedge stimuli (see methods). As shown in Fig.2A,B, all subjects showed normal retinotopic organization. The V1/V2 and V2/V3 borders were identified by the location of the vertical and horizontal meridians respectively (Fig.2B). The border location was confirmed anatomically, as in the macaque visual area boundaries have stereotypical anatomical locations (see methods).

Following a homonymous retinal lesion, parts of the visual cortex become deafferented. This results in a series of lesion projection zones (LPZ), one per retinotopic visual area. Our goal was to define the LPZ in areas V2/V3 and follow how the strength of its visual modulation changed over time. Since the retinal lesions cross the horizontal meridian (shared by V2/V3) we expected to find joined LPZs along the V2-V3 border both dorsally and ventrally.

To find the V2/V3 LPZ we performed the following steps: 1) we selected V1 voxels with coherence below threshold (we set the threshold to 0.28, which corresponds to noise at our settings) on the day of the lesion, and merged them to define the V1 LPZ (Fig. 2C,D). Note that the area V1 LPZ has been shown to remain unchanged over time in this data set (Smirnakis and others 2005), 2) we fitted the pre-lesion eccentricity and polar angle maps into an atlas (see methods) using the process described in (Dougherty and others 2003), and 3) based on the pre-lesion retinotopic atlas-fit, the voxels in V2/V3 that corresponded retinotopically to the voxels belonging to the V1 LPZ, to within 0.05° of eccentricity and polar angle (on the atlas) were selected. These selected voxels were highly clustered and continuous inside the dorsal and ventral V2/V3. They were then merged to define V2/V3 LPZ (Fig. 2C,D). Once the V2/V3 LPZ was identified on the anatomical template, all quantitative analysis was done on the original data derived from voxels located inside the anatomical region corresponding to the LPZs. For each monkey, we followed the same procedure in order to define the artificial scotoma projection zones (ASPZ) in areas V1 and V2/V3 on the non-deafferented hemisphere (ipsilateral to the scotoma). Note that the monkeys were always scanned in the same position with the help of implanted fMRI-compatible headposts, and that the

LPZ was defined on the high resolution anatomical scan that serves as a template for aligning the functional data. These procedures assured we could follow the activity of the same anatomical region over time.

Figure 2

Visual modulation inside the V2/V3 LPZ

The retinal lesion crosses the horizontal meridian and so the V2/V3 LPZ is split into two parts, one across the ventral and the other across the dorsal V2/V3 border (Fig.2C). From the coherence maps (Fig.2C) it is evident that even on the day of the lesion (D1), the V2/V3 LPZs are on average significantly visually modulated. Therefore the V2/V3 LPZ appears to receive visually modulated input outside the retinotopically corresponding V1 LPZ, which shows no significant visual modulation over its entire extent (Smirnakis and others 2005). The average fraction of voxels inside the V2/V3 LPZ that were visually modulated (> 2 standard deviations above noise level) on the day of the lesion (D1) was 50.4% ± 12% (standard deviation across subjects). This was consistent with observations made in the artificial scotoma (AS) control condition: the average fraction of voxels that were visually modulated inside the ASPZ was similar at 53.5% ±10% (standard deviation, Fig. 3).

Figure 3

Importantly, in addition to the voxels that were visually modulated immediately after the lesion, a fraction of voxels that were not significantly modulated on the day of the lesion (D1) recovered the ability to be visually modulated by day 14 post lesion (D14, Fig. 2D). We compared the distribution of coherence values measured across all the LPZ voxels pre-lesion (PRE) with the distribution on the day of the lesion (D1) and 14 days post-lesion (D14) (Fig. 4B). Because the overall level of the BOLD signal can fluctuate on different measuring sessions, the coherence of each voxel inside the LPZ was expressed as a fraction of the average coherence computed across all voxels within the non-deafferented region of V2/V3 in the same hemisphere (normalized coherence). Note that the distribution of normalized coherences derived from all voxels inside the V2/V3 LPZ (Fig. 4B) shifts initially toward lower coherence values on the day of the lesion (D1), but returns close to pre-lesion levels 14 days later (D14). Kruskal-wallis tests were performed comparing average normalized coherence over time (PRE, D1 and D14) across all of the V2v/V3v and V2d/V3d LPZ voxels in all 4 monkeys. There were significant differences of coherence over time in both the dorsal and ventral LPZ (H=32.54, $p<10^{-7}$ for V2v/V3v LPZ and H=17.83, $p<10^{-4}$ for V2d/V3d LPZ). Statistics were performed using the functional voxels (a total of 58, 45 voxels for the V2v/V3v and V2d/V3d LPZ respectively, across all monkeys). Post-hoc pairwise comparisons showed significant differences between the mean level of coherence pre-lesion (PRE) and day 1 (D1), D1 and day 14 (D14) for both LPZs, as well as the differences between PRE and D14 for V2d/V3d LPZ ($p<0.05$; Fig. 4B). In fact, the number of voxels with low coherence inside the V2/V3 LPZ also changes following the lesion. The average fraction of voxels inside the V2/V3 LPZ that had low coherence (<2 standard deviations above

noise level) across subjects was 14.1% ±8% (standard deviation) pre-lesion, increased to 49.6% ±12% on D1, and dropped back to 14.8% ±9% on D14, close to pre-lesion levels.

To study how the strength of visual modulation inside the LPZ of area V2/V3 evolves over time, we focused on voxels that were in the central area of the LPZs. These voxels were selected on the pre-lesion atlas. For the sake of comparison, the coherence of each voxel in the LPZ was normalized by the average coherence across voxels of the non-deafferented control V2/V3 ROI as described before. As shown in Fig. 4C left two panels, the mean coherence of these voxels was high pre-lesion, dropped on the lesion day, increased markedly as early as two weeks after the lesion and then remained approximately at the same level over time. The same Kruskal-wallis tests were performed comparing average normalized coherence of voxels over time across all of the central V2v/V3v and V2d/V3d LPZ in all 4 monkeys. There were significant differences of coherence over time in both the dorsal and ventral LPZ (H=54.78, $p<10^{-8}$ for V2v/V3v LPZ and H=18.64, $p<10^{-5}$ for V2d/V3d LPZ). As control, ROIs outside but close to the LPZs were selected. The coherence of these voxels over time were compared. Kruskal-wallis tests showed no significant differences (Fig. 4C right two panels).

Fig. 4D, top row, plots the percent modulation of the BOLD signal as a function of the stimulus cycle of voxels taken from the center of monkey M1's V2v/V3v LPZ. Note how the strength of the visual modulation initially drops following the lesion (D1) but then recovers over time from day 1 (D1) to day 14 (D14). Fig. 4D, bottom row, shows the signal amplitude as a function of temporal frequency for the same voxels.

This contrasts, with the case of the ASPZ where the coherence was decreased and remained stable overtime (Fig. 3), with the areas adjacent to the LPZ where the signal remained unchanged (Fig. 4C right two panels), and also with V1 LPZ where the signal dropped to noise levels following the lesion and did not change significantly over time (Smirnakis and others 2005).

Overall, across all four subjects, we found that the strength of the visual modulation inside the V2/V3 LPZ increased over time following the lesion, arguing for potential reorganization in area V2/V3.

Figure 4

Eccentricity map changes in V2/V3 LPZ

The next step was to look for the source of the input leading to the increase in visual modulation inside the V2/V3 LPZ over time. Although part of the sensory input of the voxels inside the LPZ has been cut off because of the retinal lesion, neurons inside the LPZ may still receive input from visual field locations that are outside the border of the scotoma. To test this, we compared the range of eccentricities of the voxels inside the V2/V3 LPZ before and 14 days after the lesion. We focused on the voxels whose strength of visual modulation recovered as a function of time following the lesion. Such voxels were from the center of the V2/V3 LPZ based on pre-lesion retinotopy, and were modulated above noise level both before and 14 days following the lesion. For each subject, we performed the eccentricity analysis in the dominant (largest) V2/V3 LPZ, dorsal or ventral. This is compared to controls (Fig. 5A, top row) from an approximately

iso-angular non-deafferented area V2 ROI in each subject (see Fig. 2). Eccentricity measurements in control ROIs (Fig. 5A, top row) demonstrate the reliability of this analysis. As expected, all control ROIs showed strong correlation between eccentricities measured pre-lesion and on day 14, with slopes near one (b=1.54, 0.98, 0.71, 0.94; R^2=0.91, 0.93, 0.79, 0.86; p<10^{-7} for M1, M2, M3 and M4 respectively, illustrated in dashed lines). Fig. 5A, bottom row presents the eccentricity scatter plots of voxels inside the dominant V2/V3 LPZ before and after the lesion. Voxel eccentricities pre-lesion were significantly correlated with eccentricities measured on day 14 all 4 subjects, but slopes were significantly smaller than one (b=0.23, 0.56, 0.3, 0.51; R^2=0.22, 0.34, 0.28, 0.47; p<0.01 for M1, M2, M3 and M4 respectively; illustrated in dashed lines). Overall, the eccentricities inside the LPZ span a wider range following the lesion compared to pre-lesion for each subject. Voxels with small eccentricity pre-lesion tend to have smaller eccentricity after the lesion, while, voxels with large eccentricity pre-lesion tend to have larger eccentricity after the lesion.

Distribution of eccentricity from voxels in the central V2/V3 LPZ (same voxels as panel A, bottom row) across all subjects pre-lesion and post-lesion were plotted in Fig. 5B. Because the retinotoppy of each LPZ is different. To align the LPZs, the mean eccentricity of the central V2/V3 LPZ pre-lesion was first subtracted for each subject, the relative eccentricities were then accumulated together across subjects. The distribution pre-lesion is significantly different from post-lesion (p<0.01). There are more instances of lower and higher eccentricities in the V2/V3 LPZ post-lesion, but less in the middle, compared with pre-lesion data. This agrees with panel A, bottom row, suggests that lateral inputs are likely responsible for the activation of the V2/V3 LPZ region.

Neurons inside the LPZ may regain their activity by receiving input either from the foveal or the peripheral border of the LPZ, depending on which one is closer.

Figure 5

Discussion

We found that the lesion projection zone (LPZ) in area V2/V3 could be visually modulated at the first post-lesion imaging time point, 2-6 hours following retinal photocoagulation. Approximately ~50% ± 12% (standard deviation) of the voxels inside the V2/3 LPZ were visually modulated 2-6hrs post-lesion, similar to the fraction observed inside the V2/V3 projection zone of the artificial scotoma control (ASPZ). In contrast, no visually driven activity was seen inside the V1 LPZ of the same animals (Smirnakis and others 2005). These observations are consistent with DeWeerd et al. (De Weerd and others 1995), who showed that multi-unit activity can be elicited in area V2 and V3 but not area V1 locations, if distant surround is visually stimulated. A dynamic change in the balance between excitation and inhibition affecting the range over which receptive fields receive inputs may be the cause of this relatively rapid adaptation (Knierim and van Essen 1992). Given its rapid time course, this phenomenon is likely to be mediated by pre-existing wiring, although we cannot exclude conclusively the possibility that plasticity mechanisms operating over the course of several hours may play a role.

Our results show that, over longer time periods, V2/V3 has a noticeable capacity for reorganization. Overall, ~70% of the V2/V3 LPZ voxels that do not show visual modulation on the day of the lesion (D1) can be visually modulated two weeks later. The mean coherence of V2/V3 LPZ voxels whose activity drops hours after the lesion (D1) increases markedly by two weeks post-lesion and remains approximately at the same level thereafter (see Fig. 4C). In marked contrast, visually driven activity does not recover inside the area V1 LPZ, whose border remains stable to within 1mm (Smirnakis and others 2005). Therefore the increase in the strength of visual modulation inside the V2/V3 LPZ is unlikely to be caused by area V1 recovery or even by significant retinal surround recovery, which presumably would first leave a signature in area V1.

Fig. 5A suggests that following the retinal lesion, the eccentricities of visually modulated voxels inside the V2/V3 LPZ span a wider range than pre-lesion. The form of the eccentricity change suggests that neurons inside the LPZ may reorganize by receiving intra-areal input either from the foveal or the peripheral border of the LPZ, depending on which one is closer. It is likely that this plastic reorganization is mediated by local cortico-cortical connections between the V2/V3 LPZ and its surround. Strengthening of projections from the surround of the V1 LPZ to area V2 may also play a role. We believe that similar processes likely operate along iso-angular lines. However, since we followed reorganization just by using expanding/contracting ring stimuli, we cannot definitively prove this.

Subcortical projections from the surround of the retinal lesion itself are not likely to play a major role, as they would first be expected to influence the extent of the V1 LPZ, which does not change. Trans-callosal connections between retinotopically

corresponding locations across hemispheres are also unlikely to play a major role as: 1) one would expect the range of eccentricities represented insight the LPZ to approximately match the pre-lesion values, which is not the case (Fig. 5), and 2) in some of the experiments an artificial scotoma was presented on the side contralateral to the actual scotoma, depriving the contralateral cortex from retinotopically corresponding visual input. Scenarios involving higher areas and pathways involving feedback are also unlikely as the monkeys were under anesthesia during the experiments.

It is interesting to speculate on the difference between V2/V3 reorganization following a retinal lesion versus following an area V1 lesion (Schmid and others 2009). In the retinal case, activity inside V2/V3 LPZ returns to nearly normal levels (Fig. 4). By contrast Schmid et al. showed that visual modulation strength in area V2/V3 following a V1 lesion returns to only ~20-30% of prior activity levels (Schmid and others 2009) and depends mostly on subcortical projections from the LGN (Schmid and others 2010). This difference is surprising in view of the fact that retinotopically corresponding parts of area V2/V3 were visually deprived in both cases, and V2/V3 LPZ size was commensurate in both studies. This suggests that, the existence of healthy V1 cortex and its upstream connections may be important for potentiating part of the reorganization seen in extrastriate areas after retinal lesions. Alternatively, the existence of functional retinotopically corresponding subcortical inputs, which are preserved in the case of the V1 lesion but silenced in the case of the retinal lesion, may limit the ability of lateral intra-areal connections to reorganize.

Human subjects suffering from macular degeneration exhibit perceptual filling-in in their blind visual field as well as an associated distortion of visual space (Burke 1999; Gerrits

and Timmerman 1969; Kapadia and others 1994; Zur and Ullman 2003). It has been argued that primary visual cortex is able to reorganize (Calford and others 2003; Darian-Smith and Gilbert 1994; 1995) and could provide a contribution to this phenomenon (Gilbert and Li 2012). However, the degree of V1 reorganization following retinal lesions has been questioned (Horton and Hocking 1998; Murakami and others 1997; Smirnakis and others 2005; Wandell and Smirnakis 2009), and De Weerd et al.'s filling-in study in animals with intact visual system suggests that higher areas may be involved. Our results suggest that adult extrastriate cortex exhibits significant capacity for reorganization following retinal injury, and may potentially contribute to the phenomenon of perceptual "filling-in" in subjects with retinal lesions.

Notes

Conflict of Interest: None declared.

References

Amano K, Wandell BA, Dumoulin SO. 2009. Visual field maps, population receptive field sizes, and visual field coverage in the human MT+ complex. Journal of Neurophysiology 102(5):2704-18.

Baker CI. 2005. Reorganization of Visual Processing in Macular Degeneration. Journal of Neuroscience 25(3):614-618.

Baker CI, Dilks DD, Peli E, Kanwisher N. 2008. Reorganization of visual processing in macular degeneration: Replication and clues about the role of foveal loss. Vision Research 48(18):1910-1919.

Baseler HA, Gouws A, Haak KV, Racey C, Crossland MD, Tufail A, Rubin GS, Cornelissen FW, Morland AB. 2011. Large-scale remapping of visual cortex is absent in adult humans with macular degeneration. Nature Neuroscience 14(5):649-655.

Baseler HA, Morland AB, Wandell BA. 1999. Topographic organization of human visual areas in the absence of input from primary cortex. Journal of Neuroscience 19(7):2619-2627.

Brewer AA, Press WA, Logothetis NK, Wandell BA. 2002. Visual areas in macaque cortex measured using functional magnetic resonance imaging. Journal of Neuroscience 22(23):10416-26.

Burke W. 1999. Psychophysical observations concerned with a foveal lesion (macular hole). Vision Research 39(14):2421-7.

Calford MB, Wang C, Taglianetti V, Waleszczyk WJ, Burke W, Dreher B. 2000. Plasticity in adult cat visual cortex (area 17) following circumscribed monocular lesions of all retinal layers. Journal of Physiology-London 524(2):587-602.

Calford MB, Wright LL, Metha AB, Taglianetti V. 2003. Topographic plasticity in primary visual cortex is mediated by local corticocortical connections. The Journal of neuroscience : the official journal of the Society for Neuroscience 23(16):6434-42.

Darian-Smith C, Gilbert CD. 1994. Axonal sprouting accompanies functional reorganization in adult cat striate cortex. Nature 368(6473):737-40.

Darian-Smith C, Gilbert CD. 1995. Topographic reorganization in the striate cortex of the adult cat and monkey is cortically mediated. The Journal of neuroscience : the official journal of the Society for Neuroscience 15(3 Pt 1):1631-47.

De Weerd P, Gattass R, Desimone R, Ungerleider LG. 1995. Responses of cells in monkey visual cortex during perceptual filling-in of an artificial scotoma. Nature 377(6551):731-4.

Dilks DD, Baker CI, Peli E, Kanwisher N. 2009. Reorganization of visual processing in macular degeneration is not specific to the "preferred retinal locus". Journal of Neuroscience 29(9):2768-73.

Dougherty RF, Koch VM, Brewer AA, Fischer B, Modersitzki J, Wandell BA. 2003. Visual field representations and locations of visual areas V1/2/3 in human visual cortex. Journal of Vision 3(10):586-98.

Engel SA, Glover GH, Wandell BA. 1997. Retinotopic organization in human visual cortex and the spatial precision of functional MRI. Cerebral Cortex 7(2):181-92.

Gattass R, Nascimento-Silva S, Soares JGM, Lima B, Jansen AK, Diogo ACM, Farias MF, Botelho MMEP, Mariani OS, Azzi J et al. . 2005. Cortical visual areas in monkeys: location, topography, connections, columns, plasticity and cortical dynamics. Philosophical Transactions of the Royal Society B: Biological Sciences 360(1456): 709-731.

Gerrits HJ, Timmerman GJ. 1969. The filling-in process in patients with retinal scotomata. Vision Research 9(3):439-42.

Giannikopoulos DV. 2006. Dynamics and specificity of cortical map reorganization after retinal lesions. Proceedings of the National Academy of Sciences 103(28):10805-10810.

Gilbert CD, Li W. 2012. Adult visual cortical plasticity. Neuron 75(2):250-64.

Gilbert CD, Wiesel TN. 1992. Receptive-Field Dynamics in Adult Primary Visual-Cortex. Nature 356(6365):150-152.

Girard P, Bullier J. 1989. Visual activity in area V2 during reversible inactivation of area 17 in the macaque monkey. Journal of Neurophysiology 62(6):1287-302.

Girard P, Salin PA, Bullier J. 1991. Visual activity in areas V3a and V3 during reversible inactivation of area V1 in the macaque monkey. Journal of Neurophysiology 66(5): 1493-503.

Heinen SJ, Skavenski AA. 1991. Recovery of Visual Responses in Foveal V1 Neurons Following Bilateral Foveal Lesions in Adult Monkey. Experimental Brain Research 83(3): 670-674.

Horton JC, Hocking DR. 1998. Monocular core zones and binocular border strips in primate striate cortex revealed by the contrasting effects of enucleation, eyelid suture, and retinal laser lesions on cytochrome oxidase activity. The Journal of neuroscience : the official journal of the Society for Neuroscience 18(14):5433-55.

Kaas JH, Krubitzer LA, Chino YM, Langston AL, Polley EH, Blair N. 1990. Reorganization of retinotopic cortical maps in adult mammals after lesions of the retina. Science 248(4952):229-31.

Kapadia MK, Gilbert CD, Westheimer G. 1994. A quantitative measure for short-term cortical plasticity in human vision. The Journal of neuroscience : the official journal of the Society for Neuroscience 14(1):451-7.

Keliris GA, Shmuel A, Ku SP, Pfeuffer J, Oeltermann A, Steudel T, Logothetis NK. 2007. Robust controlled functional MRI in alert monkeys at high magnetic field: Effects of jaw and body movements. Neuroimage 36(3):550-570.

Knierim JJ, van Essen DC. 1992. Neuronal responses to static texture patterns in area V1 of the alert macaque monkey. Journal of Neurophysiology 67(4):961-80.

Levin N, Dumoulin SO, Winawer J, Dougherty RF, Wandell BA. 2010. Cortical Maps and White Matter Tracts following Long Period of Visual Deprivation and Retinal Image Restoration. Neuron 65(1):21-31.

Logothetis NK, Guggenberger H, Peled S, Pauls J. 1999. Functional imaging of the monkey brain. Nature Neuroscience 2(6):555-62.

Masuda Y, Dumoulin SO, Nakadomari S, Wandell BA. 2008. V1 Projection Zone Signals in Human Macular Degeneration Depend on Task, not Stimulus. Cerebral Cortex 18(11): 2483-2493.

Murakami I, Komatsu H, Kinoshita M. 1997. Perceptual filling-in at the scotoma following a monocular retinal lesion in the monkey. Visual Neuroscience 14(1):89-101.

Schiller PH, Malpeli JG. 1977. Effect of Striate Cortex Cooling on Area 18 Cells in Monkey. Brain Research 126(2):366-369.

Schmid MC, Mrowka SW, Turchi J, Saunders RC, Wilke M, Peters AJ, Ye FQ, Leopold DA. 2010. Blindsight depends on the lateral geniculate nucleus. Nature 466(7304):373-377.

Schmid MC, Panagiotaropoulos T, Augath MA, Logothetis NK, Smirnakis SM. 2009. Visually driven activation in macaque areas V2 and V3 without input from the primary visual cortex. PLoS One 4(5):e5527.

Schumacher EH, Jacko JA, Primo SA, Main KL, Moloney KP, Kinzel EN, Ginn J. 2008. Reorganization of visual processing is related to eccentric viewing in patients with macular degeneration. Restorative Neurology and Neuroscience 26(4-5):391-402.

Shao Y, Keliris GA, Papanikolaou A, Fischer MD, Zobor D, Jagle H, Logothetis NK, Smirnakis SM. 2013. Visual cortex organisation in a macaque monkey with macular degeneration. The European journal of neuroscience 38(10):3456-64.

Smirnakis SM, Brewer AA, Schmid MC, Tolias AS, Schüz A, Augath M, Inhoffen W, Wandell BA, Logothetis NK. 2005. Lack of long-term cortical reorganization after macaque retinal lesions. Nature 435(7040):300-307.

Sunness JS, Liu T, Yantis S. 2004. Retinotopic mapping of the visual cortex using functional magnetic resonance imaging in a patient with central scotomas from atrophic macular degeneration. Ophthalmology 111(8):1595-1598.

Wandell BA, Chial S, Backus BT. 2000. Visualization and measurement of the cortical surface. Journal of Cognitive Neuroscience 12(5):739-752.

Wandell BA, Smirnakis SM. 2009. Plasticity and stability of visual field maps in adult primary visual cortex. Nature Reviews Neuroscience 10(12):873-84.

Zur D, Ullman S. 2003. Filling-in of retinal scotomas. Vision Research 43(9):971-82.

Figure Legends
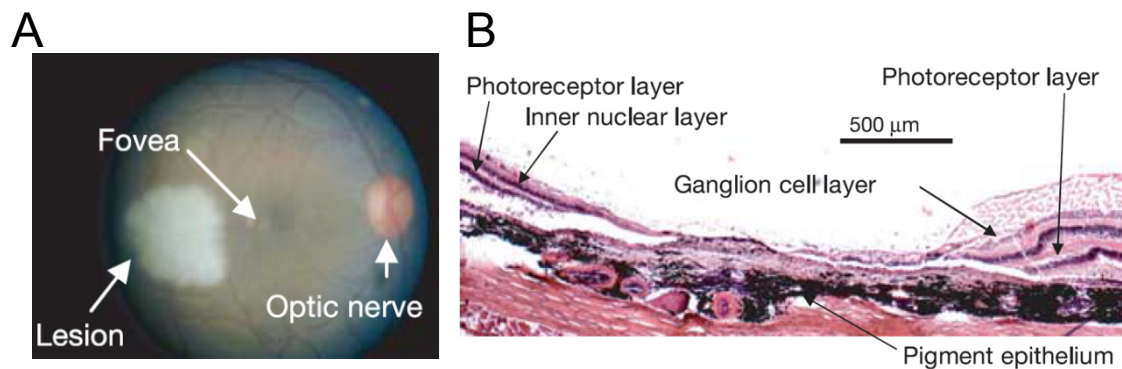
Fig.1 A. Retinal lesion. The right retinal fundus 1-2 hours following photocoagulation. The lesion appears pale white. Note that a corresponding lesion was made on the other side of the fovea in the left eye resulting in a homonymous left visual field scotoma (data not shown). Visual stimulation was always presented monocularly, on the right eye for this monkey, thus avoiding activity changes that may be due to potential eye misalignment. **B.** Haematoxylin-eosin stain of a 15µm thick section through the lesion in the right eye, where the visual stimulus was presented. Note the complete destruction of the photoreceptor layer, and the near complete destruction of the inner nuclear and ganglion cell layers (see Fig. 1 in reference (Smirnakis and others 2005) for a full description).
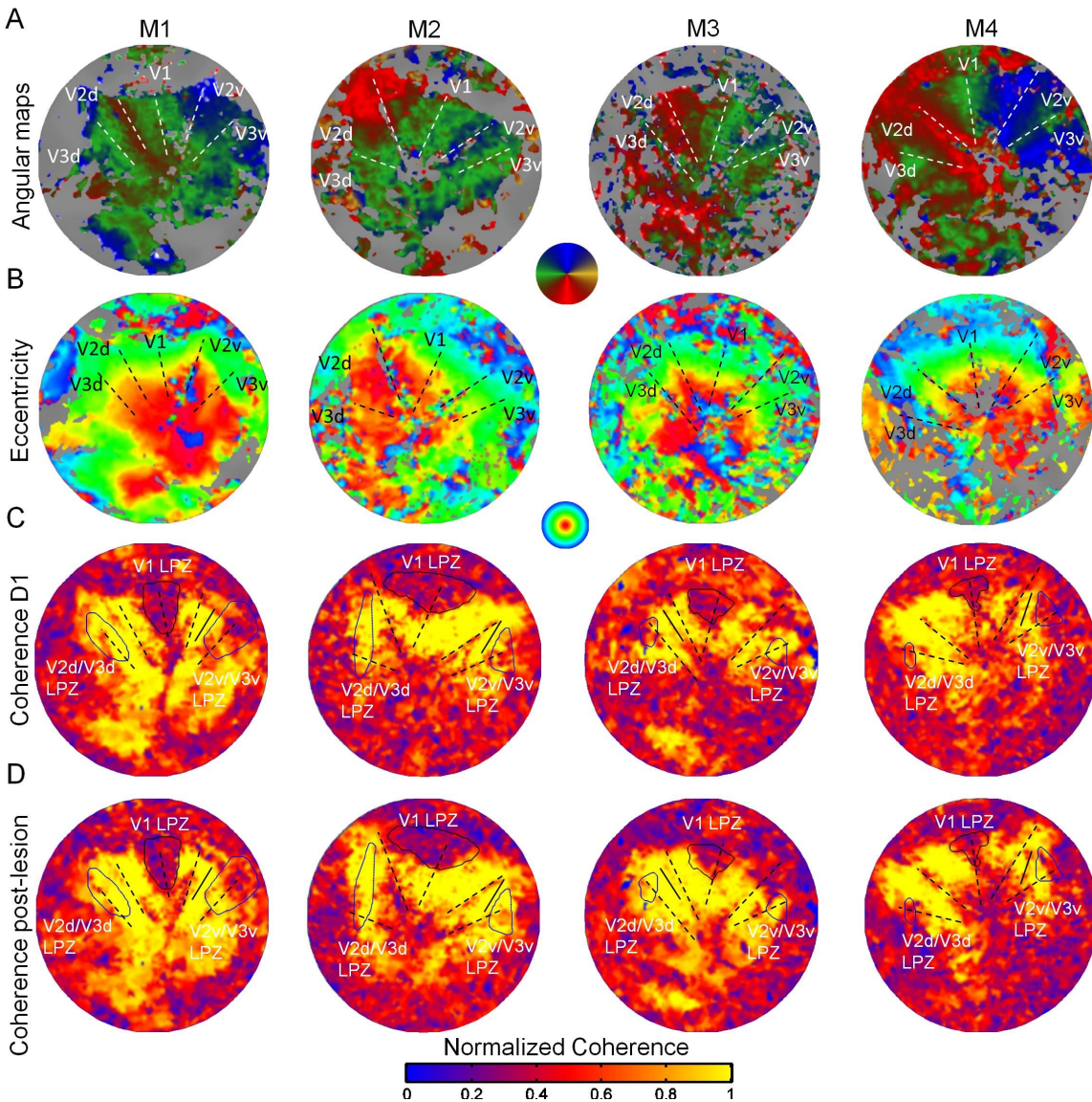
Fig.2 Pre-lesion retinotopy and LPZ definition. A. Polar angle and **B.** eccentricity functional activation maps obtained pre-lesion and overlaid on the flattened representation of early visual cortex in monkeys M1, M2, M3 and M4. **C.** Normalized coherence maps of the hemispheres affected by the retinal lesion, obtained on the day of the lesion (D1) and **D.** at least 14 days post-lesion using the ring stimulus (14 days

post-lesion for monkeys M1, M3 and M4, 62 days post-lesion for M2). The V1 LPZs were selected directly based on the coherence maps (see methods). V2v/V3v and V2d/V3d LPZs were defined on the atlas fit of the pre-lesion retinotopic maps (Dougherty and others 2003), by extracting voxels in areas V2 and V3 with similar eccentricities and polar angles as voxels in the V1 LPZ (see methods). The color map of coherence is normalized with respect to the average coherence across the voxels of an approximately iso-angular non-deafferented area V2 ROI (solid black line segment). The V1/V2 and V2/V3 borders and the V1 horizontal meridian are shown as dashed lines.
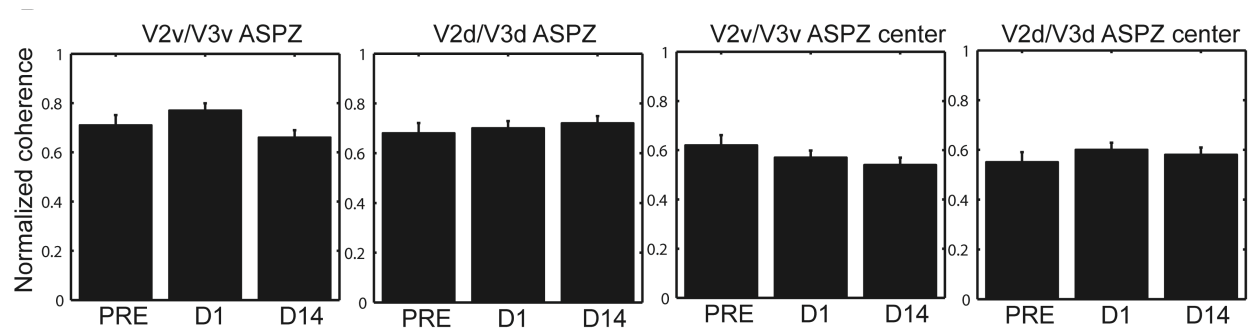
Fig.3 Coherence changes inside ASPZ. Mean normalized coherence across all voxels (the left two panels) and the center (the right two panels) of the V2v/V3v and V2d/V3d LPZ pre-lesion, as well as on day 1 and day 14 following the lesion, plotted across all monkeys. Kruskal-wallis tests were performed, no significant differences were found.
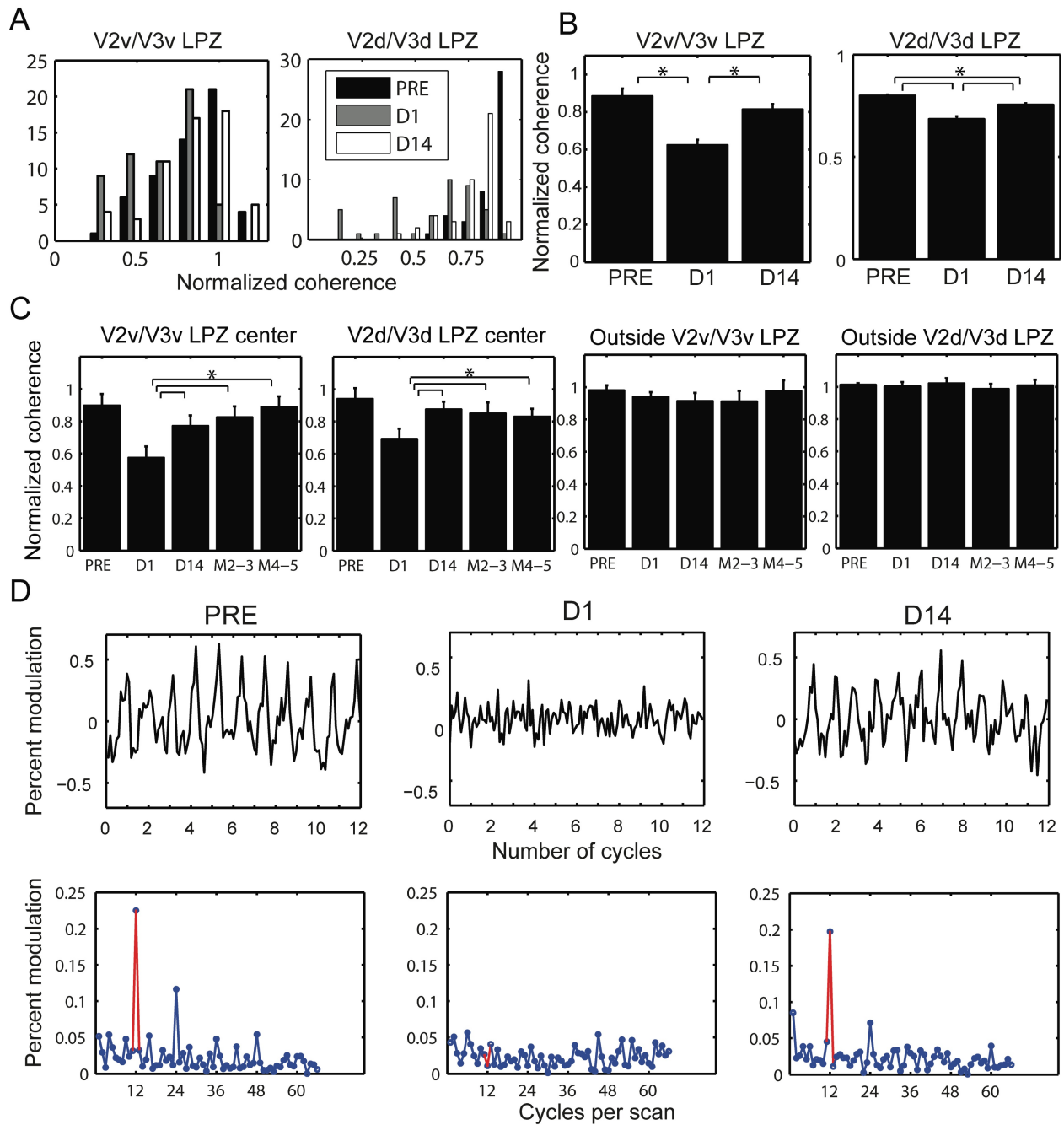
Fig.4 Longitudinal changes in the strength of visual modulation inside the V2/V3 LPZ. A. Distribution of normalized coherence values (the coherence of each voxel inside the LPZ was expressed as a fraction of the average coherence computed across all voxels within the non-deafferented region of V2/V3 in the same hemisphere) of all functional voxels inside the V2v/V3v and V2d/V3d LPZs pre-lesion and at D1 and D14

post-lesioned histogrammed across all monkeys. Note that the number of voxels with low coherence inside the V2/V3 LPZ increases on the day of the lesion, then appears to substantially recover by day 14. **B.** Mean normalized coherence across all functional voxels inside the V2v/V3v and V2d/V3d LPZ pre-lesion, as well as on day 1 and day 14 following the lesion, plotted across all monkeys. Kruskal-wallis test shows a significant effect for both LPZ's over time (H=32.54, $p<10^{-7}$ for V2v/V3v LPZ and H=17.83, $p<10^{-4}$ for V2d/V3d LPZ). Post-hoc pairwise comparisons show that the strength of visual modulation dropped significantly on Day 1 compared to pre-lesion values, and then rose again significantly from Day 1 to D14 post-lesion in both the ventral and the dorsal LPZ. Error bars represent s.e.m. across voxels * $p<0.05$. **C.** Mean normalized coherence across the voxels in the center (left two panels, these voxels were selected independently on the pre-lesion atlas) and outside (right two panels, these voxels were adjacent to the LPZ border) of the V2v/V3v or V2d/V3d LPZ is plotted as a function of time across all animals. Error bars represent s.e.m. across voxels * $p<0.05$. Note that the mean coherence for the center LPZs drops on the day of the lesion (D1) and then increases over time following the lesion. This agrees with panels A,B, which represent the aggregate response over the entire LPZ across all animals. **D.** top row: Percent BOLD signal modulation as a function of stimulus cycle from voxels in the center of the V2v/V3v LPZ of M1, plotted pre-lesion (PRE) and on days 1 (D1) and 14 (D14) post-lesion. Bottom row: Average signal amplitude as a function of temporal stimulation frequency (12 cycles per scan, indicated by the red color). Note that the strength of the visual modulation recovers over time.
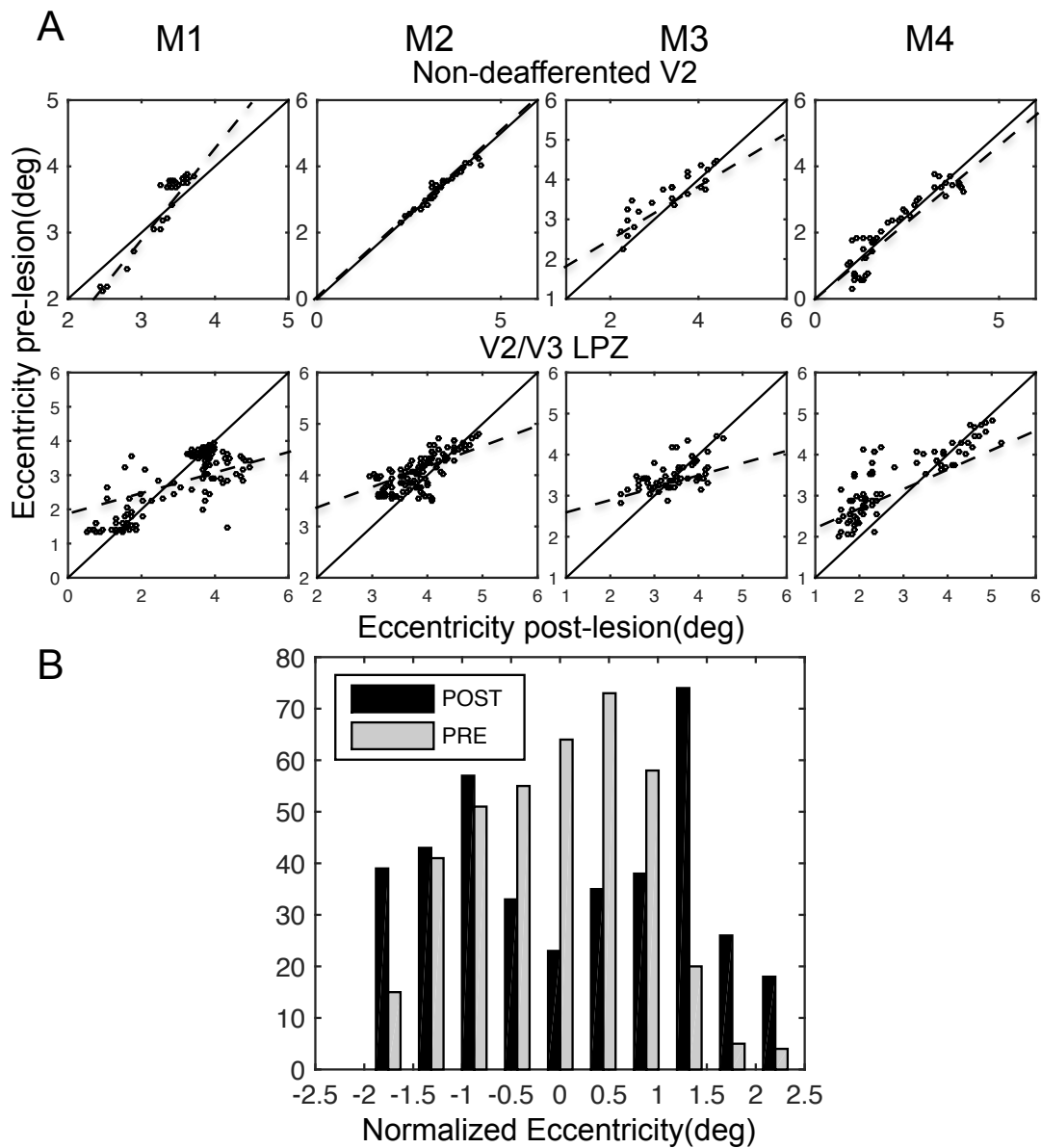
Fig.5 Eccentricity profile of V2/V3 LPZ. A. Top row, scatter plots of pre-lesion versus

post-lesion (day 14) eccentricities of voxels inside a control, non-deafferented, area V2

ROI (see Fig. 2) near the V2/V3 LPZ border. Note that the eccentricities were mainly

unchanged pre- and post- lesion (control). Bottom row, similar scatter plots of the voxels

belonging in the center of the dominant (largest) V2/V3 LPZ of each monkey. Note that

eccentricities inside the LPZ span a wider range following the lesion, with eccentricities

that started low tending to become lower and eccentricities that started higher tending to

become higher. **B.** Distribution of normalized eccentricity (The mean eccentricity of the

central V2/V3 LPZ pre-lesion was first subtracted for each subject, the relative

eccentricities were then cumulated together across subjects.) from voxels in the central V2/V3 LPZ (same voxels as panel A, bottom row) across all subjects pre-lesion and post-lesion. Noted that the distribution pre-lesion is significantly different from post-lesion (p<0.01), there are more instances of lower and higher eccentricities in the LPZ post-lesion, but less in the middle. This agrees with panel A, bottom row, suggests that lateral inputs are likely responsible for the activation of the V2/V3 LPZ region.

Population receptive field analysis of the primary visual cortex complements perimetry in patients with homonymous visual field defects

Amalia Papanikolaou[a,b], Georgios A. Keliris[a,c,1], T. Dorina Papageorgiou[d], Yibin Shao[a], Elke Krapp[e], Eleni Papageorgiou[e,f], Katarina Stingl[e], Anna Bruckmann[e], Ulrich Schiefer[e,g], Nikos K. Logothetis[a,h], and Stelios M. Smirnakis[d,i]

[a]Max Planck Institute for Biological Cybernetics, 72076 Tuebingen, Germany; [b]Graduate School of Neural and Behavioural Sciences, International Max Planck Research School, 72076 Tuebingen, Germany; [c]Bernstein Center for Computational Neuroscience, 72076 Tuebingen, Germany; [d]Departments of Neuroscience and Neurology, Baylor College of Medicine, Houston, TX 77030; [e]Center for Ophthalmology, University Eye Hospital Tuebingen, 72076 Tuebingen, Germany; [f]Department of Ophthalmology, University of Leicester, Leicester Royal Infirmary, Leicester LE2 7LX, United Kingdom; [g]Competence Center "Vision Research," Faculty of Optics and Mechatronics, Aalen University of Applied Sciences, 73430 Aalen, Germany; [h]Division of Imaging Science and Biomedical Engineering, University of Manchester, Manchester M13 9PT, United Kingdom; and [i]Michael E. Debakey VA Medical Center, Houston, TX 77030

Injury to the primary visual cortex (V1) typically leads to loss of conscious vision in the corresponding, homonymous region of the contralateral visual hemifield (scotoma). Several studies suggest that V1 is highly plastic after injury to the visual pathways, whereas others have called this conclusion into question. We used functional magnetic resonance imaging (fMRI) to measure area V1 population receptive field (pRF) properties in five patients with partial or complete quadrantic visual field loss as a result of partial V1+ or optic radiation lesions. Comparisons were made with healthy controls deprived of visual stimulation in one quadrant ["artificial scotoma" (AS)]. We observed no large-scale changes in spared-V1 topography as the V1/V2 border remained stable, and pRF eccentricity versus cortical-distance plots were similar to those of controls. Interestingly, three observations suggest limited reorganization: (*i*) the distribution of pRF centers in spared-V1 was shifted slightly toward the scotoma border in 2 of 5 patients compared with AS controls; (*ii*) pRF size in spared-V1 was slightly increased in patients near the scotoma border; and (*iii*) pRF size in the contralesional hemisphere was slightly increased compared with AS controls. Importantly, pRF measurements yield information about the functional properties of spared-V1 cortex not provided by standard perimetry mapping. In three patients, spared-V1 pRF maps overlapped significantly with dense regions of the perimetric scotoma, suggesting that pRF analysis may help identify visual field locations amenable to rehabilitation. Conversely, in the remaining two patients, spared-V1 pRF maps failed to cover sighted locations in the perimetric map, indicating the existence of V1-bypassing pathways able to mediate useful vision.

cortical blindness | quadrantanopia | plasticity | retinotopy | hemianopia

Cortical damage of the visual pathway often results from posterior or middle cerebral artery infarcts, hemorrhages, and other brain injuries. The most common visual cortex lesions involve the primary visual cortex (V1), the chief relayer of visual information to higher visual areas. Damage to area V1 or its primary inputs leads to the loss of conscious vision in the corresponding region of the contralateral visual hemifield, producing a dense contralateral scotoma that often covers a hemifield (hemianopia) or a single visual field quadrant (quadrantanopia).

A much-debated issue is whether the adult V1 is able to reorganize after injury. Reorganization refers to long-term changes in the neuronal circuit (1) and generally requires the growth of new anatomic connections or a permanent change in the strength of existing connections. Several studies report significant remapping in area V1 of patients suffering from macular degeneration and other retinal lesions (2–12). The extent of this remapping has

recently been called into question, however (1, 13–19). Less is known about how the visual system remaps to cover the visual field after injury to area V1 or its input projection from the lateral geniculate nucleus (LGN). Enlarged receptive fields have been found in areas surrounding chronic V1 lesions in cats (20–22), and visual point spread functions were seen to enlarge over time in the areas surrounding focal V1 lesions in kittens (23). Smaller, short-term changes (2 d after the lesion) have been reported as well (24). As expected, reorganization is more extensive in young animals (23, 25) compared with adults (26). A change in the balance between excitation and inhibition may underlie this functional reorganization (27–31).

In humans, V1 injury is typically followed by a brief period of spontaneous recovery, which rarely lasts beyond 6 mo (32). Whether this recovery is the result of true visual system plasticity or is related to the gradual resolution of perilesional edema and general clinical improvement of the patients is unclear. A recent study in an adult human subject suggested that large-scale reorganization occurs in area V1 after partial deafferentiation by an optic radiation lesion (33); however, quantitative measurements were not performed. To date, there has been no systematic study in humans investigating how spared V1 cortex covers the visual field after chronic V1 injury. The present work is an effort in this direction.

Significance

Partial damage of the primary visual cortex (V1), or damage to the white matter inputs to V1 (optic radiation), cause blindness in specific regions of the visual field. We use functional MRI to measure responses in individual patients with a localized, chronic V1 injury that resulted in blindness in a quarter of the visual field. The fMRI responses of patients and controls are generally similar, but in some patients differences from controls can be measured. Importantly, responses in spared early visual cortex are not always congruent with visual perception. Understanding how the properties of early visual areas respond to injury will lead to better strategies for visual rehabilitation.

We used the population receptive field (pRF) mapping method (34) to study how spared area V1 covers the visual field after chronic injury in five adult human subjects suffering from partial or complete quadrantanopia. Our findings suggest that there is at best a limited degree of reorganization in the spared part of area V1 after partial V1 injury. Interestingly, the pattern of coverage of the visual field measured in spared V1 cortex by functional magnetic resonance imaging (fMRI) typically does not match predictions derived from perimetry maps. Identifying the patterns of mismatch and how they relate to the capacity of early visual areas to reorganize after injury will eventually allow the adoption of more rational strategies for visual rehabilitation.

Results

Retinotopic Mapping of Spared Area V1. We studied five patients with partial V1 or optic radiation lesions resulting in partial or complete quadrantanopia (Table S1) and examined how the adjacent spared area V1 organization changes after the injury. We expected that in the absence of significant reorganization, reti-

notopic organization in the spared-V1 cortex would remain unchanged compared with controls. The patient's lesions are described in detail in Fig. 1. In brief, patient P1 had a lesion of the right inferior calcarine cortex (Fig. 1 *A, a*), resulting in a superior quadrantanopic defect of the left visual field (Fig. 2 *A, b*). Patient P2 had a right superior quadrantanopia (Fig. 2 *A, c*) after sustaining a temporal optic radiation infarct of the left hemisphere. Patient P3 had a lesion of the left inferior calcarine region resulting in a central (<10° radius) right superior quadrantanopia (Fig. 2 *A, d*), which spread slightly into the inferior right quadrant. Patient P4 had a lesion of the left inferior calcarine cortex, resulting in a right superior quadrantanopia (Fig. 2 *A, e*). Patient P5 had a partial left superior quadrantanopia extending to the inferior quadrant across the horizontal meridian (Fig. 2 *A, f*), resulting from an infarct in the right midposterior temporoparietal region (Fig. 1 *A, e*).

We observed two general patterns in the five patients examined. In patients P1, P2, and P3, spared (i.e., not completely deafferented) area V1 seems to retain its "coarse" retinotopic
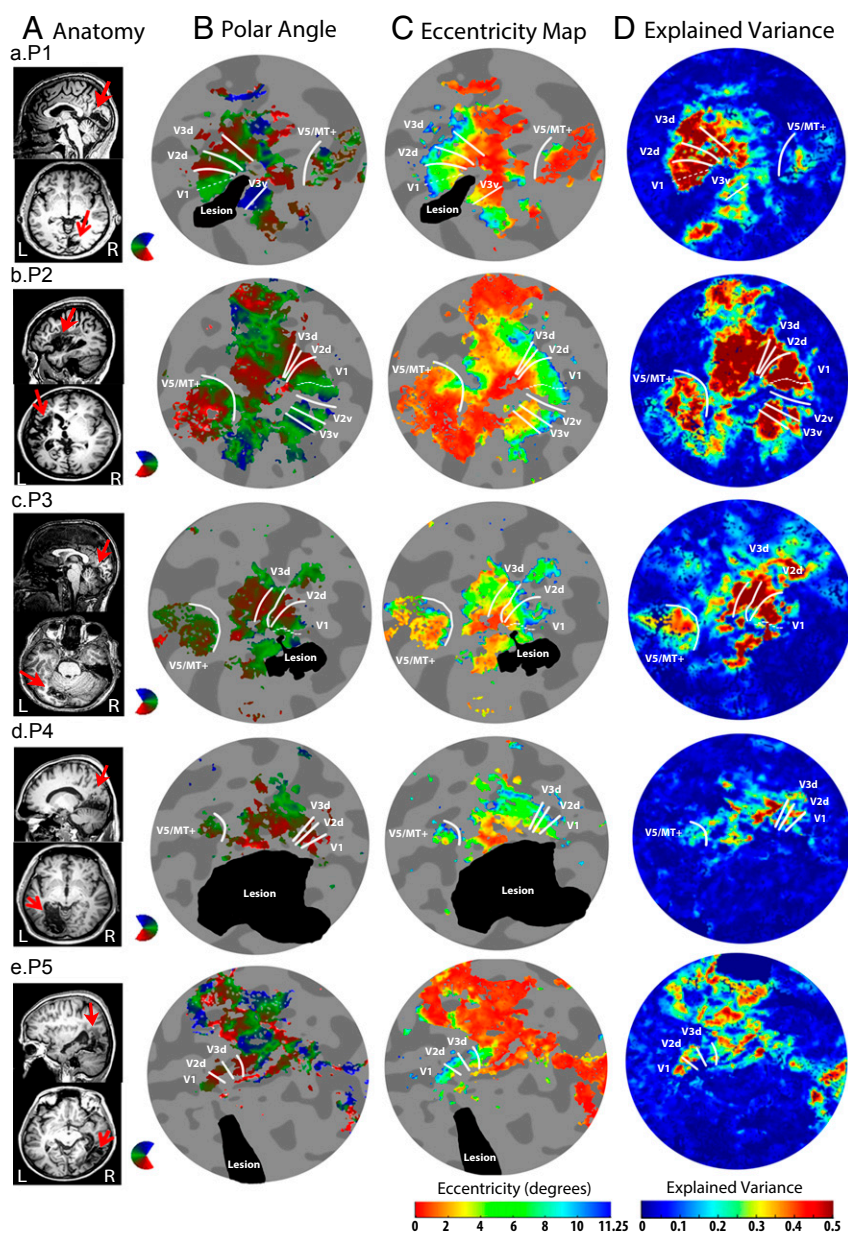
Fig. 1. Anatomic location of the lesion and retinotopic mapping. (*A*) Sagittal (*Upper*) and axial (*Lower*) slice showing each patient's anatomic lesion (a red arrow points to the lesion). Patient P1 had a lesion of the right inferior calcarine cortex involving the part of the V1 area inferior to the calcarine sulcus and the part of the extrastriate cortex corresponding to the ventral visual areas V2 and V3, with the foveal part of the vertical meridian at the border of ventral V3 and V4 spared. Patient P2 had a temporal optic radiation infarct of the left hemisphere located along the territory of the middle cerebral artery, sparing the gray matter of area V1 but deafferenting a significant portion of it by injuring the optic radiation. Patient P3 had a lesion of the left inferior calcarine cortex as a result of an ischemic event at the left inferior territory of the posterior cerebral artery, resulting in a right upper quadrantanopia. This lesion also involves part of the peripheral (>10° radius) area V1 superior to the calcarine, as well as extrastriate cortex corresponding to ventral visual areas V2, V3, and V4. Patient P4 had a lesion of the left inferior calcarine cortex caused by an infarct to the lower bank of the calcarine fissure. It involves left ventral area V1, left ventral extrastriate areas V2, V3, and V4, as well as part of the cortex near the fovea. Patient P5 had an infarct of the right midposterior temporoparietal lobes that damaged the temporal optic radiation and part of the parietal optic radiation. White matter tracts in the temporal lobe were affected, but deafferented V1 gray matter remained intact; the area corresponding to the anatomic lesion does not include early visual areas. (*B* and *C*) Polar angle (*B*) and eccentricity maps (*C*) overlaid on the flattened occipital lobe of the lesioned hemisphere for each patient. The lesioned area is colored black (Fig. S4 and *SI Materials and Methods*). (*D*) As expected, no significant activity was found inside the area of the lesion, as shown in the explained variance map. White contour lines indicate borders between visual areas. The dashed white line indicates the middle of the calcarine sulcus as identified by its anatomic localization (i.e., bottom of the calcarine sulcus).

Fig. 2. Perimetry maps versus visual field coverage maps of spared area V1. (*A*) (*a*) Sketch of the visual field indicating the location of the artificial scotoma (shaded gray area). (*b–f*) Pattern deviation probability plots of the 10° Humphrey type (10, 2) visual field test for patients P1, P2, P3, P4, and P5. The small black dots show the locations in the visual field that are normal, and the black squares indicate a visual field defect at a $P < 0.5\%$ level according to the pattern probability plot (meaning that <0.5% of normal subjects would be expected to have such a low sensitivity at this visual field location). Pattern deviation numeric plots for patients P1, P2, P3, and P4 had a visual sensitivity of <-20 dB, indicating absolute visual field scotoma (56), at all visual field locations within the affected quadrants. Black squares outside the affected quadrants had a visual sensitivity of <-10 dB (most still <-20 dB) for these patients. Patient P5 had a visual sensitivity of <-20 dB (absolute scotoma) in all of the black square locations. (*B*) Visual field coverage maps of area V1 for a control subject with AS in the upper left quadrant and for each patient. The color map indicates the maximum pRF amplitude at each visual field location of all of the pRFs covering that location. The pRF centers across all voxels within the spared V1 are plotted with gray dots. In the normalized maps (*Left*), values range between 0 and 1, because the fitted Gaussian model is normalized to 1. In the nonnormalized maps (*Right*), the maximum pRF amplitude of the nonnormalized Gaussian pRFs is plotted. The nonnormalized color map is plotted with the maximum color value taken at the median pRF amplitude across all pRFs (*SI Materials and Methods*) to maintain sensitivity to relatively low values. The V1 coverage maps of patients P1, P2, and P3 overlap significantly with locations of the perimetric map that show an absolute scotoma (black squares with decibel deviations of <-20 dB). Only a few pRFs (~6%) of patient P2's spared-V1 overlap with locations of the perimetric map (black squares) that have a lower decibel deviation, between -10 dB and -20 dB. (*C*) Eye positions plotted at 60 Hz for each subject for one entire session (6.4 min). The number of eye deviations, defined as excursions >1.5° from the fixation point, is indicated next to the graphs with #. Patient P3 was scanned without eye-tracking while performing a task at fixation. All other patients were able to maintain fixation.

organization, similar to control subjects. In particular, the pRF center eccentricity maps (Fig. 1 *C, a–c*) show that the foveal representation was in the occipital pole, as expected, and that increasingly anterior locations responded to increasingly eccentric stimuli. In addition, the representation of the visual field in the dorsal spared V1 corresponding to the sighted quadrant extended from the horizontal meridian to the lower vertical meridian, as shown on the pRF polar angle maps (Fig. 1 *B, a–c*), similar to controls. Surprisingly, in these patients, the polar angle map shows significant activity in locations ordinarily corresponding to the inferior part of the calcarine (separated by the dotted line; Fig. 1 *B, a–c*), a region normally activated by stimuli presented in the superior part of the visual field, where the perimetry shows a dense scotoma (Fig. 2 *A, b–d*). We investigated this pattern in more depth, as discussed in the next section.

Patients P4 and P5 exhibited a different pattern. In these patients, the extent of the retinotopic topography of area V1 that was activated was considerably less than would be predicted from the visual field maps. Specifically, for patient P4, the organization of spared area V1 was severely disrupted, and almost the entire dorsal V1, except for a sliver near the lower vertical meridian, was devoid of activity (Fig. 1 *B–D, d*). Nevertheless, the perimetry map of this patient closely conforms to a superior quadrantanopia, with only a slight extension below the horizontal meridian. The relatively well-preserved perimetry map of the right lower visual field quadrant (Fig. 2 *A, e*) suggests either the presence of sufficient intact dorsal V1 islands to compensate (even though they are not visible on the retinotopic map) or the presence of functional V1-bypassing pathways to higher areas that may have more complete retinotopic coverage maps (35).

Similarly, patient's P5 visual cortex inferior to the calcarine was severely affected, with no visually driven functional activity present in the ventral occipital region as a whole (Fig. 1 *B–D*, *e*). However, this subject shows a sparing along the left upper vertical meridian in the perimetry map (Fig. 2 *A*, *f*). Presumably, preserved visual function in the left upper visual field is mediated by V1-bypassing pathways, likely involving areas beyond V3 (*Discussion*), or perhaps via the contralesional hemisphere (left area V1). We explore this in more details in the next section.

In summary, we observed two different patterns in the five patients that we examined. Patients P1, P2, and P3 had visually driven activity in spared V1 regions that corresponded to dense locations of their perimetric scotoma. In contrast, patients P5 and P4 had intact perimetric maps in locations corresponding to area V1 regions, with an absence of visually driven activity. We analyzed these patterns further using the concept of visual field coverage maps.

Correspondence Between Visual Field Coverage Maps and Perimetric Scotomas. To estimate how the visual field is represented in spared area V1, we superimposed appropriately normalized pRFs arising from all of the spared V1 voxels to derive visual field coverage maps (Fig. 2*B* and *SI Materials and Methods*). The visual field coverage maps define the locations within the visual field that evoke a significant response from voxels within a region of interest (ROI) in the cortex. Determining the degree to which visual field coverage maps match perimetric maps, which indicate the patients' perceptual scotoma, is of interest.

To ensure that the patients' visual field coverage maps are not an artifact of poor pRF estimation caused by the presence of the visual field scotomas, we tested the effect of an "artificial scotoma" (AS) on normal subjects. We measured responses in five control subjects while masking the left superior quadrant of the visual field, thereby simulating a left upper quadrantanopia. As expected, the visual field coverage maps of the right V1 hemisphere in AS controls reveal visually driven activity only for stimuli presented in the left inferior visual field quadrant (Fig. 2 *B*, *a*). No activity was observed in the left upper visual field quadrant in any of the five AS control subjects.

In contrast, the visual field coverage maps of spared V1 in patients P1, P2, and P3, who had a quadrantic visual field defect similar to AS controls, contain pRF centers that extend well beyond the border of the perimetric scotoma into the superior (anopic) visual field quadrant (Fig. 2 *B*, *b–d*). The pRFs, whose centers fall inside the area of the scotoma, belong to voxels at the correct anatomic location, inferior to the calcarine, which do not appear to be grossly ectopic (Fig. 3). Thus, the observed activity likely reflects islands of V1 that were spared or only partially damaged. Interestingly visually driven activity in this spared V1 region is not sufficient to guarantee visual awareness, as measured by standard perimetry.

One possibility is that the blood oxygen level-dependent (BOLD) signal amplitude is lower at V1 locations covering the interior of the scotoma and thus cannot mediate visual perception. However, for patients P1 and P3, the mean amplitude of the pRF centers that fall inside the perimetric scotoma was similar to the mean amplitude of pRF centers located outside the scotoma, as shown in the nonnormalized visual field coverage maps (Fig. 2 *B*, *b* and *d*). In this case, the dense perimetric defect near the horizontal meridian might be explained by injury in downstream extrastriate areas, such as V2/V3 (36, 37), or the interruption of V1 projections to extrastriate areas. In fact, the lesion of these patients involves areas V2v and V3v, supporting the first possibility.

On the other hand, for patient P2, who had an optic radiation lesion, the loss of visual perception cannot be attributed to a lesion downstream from area V1, because the visual cortex remained intact. Responses in ventral areas V2 and V3 overlapped with the area of the scotoma, similar to V1 ([Fig. S1*A*](#)). In this case, the
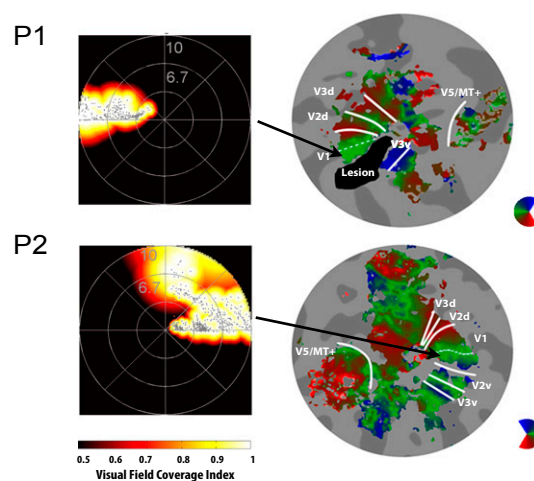

P1

P2

Fig. 3. Anatomic localization of area V1 population receptive fields within the scotoma. (*Left*) Visual field coverage maps obtained from the region of spared V1 inferior to the bottom of the calcarine sulcus (anatomic location of the horizontal meridian) for patients P1 and P2. (*Right*) Anatomic location of the bottom of the calcarine sulcus indicated by a dashed line on the polar angle flat maps. Note that pRFs with centers falling within the scotomatous area in these patients map to the correct anatomic location, inferior to the calcarine (black arrow).

nonnormalized visual field coverage maps showed a significantly lower mean amplitude of pRF centers falling inside the scotoma compared with those in the inferior (sighted) quadrant (Fig. 2 *B*, *c* and [Fig. S1*A*](#)). Thus, it is possible, at least in principle, that this decreased level of visually driven activity is responsible for the loss of visual perception as measured by perimetry. Interestingly, scattered pRF centers with high amplitude remained inside the scotoma. One possible explanation for this finding is that intact islands of spared, partial axonal tracts in the optic radiation survived after the ischemic event and activate corresponding locations in area V1. Despite being visually driven, however, these islands were unable to mediate visual perception as measured on perimetric maps and cannot be detected even with the relatively sophisticated perimetry mapping methods used here (*SI Materials and Methods*).

The mismatch between the visual field coverage map and perimetric scotoma does not manifest in the same way in every individual. For example, the visual field coverage of the spared V1 in patient P4 shows pRF centers within the inferior quadrant, outside the visual field scotoma (Fig. 2 *A* and *B*, *e*). In patient P5, a few pRF centers below the horizontal meridian seemed to fall in areas where the perimetry test showed a dense defect, as in patients P1, P3, and P2 (Fig. 2 *A* and *B*, *f*). However, the more striking observation in both these patients is the smaller than expected (based on the perimetry map) activated area in V1. In patient P4, the activation pattern seen in area V1 (Fig. 2 *B*, *e*) was patchy and smaller than expected based on the perimetric map. The visual field coverage map of the right inferior (sighted) quadrant contained significantly fewer pRF centers compared with controls, although the corresponding pRFs cover most, but not all, of the quadrant.

It is possible that pRFs in surviving islands of area V1 enlarged over time, producing a confluent visual field coverage map that partially mediated the residual visual function. However, even taking this into account, the pRF coverage map appeared to miss portions of the visual field where the perimetric map showed normal vision. This finding suggests that part of the residual visual function may be mediated through spared V1-bypassing pathways. In fact, dorsal areas V2 and V3 showed full coverage of the lower visual field quadrant, supporting this hypothesis

(Fig. S1B). Similarly, the perimetry map of patient P5 showed a significant area of sparing along the vertical meridian and beyond, within the left upper visual field quadrant (Fig. 2 A, f). Surprisingly, there was no contralateral V1 activation corresponding to that quadrant, despite the fact that a significant portion of the quadrant was essentially normal on the perimetry map (Fig. 2 A, f). One possibility is that visual perception near the vertical meridian might arise from V1-bypassing pathways providing direct input to extrastriate areas beyond V3 (35), or perhaps from ectopic V1 activation in the contralesional hemisphere.

The differences in visual field coverage maps between patients and AS controls cannot be explained by eye movements. Subjects were able to maintain fixation within a 1.5° radius from the center of fixation as measured with our eye-tracking system (Fig. 2C and *SI Materials and Methods*), except for very occasional excursions beyond this range (Fig. 2). The results remained unchanged after the epochs in which the patients had eye deviations (>1.5°) from the fixation point were removed from the analysis. Patient P3's eye movements were not recorded, but he performed a challenging detection task at fixation, and his performance was always >80% correct. The retinotopic maps of his healthy hemisphere were well organized, suggesting that he did not make large, confounding eye movements. In addition, to ensure intrasubject reproducibility, we repeated the experiment on another day for patients P2 and P5 and confirmed the findings across days. Patients P1, P3, and P4 could not repeat the session; however, we analyzed each scan separately before averaging and confirmed the reliability across different scans obtained on the same day.

In summary, our comparison of perimetric maps and pRF coverage maps of the visual field confirmed the two patterns of mismatch noted in the previous section. In three of the five patients, spared area V1 pRF maps overlapped significantly with the scotoma, suggesting remaining visually responsive islands of V1 that cannot contribute to visual perception, perhaps because of damage to downstream areas or damage to the inputs that they receive from area V1. In the remaining two patients, spared V1 pRF maps failed to completely cover locations that were found to have intact thresholds on perimetry. In these patients, the observed mismatch might indicate the existence of V1-bypassing pathways able to mediate useful vision. The information obtained from pRF analysis complements that obtained

Fig. 4. Cortical distance between the V1 horizontal meridian and dorsal V1/V2 border for patients P1–P5. The cortical distance is calculated by measuring the surface area of seven isoeccentric ROIs (range of eccentricities, 2–9°; bin size, 1°) and dividing by the cortical magnification factor (mm/°) at each eccentricity. The mean cortical distance of the controls (mm) is plotted as an orange dotted line. The gray shaded area indicates the SD (*n* = 16 hemispheres).

by standard perimetry maps, and can be used to further characterize the underlying etiology of cortical visual field defects.

pRF Center Distributions in Spared Area V1 Show at Best Limited Reorganization. A general finding in all five patients was that the retinotopic representation of the spared V1 remained grossly unaffected (Fig. 1). The borders between visual areas, as marked by polar angle reversals, were detected at the expected locations. We measured the cortical distance from the V1 horizontal meridian to the dorsal V1/V2 border along isoeccentricity contours, and plotted it as a function of eccentricity. Plots for all patients were within the range of controls (Fig. 4). Furthermore, the Talairach coordinates at an eccentricity of 8° along the horizontal meridian of V1 and the dorsal V1/V2 border were similar to those of controls (Table S2), and consistent with previous reports (38). In addition, the eccentricity maps exhibited a monotonic progression of phase, as expected (Fig. 1C). These results reveal that large-scale retinotopic distortions do not occur; however, the possibility of fine changes in the retinotopic structure of spared V1 cortex cannot be excluded and merits quantitative assessment.

To do so, we compared the distributions of pRF center locations between patients and AS controls. The AS serves as a baseline to control for pRF changes that may arise from reorganization versus simple stimulus deprivation. This control might not always be completely adequate, however, given that partial deafferentiation of the visual pathways may affect the pRFs corresponding to visual field locations that do not belong to the scotoma. Thus, a case-by-case evaluation of whether pRF differences between patients and AS controls are result of partial deafferentiation as opposed to remapping or true reorganization is needed.

pRF center distribution as a function of distance from the scotoma border. In two of the five patients (P1 and P2), the distribution of pRF centers as a function of distance from the horizontal border of the scotoma (elevation) differed significantly from that of AS controls [two-sample Kolmogorov–Smirnov test; significance is reported as $P = a < b$, where b is the value selected to reject the null hypothesis (*Materials and Methods*); P1: $P = 8.09 \times 10^{-63} < 10^{-27}$; P2: $P = 7.62 \times 10^{-42} < 10^{-27}$]. Specifically, pRF centers were seen to cluster near the border of the scotoma, that is, the horizontal meridian (Fig. 5A). In fact, in these patients, a number of pRF centers crossed the scotoma border to lie inside the scotoma (i.e., with elevation > 0°), as seen in the visual field coverage maps (Fig. 5A, *Insets*). These pRFs belonged to voxels that were not anatomically ectopic but mapped roughly at the correct anatomic location, the lower bank of the calcarine sulcus (Fig. 3). One may then wonder whether they are the reason that pRF centers cluster more strongly near the border of the scotoma in patients compared with AS-controls. However, the distribution of pRFs of the spared dorsal V1, defined by its anatomic location, was also significantly shifted toward the scotoma border, with voxels clustering near the border (0° elevation) (Fig. 5B; P1: $P = 8.09 \times 10^{-38} < 10^{-26}$; P2: $P = 8.09 \times 10^{-38} < 10^{-26}$). This finding suggests that the observed shift in the distribution of pRF centers likely corresponds to a slight reorganization of the visual field coverage map in unlesioned portions of area V1 that are located close to the scotoma border, perhaps because of a change in local excitation/inhibition balance as a result of the lesion.

This effect was not seen in every patient. The distribution of pRFs in the dorsal V1 of patient P3 did not show significant clustering near the border of the scotoma compared with AS controls ($P = 1.4 \times 10^{-15} > 10^{-28}$) (Fig. 5B). Patients P4 and P5 had fewer voxels with pRFs inside the sighted quadrant compared with AS controls, and P4 also showed a trend toward clustering of pRF centers at the scotoma border, but this did not reach significance under our relatively strict comparison criterion (P4: $P = 1.48 \times 10^{-04} > 10^{-07}$; P5: $P = 9.6 \times 10^{-04} > 10^{-11}$) (Fig. 5A). Regardless, the lesions of patients P4 and P5 extended to
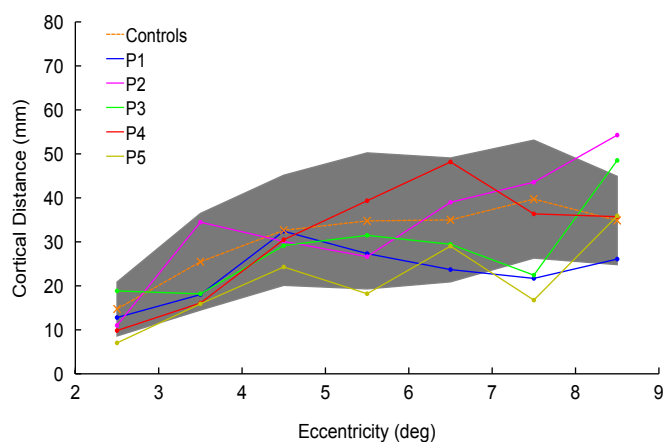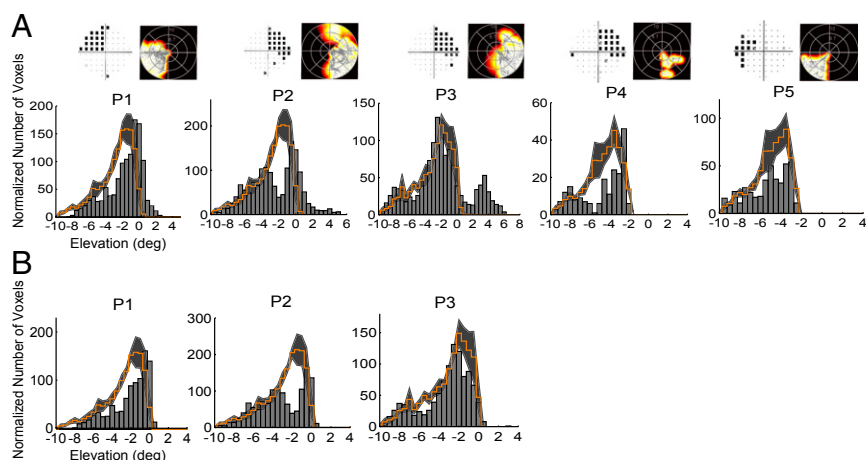
Fig. 5. pRF center distribution as a function of distance from the scotoma border. (*A*) Histograms (gray bars) showing the number of voxels as a function of the pRF center elevation, that is, the distance of the pRF center from the horizontal meridian border of the scotoma (coordinate Y), for patients P1–P5. Units are degrees of visual angle. The mean distribution of voxels in the control subjects with AS is overlaid as a step histogram in orange. To adjust for V1 size, the distributions of the controls were normalized according to the relative size of the retinotopically corresponding V1 regions that were activated in patients versus controls under the full stimulation condition (*SI Materials and Methods*). The shaded area represents the SEM for the control group (*n* = 5). The pRF center elevation distributions of patients P1, P2, and P3 show pRFs within the area of the scotoma (elevation >0), as also shown in the visual field coverage maps (*Insets* and Fig. 2 *B, b–d*). However, for patients P1 and P2, there was also a clustering of voxels near the scotoma border. The pRF center elevation distributions of patients P4 and P5 show fewer voxels within the sighted quadrant compared with AS controls and a clustering near the scotoma border for P4, but the effect did not reach significance. The observed differences between these patients and AS controls are likely related to partial deafferentiation of the voxels plotted. (*B*) pRF center elevation distributions of the significantly activated voxels in the anatomically defined intact dorsal V1 of patients P1, P2, and P3. For patients P1 and P2, pRFs clustered significantly near the scotoma border, suggesting reorganization. This effect was not seen in patient P3.

partially involve dorsal V1 or its inputs (Fig. 1 *A, d* and *e*), making it difficult to determine whether observed changes are related to true reorganization or to partial deafferentiation.

In summary, these results suggest that in some patients with partial lesions of area V1 or its inputs (here P1 and P2), the pRF centers of spared V1 cortex cluster near the border of the scotoma. This clustering is seen primarily within 1–2° of the scotoma border. The magnitude of the shift is small, suggesting a limited degree of reorganization. One patient (P3) did not exhibit this effect; however, this patient's injury occurred only 6 mo before recruitment, compared with the chronic lesions of the other patients, and we cannot exclude the possibility that time may affect the degree of the observed reorganization. In patients P4 and P5, the observed differences are more likely related to partial deafferentiation or partial injury of the corresponding voxels.

Population receptive field size. We found a larger mean pRF size in the spared V1 area in patients compared with AS controls (Fig. 6). Specifically, the mean pRF size in the spared V1 of patients P1, P2, P4, and P5 was increased by ~25% compared with AS controls. A larger increase was seen in patient P3, ~90% compared with AS controls. The pRF size distributions of patients P1, P2, and P3 were significantly shifted toward larger sizes compared with the AS controls ($P = 1.4 \times 10^{-76} < 10^{-63}$, $P = 1.67 \times 10^{-78} < 10^{-70}$, and $P = 1.13 \times 10^{-165} < 10^{-66}$, respectively) (Fig. 6*A*). The same trend was seen for patients P4 and P5, but it did not reach significance ($P = 7.4 \times 10^{-09} > 10^{-39}$ and $P = 1.19 \times 10^{-33} > 10^{-62}$) (Fig. 6*A*). V1 lesions were larger in these patients (Fig. 1 *B, d* and *e*), leading to few visually modulated area V1 voxels and thus more measurement variability. In addition, in these patients, the pRFs were located at higher eccentricities, where pRF sizes are larger. In general, the mean pRF size for each patient was greater than the corresponding mean of the distribution of pRF sizes of the AS controls (Table S3).

We examined whether the pRF size increase depends on eccentricity and distance of the voxel from the scotoma border. To do so, we divided voxels in the spared V1 of patients and AS controls into two categories: voxels with pRF centers within 2° of the horizontal scotoma border and voxels with pRF centers >2°

from this border, and plotted mean pRF size versus eccentricity (Fig. 6 *B* and *C*). We found that for all patients, mean pRF size was increased for voxels located within 2° of the scotoma border (Fig. 6*B*), with increases of ~40% for patients P2, P4, and P5; ~75% for patient P1; and ~120% for patient P3. For patients P1, P2, P3, and P5, the increase occurred across almost the whole range of eccentricities, whereas for P4, it was more profound for large eccentricities (>6°). In contrast, the mean pRF size of voxels >2° away from the scotoma was more similar in patients P1, P2, P4, and P5 and AS controls (Fig. 6*C*). For P3, the mean pRF size was increased for voxels away from the scotoma as well, but to a lesser degree (~40%) compared with voxels near the scotoma. The larger increase observed in this patient might be attributed to the relatively recent lesion compared with the other patients, but we cannot exclude the possibility that small eye movements might have affected the pRF size, considering that this patient was not eye-tracked. However, eye movements would be expected to increase pRF size in higher areas in a comparable way as in V1 (39). In patient P3, pRF size in areas V2d and V3d was slightly larger (~15%) compared with that in AS controls, but the magnitude of the increase was considerably less than observed in area V1 and did not occur for all eccentricities (Fig. S2). Thus, eye movements cannot be the sole explanation for the pRF size increase observed in area V1 of this patient.

In summary, the pRF size distribution in the spared V1 regions of patients with partial quadrantanopia appeared to shift toward larger values compared with the AS controls, particularly near the scotoma border.

Contralesional Hemisphere. Previous reports have suggested that in some cases, residual vision in the blind hemifield might be mediated by visual areas in the intact hemisphere (40–43). It is then possible that after area V1 injury, reorganization might occur in the contralateral, healthy hemisphere. Because in primates, callosal projections are concentrated along the V1/V2 boundary (44), the vertical meridian is the most natural place in the contralesional hemisphere to look for potential reorganization. We compared pRF sizes between the dorsal and ventral V1 and
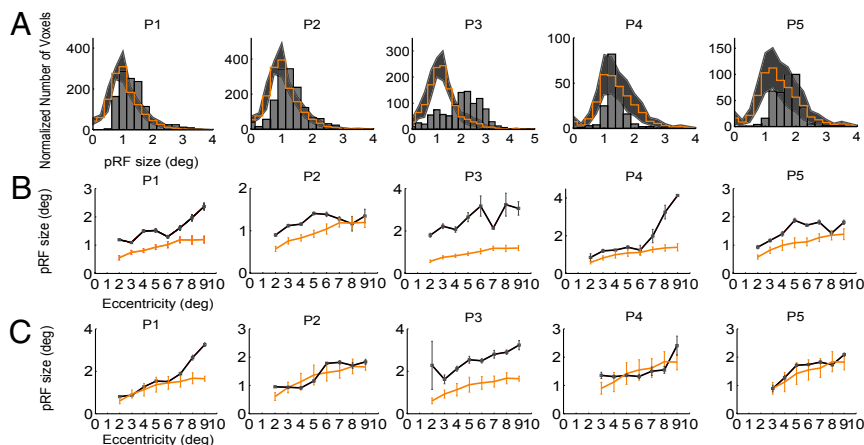
Fig. 6. pRF size in spared V1 areas. (*A*) Histograms of the distribution of pRF size from the spared V1 of all patients (gray bars) compared with the mean distribution of AS controls (orange stairs). The shaded area indicates the SEM across the AS controls. The pRF size distribution of all patients is shifted toward larger pRF sizes compared with the AS controls. (*B*) Mean pRF size versus eccentricity for voxels located near the scotoma border (<2°) in patients (black) and AS controls (orange). The orange error bars indicate the SEM across AS control subjects (*n* = 5). The gray error bars indicate the SEM across voxels within an eccentricity bin (bin size, 1°) for each patient. Mean pRF size is larger in patients compared with AS controls across eccentricities. pRFs within the area of the scotoma of patients P1, P2, and P3 were not included in the plots; however, results remain the same when these voxels are included. (*C*) Mean pRF size versus eccentricity for voxels located away from the scotoma border (>2°) in patients (black) and AS controls (orange). Mean pRF size was similar in patients P1, P2, P4, and P5, and AS controls across eccentricities, with only P1 having a slightly increased pRF size for eccentricities >7°. For P3, the mean pRF size was larger than that of AS controls for all eccentricities. Eye movements cannot explain the observed differences for patients P1, P2, P4, and P5, given that the distribution of eye movements was similar in patients and controls (Fig. 2*B*) and eye movements would have caused an increase in pRF size at low eccentricities irrespective of distance from the scotoma border. Patient P3 was not eye-tracked, and thus we cannot completely exclude that possibility. However, pRF sizes in areas V2d and V3d did not increase similarly to those in V1, suggesting that eye movements might not be responsible for the large increase observed in V1 (Fig. S2).

between the vertical and horizontal V1 meridians of the hemisphere ipsilateral (contralesional) to the visual field scotoma in patients and in AS controls. Patients P1, P2, P3, and P4 showed no significant difference in mean pRF size between contralesional dorsal and ventral V1 or between vertical and horizontal V1 meridians (Fig. S3); however, the pRF size distribution of the entire contralesional V1 in each patient showed a significant shift to larger pRF sizes in patients P2, P5, and P3 compared with AS controls ($P = 1.63 \times 10^{-64} < 10^{-62}$, $P = 2.55 \times 10^{-167} < 10^{-70}$, and $P = 4.93 \times 10^{-236} < 10^{-63}$ respectively) (Fig. 7*A*). The increase occurred across all eccentricities in patients P3 and P5 and mainly for eccentricities >5° in patient P2 (Fig. 7*B*). Patients P1 and P4 had a pRF size distribution more similar to that of AS controls, with differences that did not reach significance (P1: $P = 8.34 \times 10^{-34} > 10^{-64}$; P4: $P = 7.53 \times 10^{-18} > 10^{-55}$) (Fig. 7*A*); however, these patients had a larger pRF size for eccentricities >7° compared with AS controls (Fig. 7*B*).

Only patient P5 had significantly larger pRFs in the ventral contralesional V1 than in the dorsal contralesional V1, particularly along the upper vertical meridian (Fig. S3). This finding is intriguing, and it is tempting to associate it with the sparing seen in the perimetric map of this patient along the left upper vertical meridian (Fig. 2 *A*, *f*). This association is not certain, however, for several reasons: (*i*) Although larger, patient P5's pRFs along the vertical meridian crossed only modestly (~1–2°) into the contralateral visual field, and this cannot readily explain the relatively larger sparing seen on perimetric maps; (*ii*) the degree of crossover was commensurate with the size of patient P5's eye movements (~1.3°); and (*iii*) we cannot completely exclude the possibility that area V1 of the lesioned hemisphere could be mediating visual perception in the spared region seen on visual perimetry while being too weakly visually driven to be evident on the pRF maps.

Discussion

The few published studies of human visual system organization in the setting of area V1 injury are mainly case reports (33, 45). Naturally occurring cortical lesions show considerable variability,

making it difficult to draw definite conclusions from isolated case studies. Dilks et al. (33) studied a subject with left upper quadrantanopia after damage to the optic radiation and report significant ectopic activity in area V1 at 6 mo after the ictus. Specifically, activity elicited by stimuli presented in the sighted left lower visual field quadrant mislocalized to V1 regions ordinarily corresponding to the blind left upper quadrant, suggesting the occurrence of large-scale reorganization. Whether the ectopic V1 activity that Dilks et al. reported is the result of reorganization or simply the result of a different pattern of visual input between patient and controls is unclear, however. The authors attempted to control for this by removing stimulation epochs corresponding to the left upper quadrant from their analysis in the controls, but this was not necessarily definitive, because the stimulus was in fact presented there. A more appropriate control would have been to mask the stimulus presentation space in the controls to simulate a quadrantic scotoma (AS condition). Given the high intersubject variability, further studies are needed to characterize how the functional properties of the visual cortex change in the context of injury.

Here we used quantitative pRF analysis (34, 46–48) to study the properties of spared V1 cortex in five patients with chronic postchiasmatic lesions resulting in homonymous visual field quadrantanopia. We derived detailed retinotopic maps and visual field coverage maps of spared area V1 for each patient and made the following observations: (*i*) The spared V1 region of the lesioned hemisphere retained its coarse retinotopic organization, as described previously (35, 45), the V1/V2 border remained stable, and retinotopic maps showed a monotonic progression of phase, as expected; and (*ii*) visual field coverage maps of the spared V1 area generally did not exactly match the area of the dense perimetric scotoma (Fig. 2). Two main patterns of mismatch were identified.

Pattern 1: Visual Field Coverage Maps of Spared-V1 Overlapped Significantly with the Dense Perimetric Scotoma in Three of the Five Patients. pRFs activated inside the scotoma were found in the proper anatomic locations. Thus, in patient P2, whose scotoma
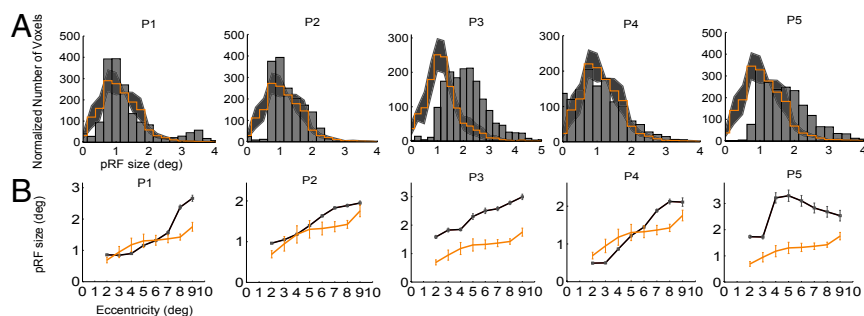
Fig. 7. pRF size of the contralesional V1. (*A*) Histograms of the distribution of pRF sizes from the contralesional V1 of all patients (gray bars) compared with the mean distributions of AS controls (orange stairs). The shaded area indicates the SEM across AS controls (*n* = 5). The distributions show a significant shift to larger pRF sizes for patients P2, P3, and P5. Patients P1 and P4 showed a significant increase in pRF size only for eccentricities >7°. (*B*) Mean pRF size versus eccentricity for voxels in the contralesional V1 of patients (black) and AS controls (orange). The orange error bars indicate the SEM across AS control subjects (*n* = 5). The gray error bars indicate the SEM across voxels within an eccentricity bin (bin size, 1°) for each patient. For patients P1, P2, and P4, pRF size was larger compared with that in AS controls for eccentricities >6–7°. For patients P3 and P5, pRF size was increased across all eccentricities. As shown in Fig. 2*C*, patients P1, P2, P4, and P5 were able to ensure fixation. The amplitude of the eye movements did not differ between patients and controls (Fig. 2*C*), and epochs of significant deviation from fixation were excluded from the analysis; thus, the findings for these patients are unlikely to be attributed to eye movements. Patient P3 was not eye-tracked, however, and even though he was performing a challenging detection task at fixation, in his case we cannot completely exclude that possibility.

resulted from optic radiation injury, residual islands of V1 activity likely received inputs from axonal tracts that are only partially affected by the lesion. These tracts were able to elicit area V1 activity, but were not strong enough to elicit a visual percept (Fig. 2 *B*, *c*). In principle, lack of a percept in the presence of area V1 activity may occur because retinotopically corresponding higher pathways or areas are injured, or because the activity generated in area V1 is too weak or too disorganized to elicit a percept. Patient P2 had no lesion in higher pathways, and so the latter mechanism likely dominates. Given that the pathways from area V1 to higher extrastriate areas were intact and islands of activity were present in the V1 cortex, it is reasonable to view this patient as a prime candidate for visual rehabilitation. In theory, the capacity for recovery would be maximal in the portion of the scotoma that overlaps with the visual field coverage map of area V1.

The two other patients in this category, P1 and P3, had lesions that included ventral areas V2/V3, raising the possibility that the information flow between area V1 and higher extrastriate areas had been cut off. In that event, knowing the region of overlap between the visual field coverage map of area V1 and the scotoma might still be helpful if the projection from spared V1 cortex to extrastriate areas was not completely cut off. Regardless, the region of overlap between a visual field coverage map and the corresponding perimetrically determined visual field scotoma identifies visual field locations that can still generate some level of V1 activity and thus may have greater potential for visual rehabilitation. This strongly suggests that pRF mapping (34, 49) should be incorporated into the design of future visual rehabilitation studies.

Pattern 2: Visual Field Coverage Maps of Spared-V1 Did Not Cover Completely the Sighted Quadrant of the Perimetric Map. Two out of five patients exhibited this pattern of activity. Presumably in this case, residual visual function is mediated by V1-bypassing pathways (as supported by the visual field coverage maps of areas V2/V3 in patient P4; Fig. S1) or perhaps through the contralesional hemisphere. The latter possibility would be supported by a spreading of the pRF coverage map across the vertical meridian, as occurred to some degree in patient P5 (Fig. S3), who exhibited an area of sparing near the vertical meridian in the perimetry map. This occurred to a lesser degree than expected from the area of sparing seen in the perimetric map, however, and thus this hypothesis cannot be verified here; more research is needed. Another possible explanation that we cannot completely exclude here is that in some cases, fMRI mapping might not be sufficiently

sensitive to detect weak visually induced activity in early visual areas. This is probably not the complete explanation, however, for several reasons: (*i*) We calculated the BOLD signal-to-noise ratio (SNR) in the areas of interest in all patients and found them to be within the range obtained in controls with AS; (*ii*) the variance explained of voxels corresponding to these visual field locations is within the range obtained in nonvisually responsive areas; and (*iii*) previous studies have shown that BOLD signal amplitude correlates well with visual stimulus perception (50, 51), and in some cases even subthreshold stimuli elicit significant modulation in early visual areas (52).

Do (Spared) Area V1 pRFs Change After the Lesions? pRF measurements provide a way to gauge the degree of reorganization that occurs in early visual areas. The pRF depends on both the size and the position scatter of individual receptive fields within a voxel (53). It thus might be affected by partial deafferentiation of V1 inputs, or may reflect reorganization, that is, sprouting or strengthening of anatomic connections after V1 injury. Incomplete stimulus presentation itself might alter pRF size measurements and result in apparent remapping even in the absence of true reorganization (54). For this reason, changes can be reasonably attributed to cortical reorganization only if they are significantly different than changes observed in controls under the AS condition. Thus, we compared pRF center and size distributions between patients and AS controls.

Does the Position of pRF Centers Reorganize? One important question is whether the pRFs of spared area V1 in patients emerge from voxels that are at the correct anatomic locations versus voxels that are ectopic, suggesting possible reorganization. We have not found voxels with grossly ectopic V1 pRFs in any patient. pRFs fall in approximately correct anatomic locations; that is, pRFs located in the upper visual field belong to voxels located below the calcarine sulcus and vice versa. Finer changes in pRF localization do occur, however.

We found that for two of the five patients (P1 and P2), pRF center elevation (i.e, distance from the scotoma border) distributions differed significantly from that of the AS controls, with clustering near the scotoma border (horizontal meridian). Moreover, this occurred even when we restricted the analysis to the intact part of V1 that corresponds to a normal perimetry (dorsal V1; Fig. 5*B*). This suggests that for these patients, some pRF centers shift their location over short distances to locations near the scotoma border, supporting the notion of reorganization. A

possible mechanism behind this shift is enhancement of surviving single-cell pRFs in voxels near the border of the scotoma after injury, perhaps via a change in the balance of inhibition versus excitation (27–31). The magnitude of the shift is on average only 1°, consistent with at most a limited degree of reorganization.

In contrast, patients P4 and P5 exhibited patchy activation of spared V1. The difference in pRF center distributions between these patients and AS controls may be the result of partial deafferentation. The remaining patient, P3, had similar pRF center location distributions as AS controls. A possible important difference in this patient is that V1 injury occurred only 6 mo before recruitment, whereas all other patients had been lesioned for years. None of the patients who participated in this study, including the two patients with optic radiation lesions, had ectopic pRF centers over distances comparable to those suggested by Dilks et al. (33).

Does pRF Size Change in Spared-V1 Cortex? pRF size measurements in the spared V1 cortex of patients showed pRF size increases of ∼25% for patients P1, P2, P4, and P5 and ∼90% for patient P3 compared with AS controls. The pRF size difference reached ∼40% for patients P2, P4, and P5, ∼75% for patient P1, and ∼120% for patient P3 near (<2°) the scotoma border, whereas it was correspondingly smaller far (>2°) from the scotoma border (Fig. 6 B and C). As mentioned earlier, this may stem from decreased inhibition in the area surrounding the lesion (21), or perhaps because subcortical inputs from LGN or the pulvinar may reorganize via sprouting of cortical axons (55) and contribute to the activation of area V1 areas surrounding the lesion.

pRF size in area V1 of the intact hemisphere also increased in patients compared with healthy AS controls. The relative magnitude of the increase was ∼20% for patient P2 and ∼90% for patients P3 and P5. pRFs for patients P1 and P4 increased by ∼30% but only for eccentricities 6–10°. The relative increase in pRF size seen in the contralesional hemisphere may be attributed to loss of input from interhemispheric connections (40–42), although the expectation that these would affect mainly pRFs along the vertical meridian is not well born out.

Conclusions

Although each patient is unique, several themes emerge from our study:

1. Area V1 displays at best a limited degree of reorganization in adult humans with homonymous visual field defects due to postchiasmatic lesions of the visual pathway.
2. This reorganization is manifested in some patients by a small shift in the pRF centers toward the border of the scotoma and in most patients by a slight increase in V1 pRF sizes near the border of the scotoma, as well as in the V1 of the contralesional hemisphere. Finding ways to further expand pRF size in these patients may increase coverage of the visual field defect, inducing recovery.
3. Importantly, pRF measurements in patients with cortical lesions yield information on the functional properties of spared visual cortex that complements the information provided by standard perimetry maps.
4. We identified two different patterns of mismatch between responses in early visual areas and visual perception as measured by perimetry mapping, and examined possible underlying mechanisms.

5. Understanding how surviving visual areas process visual information post-lesion could potentially help guide visual rehabilitation efforts to induce recovery. Future studies of this patient population incorporating pRF measurements are clearly warranted to improve understanding of visual processing in the context of injury.

Materials and Methods

Patients. Four adult patients (age 27–64 y; two females and two males) with visual cortical lesions were recruited at the Center for Ophthalmology of the University Clinic in Tuebingen. One patient (male, age 33 y) was recruited at the Center for Advanced MR Imaging at Baylor College of Medicine. Four of the participants had homonymous visual field defects as a result of ischemic or hemorrhagic stroke at 7–10 y before enrollment in this study, and one patient had sustained an ischemic stroke at 0.5 y before recruitment (Table S1). Nine participants (age 26–65 y; eight males and one female) were recruited as controls. All patients had normal or corrected-to-normal visual acuity. The experiments were approved by the Ethical Committee of the Medical Faculty of the University of Tuebingen and the Institutional Review Board of Baylor College of Medicine.

Scanning. At least two T1-weighted anatomic volumes and a minimum of five fMRI scans were acquired for each patient and averaged to increase the SNR.

Stimuli. The patients were presented with moving square-checkerboard bars that traveled sequentially in eight different directions spanning a circular aperture with a radius of 11.25° around the fixation point. The bar width was 1.875°, and it was moved in a step of half its size (0.9375°) at each image volume acquisition (repetition time, 2 s). Five control subjects were asked to participate in a second session, during which an isoluminant mask was placed in the upper left quadrant of the visual field. The mask covered the area of the stimulus and created an AS.

Data Analysis. Data analysis was performed in MATLAB using the mrVista toolbox (http://white.stanford.edu/software/). Reliable pRF measurements and visual field coverage maps were derived using the direct isotropic Gaussian pRF method (Fig. S5) (34).

Normalization of pRF Center Voxel Distributions. To test for significant differences between individual patients and the mean distribution from controls (38), we normalized the distributions derived from the AS controls separately for each patient. To do so, we scaled these distributions by the ratio of active spared voxels in V1 of each patient divided by the number of active voxels in the retinotopically corresponding V1 regions of the control subjects during full stimulation (i.e., without AS).

Statistical Analysis. We used a two-sample Kolmogorov–Smirnov test to compare pRF center locations and size distributions between the patients and AS controls. The significance level selected to reject the null hypothesis (same distributions) was estimated by comparing each of the control distributions with the mean control distribution. The minimum P value of these comparisons was then used to test for significance differences in the mean distribution between patients and controls. We report significance as $P = a < b$, where b is the value selected to reject the null hypothesis.

Detailed descriptions of the methodology used in this study are provided in SI Materials and Methods.

1. Wandell BA, Smirnakis SM (2009) Plasticity and stability of visual field maps in adult primary visual cortex. Nat Rev Neurosci 10(12):873–884.
2. Kaas JH, et al. (1990) Reorganization of retinotopic cortical maps in adult mammals after lesions of the retina. Science 248(4952):229–231.
3. Chino YM, Kaas JH, Smith EL, 3rd, Langston AL, Cheng H (1992) Rapid reorganization of cortical maps in adult cats following restricted deafferentation in retina. Vision Res 32(5):789–796.
4. Chino YM, Smith EL, 3rd, Kaas JH, Sasaki Y, Cheng H (1995) Receptive-field properties of deafferentated visual cortical neurons after topographic map reorganization in adult cats. J Neurosci 15(3 Pt 2):2417–2433.

5. Gilbert CD, Wiesel TN (1992) Receptive field dynamics in adult primary visual cortex. Nature 356(6365):150–152.
6. Schmid LM, Rosa MG, Calford MB, Ambler JS (1996) Visuotopic reorganization in the primary visual cortex of adult cats following monocular and binocular retinal lesions. Cereb Cortex 6(3):388–405.
7. Calford MB, Schmid LM, Rosa MG (1999) Monocular focal retinal lesions induce short-term topographic plasticity in adult cat visual cortex. Proc Biol Sci 266(1418):499–507.
8. Baker CI, Dilks DD, Peli E, Kanwisher N (2008) Reorganization of visual processing in macular degeneration: Replication and clues about the role of foveal loss. Vision Res 48(18):1910–1919.

9. Baker CI, Peli E, Knouf N, Kanwisher NG (2005) Reorganization of visual processing in macular degeneration. *J Neurosci* 25(3):614–618.

10. Giannikopoulos DV, Eysel UT (2006) Dynamics and specificity of cortical map re-organization after retinal lesions. *Proc Natl Acad Sci USA* 103(28):10805–10810.

11. Schumacher EH, et al. (2008) Reorganization of visual processing is related to eccentric viewing in patients with macular degeneration. *Restor Neurol Neurosci* 26(4-5):391–402.

12. Dilks DD, Baker CI, Peli E, Kanwisher N (2009) Reorganization of visual processing in macular degeneration is not specific to the "preferred retinal locus." *J Neurosci* 29(9):2768–2773.

13. DeAngelis GC, Anzai A, Ohzawa I, Freeman RD (1995) Receptive field structure in the visual cortex: Does selective stimulation induce plasticity? *Proc Natl Acad Sci USA* 92(21):9682–9686.

14. Murakami I, Komatsu H, Kinoshita M (1997) Perceptual filling-in at the scotoma following a monocular retinal lesion in the monkey. *Vis Neurosci* 14(1):89–101.

15. Horton JC, Hocking DR (1998) Monocular core zones and binocular border strips in primate striate cortex revealed by the contrasting effects of enucleation, eyelid suture, and retinal laser lesions on cytochrome oxidase activity. *J Neurosci* 18(14):5433–5455.

16. Sunness JS, Liu T, Yantis S (2004) Retinotopic mapping of the visual cortex using functional magnetic resonance imaging in a patient with central scotomas from atrophic macular degeneration. *Ophthalmology* 111(8):1595–1598.

17. Smirnakis SM, et al. (2005) Lack of long-term cortical reorganization after macaque retinal lesions. *Nature* 435(7040):300–307.

18. Masuda Y, Dumoulin SO, Nakadomari S, Wandell BA (2008) V1 projection zone signals in human macular degeneration depend on task, not stimulus. *Cereb Cortex* 18(11):2483–2493.

19. Baseler HA, et al. (2011) Large-scale remapping of visual cortex is absent in adult humans with macular degeneration. *Nat Neurosci* 14(5):649–655.

20. Eysel UT, Schmidt-Kastner R (1991) Neuronal dysfunction at the border of focal lesions in cat visual cortex. *Neurosci Lett* 131(1):45–48.

21. Eysel UT, Schweigart G (1999) Increased receptive field size in the surround of chronic lesions in the adult cat visual cortex. *Cereb Cortex* 9(2):101–109.

22. Eysel UT, et al. (1999) Reorganization in the visual cortex after retinal and cortical damage. *Restor Neurol Neurosci* 15(2-3):153–164.

23. Zepeda A, Vaca L, Arias C, Sengpiel F (2003) Reorganization of visual cortical maps after focal ischemic lesions. *J Cereb Blood Flow Metab* 23(7):811–820.

24. Schweigart G, Eysel UT (2002) Activity-dependent receptive field changes in the surround of adult cat visual cortex lesions. *Eur J Neurosci* 15(10):1585–1596.

25. Payne BR, Lomber SG (2002) Plasticity of the visual cortex after injury: What's different about the young brain? *Neuroscientist* 8(2):174–185.

26. Yinon U, Shemesh R, Arda H, Dobin G, Jaros PP (1993) Physiological studies in deafferented visual cortical cells of cats following transplantation of fetal xenografts from the rat's cortex. *Exp Neurol* 122(2):335–341.

27. Rumpel S, et al. (2000) Lesion-induced changes in NMDA receptor subunit mRNA expression in rat visual cortex. *Neuroreport* 11(18):4021–4025.

28. Mittmann T, Eysel UT (2001) Increased synaptic plasticity in the surround of visual cortex lesions in rats. *Neuroreport* 12(15):3341–3347.

29. Barmashenko G, Eysel UT, Mittmann T (2003) Changes in intracellular calcium transients and LTP in the surround of visual cortex lesions in rats. *Brain Res* 990(1-2):120–128.

30. Yan L, et al. (2012) Changes in NMDA-receptor function in the first week following laser-induced lesions in rat visual cortex. *Cereb Cortex* 22(10):2392–2403.

31. Imbrosci B, Neubacher U, White R, Eysel UT, Mittmann T (2013) Shift from phasic to tonic GABAergic transmission following laser-lesions in the rat visual cortex. *Pflugers Arch* 465(6):879–893.

32. Zhang X, Kedar S, Lynn MJ, Newman NJ, Biousse V (2006) Natural history of homonymous hemianopia. *Neurology* 66(6):901–905.

33. Dilks DD, Serences JT, Rosenau BJ, Yantis S, McCloskey M (2007) Human adult cortical reorganization and consequent visual distortion. *J Neurosci* 27(36):9585–9594.

34. Dumoulin SO, Wandell BA (2008) Population receptive field estimates in human visual cortex. *Neuroimage* 39(2):647–660.

35. Schmid MC, Panagiotaropoulos T, Augath MA, Logothetis NK, Smirnakis SM (2009) Visually driven activation in macaque areas V2 and V3 without input from the primary visual cortex. *PLoS ONE* 4(5):e5527.

36. Horton JC, Hoyt WF (1991) Quadrantic visual field defects: A hallmark of lesions in extrastriate (V2/V3) cortex. *Brain* 114(Pt 4):1703–1718.

37. Slotnick SD, Moo LR (2003) Retinotopic mapping reveals extrastriate cortical basis of homonymous quadrantanopia. *Neuroreport* 14(9):1209–1213.

38. Dougherty RF, et al. (2003) Visual field representations and locations of visual areas V1/2/3 in human visual cortex. *J Vis* 3(10):586–598.

39. Levin N, Dumoulin SO, Winawer J, Dougherty RF, Wandell BA (2010) Cortical maps and white matter tracts following long period of visual deprivation and retinal image restoration. *Neuron* 65(1):21–31.

40. Ptito M, Dalby M, Gjedde A (1999) Visual field recovery in a patient with bilateral occipital lobe damage. *Acta Neurol Scand* 99(4):252–254.

41. Raninen A, Vanni S, Hyvärinen L, Näsänen R (2007) Temporal sensitivity in a hemianopic visual field can be improved by long-term training using flicker stimulation. *J Neurol Neurosurg Psychiatry* 78(1):66–73.

42. Henriksson L, Raninen A, Näsänen R, Hyvärinen L, Vanni S (2007) Training-induced cortical representation of a hemianopic hemifield. *J Neurol Neurosurg Psychiatry* 78(1):74–81.

43. Reitsma DC, et al. (2013) Atypical retinotopic organization of visual cortex in patients with central brain damage: congenital and adult onset. *J Neurosci* 33(32):13010–13024.

44. Hubel DH, Wiesel TN (1967) Cortical and callosal connections concerned with the vertical meridian of visual fields in the cat. *J Neurophysiol* 30(6):1561–1573.

45. Baseler HA, Morland AB, Wandell BA (1999) Topographic organization of human visual areas in the absence of input from primary cortex. *J Neurosci* 19(7):2619–2627.

46. Amano K, Wandell BA, Dumoulin SO (2009) Visual field maps, population receptive field sizes, and visual field coverage in the human MT+ complex. *J Neurophysiol* 102(5):2704–2718.

47. Harvey BM, Dumoulin SO (2011) The relationship between cortical magnification factor and population receptive field size in human visual cortex: Constancies in cortical architecture. *J Neurosci* 31(38):13604–13612.

48. Winawer J, Horiguchi H, Sayres RA, Amano K, Wandell BA (2010) Mapping hV4 and ventral occipital cortex: The venous eclipse. *J Vis* 10(5):1.

49. Lee S, Papanikolaou A, Logothetis NK, Smirnakis SM, Keliris GA (2013) A new method for estimating population receptive field topography in visual cortex. *Neuroimage* 81:144–157.

50. Boynton GM, Demb JB, Glover GH, Heeger DJ (1999) Neuronal basis of contrast discrimination. *Vision Res* 39(2):257–269.

51. Avidan G, et al. (2002) Contrast sensitivity in human visual areas and its relationship to object recognition. *J Neurophysiol* 87(6):3102–3116.

52. Watanabe M, et al. (2011) Attention, but not awareness, modulates the BOLD signal in the human V1 during binocular suppression. *Science* 334(6057):829–831.

53. Haak KV, Cornelissen FW, Morland AB (2012) Population receptive field dynamics in human visual cortex. *PLoS ONE* 7(5):e37686.

54. Pettet MW, Gilbert CD (1992) Dynamic changes in receptive-field size in cat primary visual cortex. *Proc Natl Acad Sci USA* 89(17):8366–8370.

55. Rose JE, Malis LI, Kruger L, Baker CP (1960) Effects of heavy, ionizing, monoenergetic particles on the cerebral cortex, II: Histological appearance of laminar lesions and growth of nerve fibers after laminar destructions. *J Comp Neurol* 115:243–255.

56. Heijl A, Patella VM, Bengtsson B (2012) *The Field Analyzer Primer: Effective Perimetry* (Carl Zeiss Meditec, Dublin, CA), 4th Ed.